APTAMER-BASED BIOSENSORS FOR PROTEIN BIOMARKERS

by

Alan Ka Ho Cheng
B.Sc., Simon Fraser University, 2003–2006
Molecular Biology and Biochemistry

THESIS SUBMITTED IN PARTIAL FULFILLMENT OF
THE REQUIREMENTS FOR THE DEGREE OF

MASTER OF SCIENCE

In the
Department of Chemistry

SIMON FRASER UNIVERSITY

Summer 2009

APPROVAL

Name: Alan Ka Ho Cheng

Degree: Master of Science

Title of Thesis: Aptamer-Based Biosensors for Protein Biomarkers

Examining Committee:

Chair

Dr. David J. Vocadlo
Associate Professor, Department of Chemistry

Dr. Hua-Zhong (Hogan) Yu
Senior Supervisor
Associate Professor, Department of Chemistry

Dr. Peter J. Unrau
Supervisor
Associate Professor, Department of Molecular Biology & Biochemistry

Dr. Michael H. Eikerling
Supervisor
Assistant Professor, Department of Chemistry

Dr. Robert N. Young
Internal Examiner
Professor, Department of Chemistry

Date Defended/Approved: **July 9, 2009**

Declaration of
Partial Copyright Licence

ABSTRACT

The revolutionary technique of "systematic evolution of ligands by exponential enrichment" (SELEX) has transformed the premise of biorecognition to encompass nucleic acids as well as protein antibodies. These synthetic counterparts – aptamers – are DNA or RNA strands that have been selected through iterative rounds of *in vitro* selection to bind with specific affinity to analytes (from small molecules to proteins) of choice. In this thesis, the voltammetric aptamer-based detection of ubiquitous glycanhydrolase lysozyme was first explored based on charge density changes on aptamer-modified electrodes upon analyte binding. Different detection methodologies (optical and electrochemical methods) were then tested for the detection of MUC1 (mucin 1), a glycoprotein overexpressed in elevated concentrations in the serum of patients with epithelial adenocarcinomas; this augments the importance for MUC1 detection as an alternative for early cancer diagnostics. Optical biosensors developed for the MUC1 detection was through a DNA hybridization scheme with quantum dot-based fluorescence readout. Electrochemical methods were based on either direct attachment of a redox center, methylene blue (MB), to the aptamer strands, or adding free MB to the electrolyte solution (intercalative binding). In both cases, quantitative detection of MUC1 was possible, although direct labeling showed a better sensitivity. To further improve the sensitivity, an intricate biochemical assay was explored featuring the fusion of anti-thrombin and anti-MUC1 aptamers, in the hope of generating a pico-Molar assay for MUC1 via the MUC1-dependent allosteric upregulation of the proteolytic activity of human α-thrombin.

Keywords: biosensor; DNA; aptamer; electrochemistry; biomarker; cancer; early diagnostics

To my family

But we have this treasure in jars of clay to show that this all-surpassing power is from God and not from us. We are hard pressed on every side, but not crushed; perplexed, but not in despair; persecuted, but not abandoned; struck down, but not destroyed. We always carry around in our body the death of Jesus, so that the life of Jesus may also be revealed in our body. For we who are alive are always being given over to death for Jesus' sake, so that his life may be revealed in our mortal body.

So then, death is at work in us, but life is at work in you. 2 Corinthians 4:7–12

我們有這寶貝放在瓦器裡，要顯明這莫大的能力是出於神，不是出於我們。我們四面受敵，卻不被困住；心裡作難，卻不至失望；遭逼迫，卻不被丟棄；打倒了，卻不至死亡。身上常帶著耶穌的死，使耶穌的生也顯明在我們身上。因為我們這活著的人是常為耶穌被交於死地，使耶穌的生在我們這必死的身上顯明出來。

這樣看來，死是在我們身上發動，生卻在你們身上發動。 歌林多後書四章 7 至 12 節

ACKNOWLEDGEMENTS

My sincere gratefulness goes to my senior supervisor, Dr. Hua-Zhong (Hogan) Yu, for challenging me and encouraging me ever since I entered his laboratory as an aimless 19 year old teenager with zero knowledge of scientific research. I am appreciative of the research opportunities that he has given me and for his patience and guidance throughout the years. I give thanks to Dr. P. J. Unrau and Dr. M. H. Eikerling for being my committee members – their advice and suggestions have tremendously helped in my studies. I would like to thank Dr. D. Sen for the valuable and constructive discussions on my research. I would like to also thank Dr. R. N. Young for taking time from his busy schedule to be the internal examiner of this thesis. Furthermore, I would like to thank the Natural Sciences and Engineering Research Council, the Provincial Government of British Columbia, British Columbia Network of Aging Research, and Simon Fraser University for funding support.

My special thanks go to Dr. Bixia Ge for inspiring me and raising my interest in the field of bioanalytical chemistry. I would like to thank past and present members of the Yu laboratory for their friendship and support. My sincere appreciation goes to my brothers and sisters in Christ who have supported and encouraged me through prayer.

I would like to express my deepest thankfulness to my parents and my brother Leslie for their unconditional and steadfast support in my academic career. My ultimate gratefulness goes to my Heavenly Father – to the only God all glory, majesty, power and authority, through Jesus Christ our Lord, before all ages, now and forevermore.

TABLE OF CONTENTS

LIST OF FIGURES

LIST OF ABBREVIATIONS

A/C/T/G	Adenosine / cytidine / thymidine / guanosine
A/C/T/GMP	Adenosine / cytidine / thymidine / guanosine 5′-monophosphate
A/C/T/GDP	Adenosine / cytidine / thymidine / guanosine 5′-diphosphate
A/C/T/GTP	Adenosine / cytidine / thymidine / guanosine 5′-triphosphate
ACV	Alternating current voltammogram / alternating current voltammetric / alternating current voltammetry
AQ	Anthraquinone
AQMS	Anthraquinone-2-sulfonic acid
BCA	Bicinchoninic acid
bp	Base pair
BSA	Bovine serum albumin
cps	Counts per second
CHCA	α-cyano-4-hydroxycinnanic acid
CV	Cyclic voltammogram / cyclic voltammetric / cyclic voltammetry
DMS	Dimethyl sulfate
DNA	Deoxyribonucleic acid
dsDNA	Double stranded deoxyribonucleic acid
ssDNA	Single stranded deoxyribonucleic acid
E-AB	Electronic aptamer-based
et al.	*et alii* (Latin expression: “and others”)
EDC	1-ethyl-3-(3-dimethylaminopropyl)carbodiimide
EDTA	Ethylenediaminetetraacetic acid

ELISA	Enzyme-linked immunosorbent assay
F-Q	bis-(p-tosyl-L-glycyl-L-prolyl-L-arginine amide), Rhodamine 110
Fc	Ferrocene
FRET	Fluorescence resonance energy transfer / Förster resonance energy transfer
G+•	Guanine radical cation
HPLC	High performance liquid chromatography
I-B	Immobilization buffer
IgA	Immunoglobulin A
IgG	Immunoglobulin G
ITO	Indium tin oxide
K_D	Dissociation constant
LB	Leucomethylene blue
MALDI-TOF	Matrix-assisted laser desorption ionization, time of flight
MB	Methylene blue
MCH	6-mercapto-1-hexanol
MUC1	Mucin 1
NHS	N-hydroxysuccinimide
nt	Nucleotide
PAGE	Polyacrylamide gel electrophoresis
PBS	Phosphate buffered saline
PCR	Polymerase chain reaction
PDGF	Platelet-derived growth factor
PEG	Poly(ethylene glycol)
POC	Point-of-care
PSMA	Prostate specific membrane antigen

QD	Quantum dot
QD-Au	Quantum dot-gold nanoparticle conjugate
regNA	Regulatory nucleic acid
R^2	Correlation of determination
RNA	Ribonucleic acid
RT-PCR	Reverse transcriptase polymerase chain reaction
SAM	Self-assembled monolayer
SELEX	Systematic evolution of ligands by exponential enrichment
SHE	Standard hydrogen electrode
SQW	Square wave voltammogram / square wave voltammetric / square wave voltammetry
TAE	40 mM Tris-acetate, 1 mM EDTA at pH 8.0
TBE	89 mM Tris-HCl, 89 mM H_3BO_3, 2 mM EDTA at pH 8.0
TCEP	Tris(2-carboxyethyl)phosphine
TE	10 mM Tris-HCl, 100 μM EDTA at pH 7.4
TEAA	Triethylammonium acetate
TRAP	Targeted reversibly attenuated probe
Tris	Tris(hydroxylmethyl)aminomethane
tRNA	Transfer ribonucleic acid
UV	Ultraviolet
W-B	Wash buffer

CHAPTER 1

DESIGN AND TESTING OF APTAMER-BASED BIOSENSORS: FROM *SELEX* TO ELECTROCHEMICAL READOUT METHODS[*]

This chapter is a general introduction to aptamers and aptamer-based electrochemical biosensors; it summarizes the fundamental concepts and recent research efforts which are pertinent as an introduction for the next four chapters of this thesis. In this chapter, aptamer-based electrochemical sensors are described and classified into three categories, for which the analyte detection relies on analyte-induced configurational changes, conformational changes, and conductivity changes, with concomitant alteration in electrochemical response. The thesis, itself, constitutes of six chapters, with the first and last being a general introduction and an overall conclusion, respectively. Chapters 2 through 5 recapitulates the research efforts geared towards the development of novel electrical and optical aptamer-based biosensors, first using lysozyme (a ubiquitous protein in mammals) as a model system (Chapter 2), followed by the development and pre-developmental steps in novel sensor development for mucin 1 (MUC1), a cell-surface glycoprotein, which has been confirmed as a potentially useful biomarker for the diagnosis of early epithelial cancers (Chapters 3 through 5).

[*] Reproduced in part with permission from Cheng, A. K. H.; Sen, D.; Yu, H. Z. (2009) Design and testing of aptamer-based electrochemical biosensors for proteins and small molecules. *Bioelectrochemistry* 75: in press.

1.1 Introduction

1.1.1 Biosensors

The realm of biosensing technology began when analytical scientists faced the challenge in developing novel methodologies for the detection and quantitation of not only simple/small molecules, but also biomedical analytes (typically biological macromolecules). The term "biosensor" refers to analytical devices that are based on biological components and are capable of sensing biologically-relevant analytes with either electrical or optical readout. Their importance is epitomized by the now commercially-ubiquitous glucose sensor, which uses an enzymatic reaction (catalyzed by the enzyme glucose oxidase).[1] The oxidation of glucose to gluconic acid by the enzyme is coupled to the reduction of ferricyanide to ferrocyanide. Such an electrocatalytic reaction on the working electrode surface is monitored, and the generated electrical current infers the concentration of glucose in the blood samples.

Like the glucose sensor, a typical biosensor contains three components: a biological sensing element (that can "recognize" or "bind" the analyte of choice), a transducing element (which converts the binding or detection event into a measurable signal), and a display (which transforms the measured electrical/optical signal into a digital format for end users). The sensing element primarily defines the selectivity and sensitivity of the biosensor. To date, many different types of biological components (enzymes, antibodies, or DNA/RNA) have been employed for highly selective responses to particular analytes. Antibodies are protein molecules generated by the immune system *in vivo*, and their binding specificity arises from a variable region in the protein that relies on non-covalent interactions (e.g., electrostatic interactions, van der Waals interactions,

and hydrophobic interactions) to recognize antigens (analytes) at particular structured regions termed antigenic epitopes. Production of a particular analyte-specific antibody can be accomplished by injecting the analyte (antigen) into an animal such as a rabbit, followed by the isolation and purification of the antibodies specific for the antigen. Modern antibody-based biosensors include the popularly enzyme-linked immuno-sorbent assay (ELISA).[2] Briefly, the antibody recognizing the analyte of choice is immobilized (with the variable recognition elements facing upwards) on a surface, typically a multi-well plate that can be read optically. The sample containing the analyte is then allowed to react with the surface-bound antibodies. A secondary antibody conjugated to an enzyme (hence, enzyme-linked) which recognizes another epitope of the same analyte is incubated in the wells. The binding event thus immobilizes the enzyme which is capable of generating a chromophore or cleaving a non-fluorescent substrate to a fluorescent product. The extent of changes in colour or fluorescence produced in each well can infer the concentration of the starting analyte. This can be accomplished by the production of a standard working curve with a set of standard controls.

1.1.2 Aptamer-Based Biosensors

While antibodies have been dominant in the realm of protein detection, the early 1990s was an era in which the development of biosensors was revolutionized by the introduction of a novel sensing element that could rival antibodies.[3,4] These are aptamers, DNA and RNA molecules that have undergone a selection process to bind with high affinity and specificity to analytes of interest. The selection is termed SELEX (systematic evolution of ligands by exponential enrichment) (Figure 1-1). A random DNA library

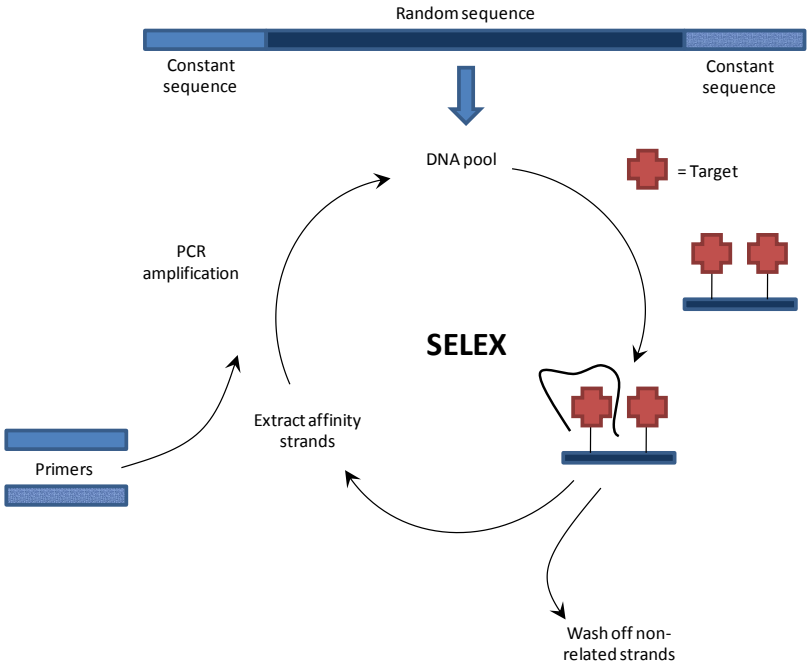

Figure 1-1. The preparation of functional DNA oligonucleotides (aptamers) that bind with high specificity to an analyte of choice via the SELEX (systematic evolution of ligands by exponential enrichment) protocol. PCR = polymerase chain reaction.

containing 10^{14} to 10^{15} sequences is produced. The analyte of interest is immobilized onto a column, and the library (DNA or RNA) is passed through. Those that do not bind to the analyte specifically are washed off, while those that do bind are retained. The ionic strength of the column buffer is then altered to release those nucleic acid molecules that have bound with high specificity. Polymerase chain reaction (PCR) or reverse-transcriptase polymerase chain reaction (RT-PCR) is performed to re-amplify the pool containing putative specific nucleic acid sequences of interest, for DNA and RNA, respectively. The cycle is repeated iteratively to isolate highly specific binding nucleic acids. The resulting sequences are then cloned in plasmids into bacteria, cultured, then subjected to modern sequencing to elucidate the analyte-specific binding sequences.

In general, aptamers are excellent alternatives for antibodies owing to their ease of handling and stability (synthetic oligonucleotides vs. biologically generated proteins), synthesis *in vitro* rather than *in vivo*, and their low elicitation of immunological response if used as an *in vivo* detection system.[5] Typically, the ability for an aptamer to bind an analyte does not in itself guarantee its application for a biosensor; the necessity for transduction of the binding event to a measurable signal is equally important. The transduction of measurable signals is usually in an electrical form or an optical form: the latter, which has been reported extensively in literature, has the binding event alter the configuration/conformation of an aptamer (which is usually conjugated to fluorophores or nanoparticles), which in turn alters the optical properties of the system.[6–9] The binding of analyte molecules induces changes in fluorescence or absorbance, which can be monitored either spectroscopically or colourimetrically. Several recent review articles have covered the development of aptamer-based biosensors with either optical[10–13] or electrochemical[14] readout; in this chapter, we focus on those that are based solely on electrochemical readout methodologies with an emphasis on the design of the constructs as sensing platforms. While the use of aptamers (as opposed to antibodies) provides a more versatile and robust platform for detection, electrochemical transduction of the aptamer-analyte binding events to digital signals is practically more appealing as it is sensitive and requires less complicated instrumentation, as discussed in detail below.

1.2 Aptamer-Based Electrochemical Sensors

A typical electrochemical biosensor makes use of an electrode surface as the platform to immobilize the biological sensing component (*e.g.*, antibodies or aptamers), and the analyte binding event is monitored based on electrical current variations.

Analogous to the commercialized glucose sensor, it is possible to produce miniature, portable, and versatile aptamer-based biosensors for both small and macromolecules.

In the fabrication of aptamer-based electrochemical biosensors, one of the most popularly used electrode materials is gold, upon which thiolated DNA/RNA strands can be immobilized via strong Au-S linkages.[15–17] The modification of DNA or RNA with a terminal thiol is straightforward: simple phosphoramidite chemistry on the DNA/RNA synthesizer suffices. The modification of Au surfaces with thiolated oligonucleotide strands is readily accomplished by dipping the cleaned Au slide into a deposition solution to form a self-assembled monolayer (SAM). Although the initial adsorption of thiolated DNA strands onto gold surfaces occurs within minutes, it is necessary to allow the reaction to continue for up to 24 hours to ensure a homogenous surface.[15–17] The resulting surface is usually subjected to a passivation step (*i.e.*, treated with 1-mercapto-6-hexanol solution) to minimize non-specifically bound oligonucleotide strands.[15,17]

In the following sections, we will describe different types of aptamer-based electrochemical biosensors that utilize various sensor designs, for instance, in the way the aptamer strands are incorporated onto the surface-bound DNA construct and how the electrochemical signal is obtained upon analyte binding. As shown in Figure 1-2 (also as an outline of this chapter), aptamer-based electrochemical biosensors can be divided into three types, which depend on changes in (i) configuration, (ii) conformation, and (iii) conductivity of the aptamer-containing DNA construct upon binding an analyte, with concomitant alteration in electrochemical response.

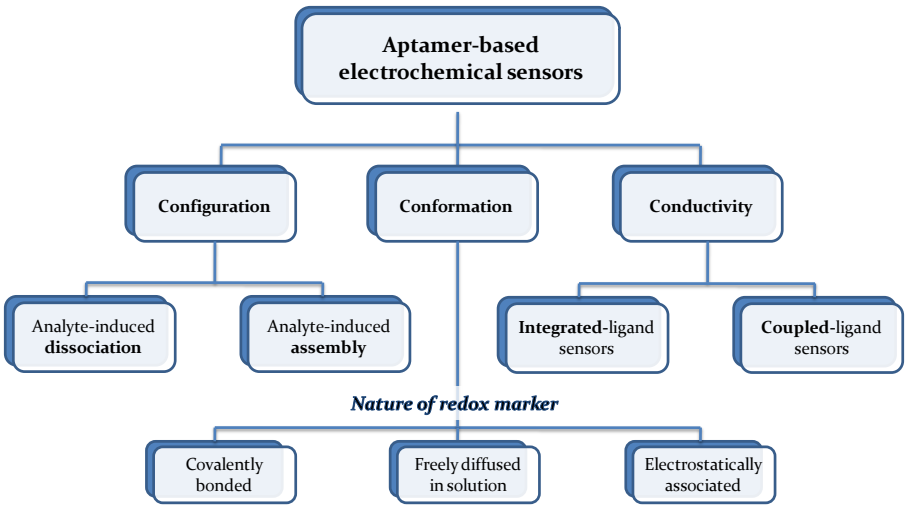

Figure 1-2. A schematic hierarchy of the different classes of aptamer-based electrochemical sensors described in this chapter.

1.2.1 Configurational Change

We define configurational change as a detection methodology for aptamer-based electrochemical biosensors in which the binding of the analyte induces either an assembly or dissociation of the sensor construct, with concomitantly altered electrochemical behaviour. Often assembly results in the formation of more intricate sandwich structures (*e.g.*, an aptamer-analyte-aptamer assembly), while dissociation results in the elimination of previously formed intramolecular Watson-Crick interactions, resulting in the release of DNA/RNA single strands. In both cases, the electrochemistry depends on redox markers that are electrostatically associated, covalently bonded, or diffusively (attraction/repulsion) interacting with surface-bound DNA strands. The application of tethered enzymes and nanoparticles for catalyzing the electrochemical signal for

biosensors involving analyte-induced dissociation/assembly processes has been also reported.

1.2.1.1 Analyte-Induced Dissociation of the Aptamer Construct

We first describe the varieties of configurational change-induced alterations in electrical signal that involve an analyte-induced dissociation. In these cases, the binding of an analyte to the preformed aptamer-containing construct grafted on a Au surface brings about a dissociation of the construct. We describe three such types of "dissociation" designs: (i) a partial double-stranded DNA construct; (ii) a complete double-stranded DNA helix; and (iii) an aptamer-extraneous analyte complex.

Disassembly of a Partial Double-Stranded DNA Construct

This type of configurational change has been demonstrated with the adenosine aptamer, which was selected by Huizenga and Szostak in 1995.[18] It is known that the binding of adenosine to the aptamer results in a generation of a localized intramolecular region with both canonical Watson-Crick interactions as well as non-canonical purine-purine interactions,[19] as shown in Figure 1-3. Researchers have taken advantage of the production of this unique tertiary structure to design and develop biosensors, which feature a partial double-stranded region (often proximal to the Au surface) that dehybridizes via an unzipping mechanism upon the binding of adenosine (or its derivatives) to a longer (aptamer-containing) DNA strand.

In early 2007, Shao and coworkers reported a chronocoulometric aptamer sensor for adenosine monophosphate (AMP) using $[Ru(NH_3)_6]^{3+}$ as an electrostatically-bound redox marker.[20] It is known that $[Ru(NH_3)_6]^{3+}$ electrostatically associates with the

phosphate backbone of both double-stranded and single-stranded DNA and displaces physiological Na^+ ions.[21,22] Theoretically, the triply charged $[Ru(NH_3)_6]^{3+}$ cations would displace three Na^+ ions upon equilibrium. Given these conditions, it is possible to use simple electrochemical techniques to determine the number of $[Ru(NH_3)_6]^{3+}$ electrostatically bound, and hence estimate its surface concentration, which in turn provides a quantitative measure of the surface density of DNA molecules. Therefore, this method is not only useful in demonstrating changes in redox activity that is pertinent to its role in a biosensor, it also helps to determine the surface density of DNA strands without the use of a more tedious radioactivity labeling protocol.[23] In fact, the surface density of DNA constructs on the electrode can directly influence the performance of

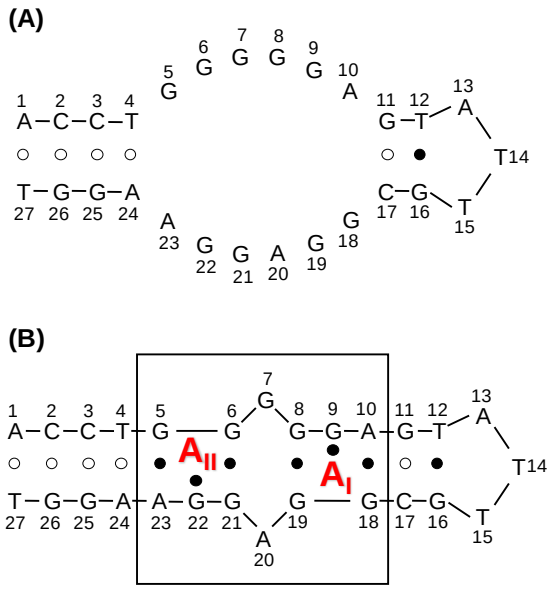

Figure 1-3. (a) The sequence and Watson-Crick pairing alignments for the 27-mer ATP-binding DNA aptamer identified via *in vitro* selection. (b) The secondary folding structure of the above aptamer upon AMP binding at the two non-equivalent sites (A_I and A_{II}). Reproduced with permission from reference 19.

DNA biosensors, as will be discussed later. The electrochemical determination of DNA surface density is based on the following equations:

$$\Gamma_{Ru} = \frac{Q}{nFA} \quad (1)$$

$$\Gamma'_{DNA} = \Gamma_{Ru}(\frac{z}{m})N_A \quad (2)$$

where Γ_{Ru} is the surface molar density of $[Ru(NH_3)_6]^{3+}$, Q is the integrated charge for the reduction of surface-bound $[Ru(NH_3)_6]^{3+}$ to $[Ru(NH_3)_6]^{2+}$, n is the number of electrons transferred, F is Faraday's constant, A is the area of the electrode, Γ'_{DNA} is the surface density of DNA, z is the valence of the redox species investigated (3 in the case of $[Ru(NH_3)_6]^{3+}$), m is the sum of the number of total nucleotides, and N_A is the Loschmidt-Avogadro's constant.[21,22]

In the paper of Shao and coworkers,[20] a partial double-stranded DNA construct was produced by the hybridization of a thiol-terminated strand with a shorter, unmodified strand, and the composite immobilized with the double-stranded region proximal to the Au surface (Panel A of Figure 1-4). The long strand contained the aptamer sequence, and hence the analyte-binding site. A similar electrode design for sensing adenosine was reported by Willner's group previously.[24] In the case of Shao and coworkers (Panel A of Figure 1-4), the DNA-modified electrode was allowed to be equilibrated with $[Ru(NH_3)_6]^{3+}$ and then tested using chronocoulometric measurements. Upon the binding of adenosine, the long DNA strand folds into its inherent tertiary structure stabilized by purine-purine interactions with adenosine acting as a "nucleobase" to complete these interactions (as discussed above). This in turn results in the "unzipping" of the pre-

formed double helix, starting at the end distal to the Au surface. Complete unzipping results in the release of the shorter strand, which can be measured from the decrease in the integrated charge of $[Ru(NH_3)_6]^{3+}$ ions bound to the DNA strands on the electrode surface. The authors demonstrated that the response of the system (change of reduction

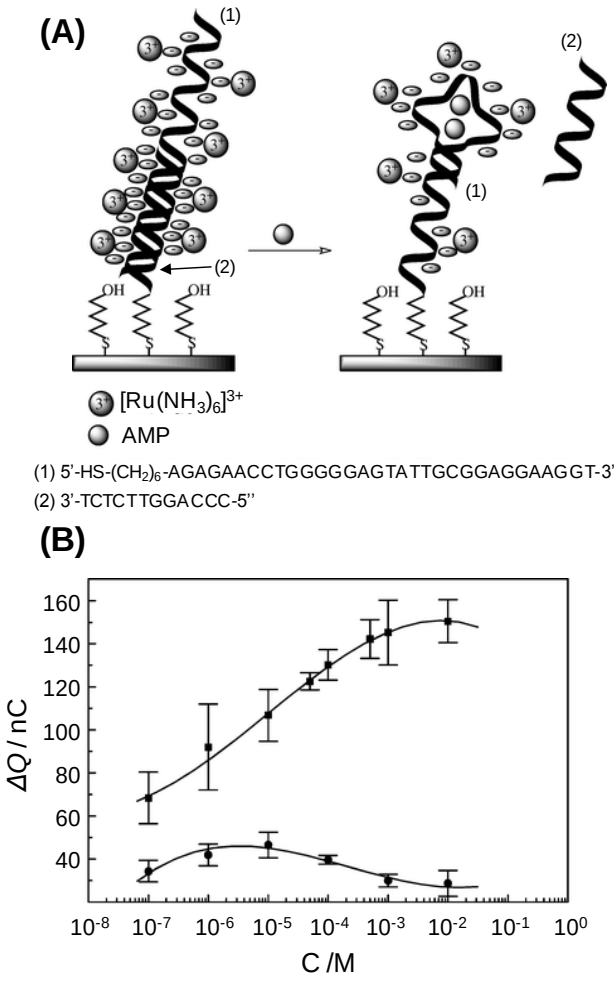

Figure 1-4. (a) A schematic representation of the chronocoulometric aptamer sensor for AMP. (b) The decrease of integrated charge (ΔQ) of the surface-bound $[Ru(NH_3)_6]^{3+}$ cations is presented as a function of the cconcentration (C) of AMP (top) and CMP (bottom), respectively. Adapted with permission from reference 20.

charge) towards AMP increases monotonically with increasing analyte concentration (Panel B of Figure 1-4); a significantly smaller response was observed with CMP (cytidine monophosphate) which does not bind the aptamer. The authors also evaluated the time-dependent response of the sensor, showing that with a concentration of AMP of 1 mM, about 10 min are required to reach equilibrium. The detection limit of the sensor was determined to be as sensitive as 0.1 μM.

Wu *et al.* designed a similar type of biosensor capable of detecting adenosine, but with covalently-tethered redox centres.[25] The preparation of redox centre-tethered DNA strands can be accomplished with either phosphoramidite chemistry or a simple amide coupling reaction: amine-terminated DNA can be coupled post-synthetically with an activated ester (typically a N-hydroxysuccinimide ester) of a redox moiety.[26] The modification of the other end of the nucleic acid with a thiol group allows the immobilization of such redox-labeled strands on Au surface. As will be discussed later, the two popular redox moieties that have been used for this purpose are ferrocene and methylene blue, both of which can be easily tethered to the end of a DNA molecule via amide coupling reactions.

In their report, Wu *et al.* modified the Au surface with gold nanoparticles in the hope of increasing the surface area of the working electrode, hence enhancing the redox signal.[25] They also used a partial double-stranded construct with the double-helical region proximal to the Au surface. The long strand (containing the analyte-binding aptamer sequence) was covalently modified with a ferrocene moiety. Thus, formation of the desired construct can be monitored by measuring the ferrocene oxidation/reduction signal. Upon incubation with adenosine, the longer strand binds two adenosine

molecules and unzips the pre-formed double helix towards the Au surface. The long strand (tethered with ferrocene) will then leave the surface, leading to a decrease in the surface concentration of ferrocene moieties (in a way that was dependent on the concentration of adenosine in the analyte sample). An improved detection limit with this methodology was achieved (20 nM).

Also in 2007, Dong and co-workers developed a similar sensor design but based on the electrochemical response of $[Fe(CN)_6]^{3-/4-}$ ions, which freely diffuse in the solution.[27] Differing from the earlier design,[20] the longer (aptamer-containing) strand dissociates from the electrode surface upon binding to adenosine, leaving the shorter thiolated strand on electrode. The extent of electrostatic repulsion of $[Fe(CN)_6]^{3-/4-}$ to the surface was reduced, leading to increased electrochemical response.

Plaxco, Heeger and coworkers designed another type of biosensor in which a methylene blue moiety is covalently linked to a strand that becomes partially dehybridized upon introduction of analyte.[28] This strand is also partially complementary to an anti-thrombin aptamer-containing strand, and the full construct in the absence of analyte consists of a partial double stranded DNA with a mismatched region in the centre (Figure 1-5: top). In the absence of thrombin, the partial double-stranded conformation of the construct places methylene blue far from the electrode surface, producing minimal current, since the electron transfer process from methylene blue to the electrode is prohibited (due to the distance). In the presence of thrombin, the aptamer folds and binds thrombin as a guanine quadruplex (G-quadruplex), releasing the complementary methylene blue-containing strand. The increased flexibility of this liberated strand now promotes the electron transfer between methylene blue and the electrode, due to their

closer physical distance with each other. The increase in the current was monitored using alternating current voltammetry (ACV) and a detection limit of 3 nM was reported (Figure 1-5: bottom).

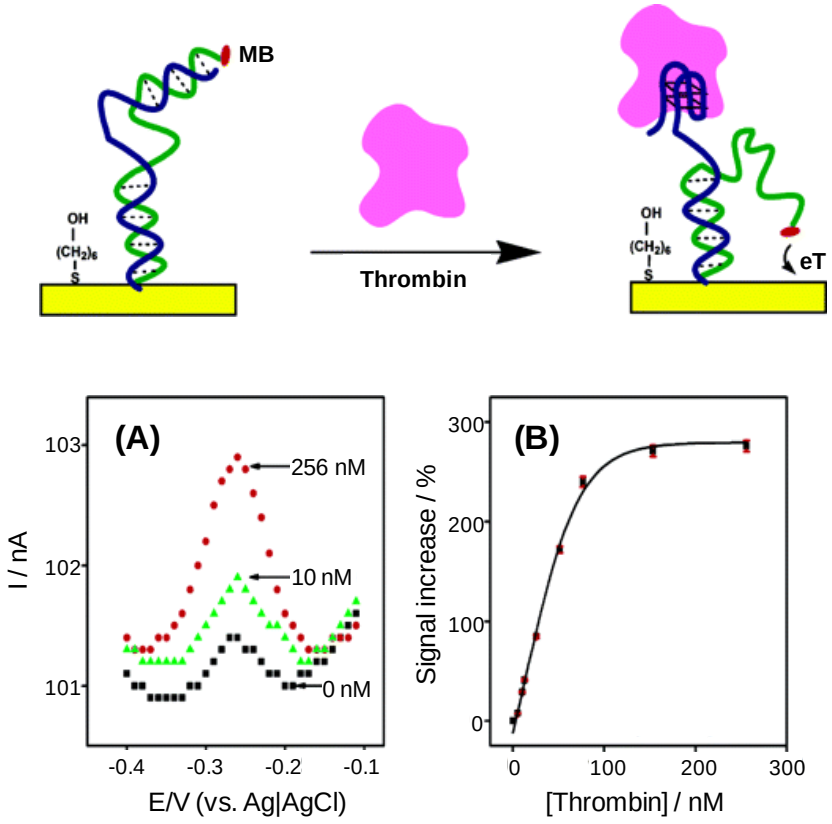

Figure 1-5. Top: the proposed mechanism of the signal-on electronic, aptamer-based (E-AB) sensor. Bottom: (A) Alternating current voltammetric (ACV) responses of the E-AB sensor-functionalized gold electrodes in 20 mM Tris-HCl, pH 7.4 with 140 mM NaCl, 20 mM $MgCl_2$, and 20 mM KCl at various thrombin concentrations. (B) The signal decrease of the E-AB sensor is presented as a function of the thrombin concentration. Adapted with permission from reference 28.

Disassembly of a Complete Double-Stranded DNA Helix

Very recently, another design of aptamer-based biosensors was developed that was based on changes in the configuration (structure) of the aptamer-DNA construct:[29–31] these types of biosensors took advantage of the strong affinity of an aptamer for its specific analyte and used a competition scheme as the detection methodology. In these designs, a complete DNA double helix was immobilized on a Au electrode, in which one of the strands contained the aptamer sequence. In the usual way, one of the two strands was tethered with a covalently-linked redox marker to assess electrochemical reactivity.

Fan and coworkers developed a sensor for adenosine triphosphate (ATP) based on the above-mentioned design (Figure 1-6).[29] The system is similar to the aforementioned designs but uses a complete DNA double helix as opposed to a partial double-stranded construct. In their design, ferrocene was attached to the surface-bound aptameric strand, which hybridized with its fully complementary strand. In its initial state, ferrocene was far from the electrode surface and thus the electron transfer process was inhibited. Upon binding of the aptamer with adenosine, the aptamer strand folded back, dehybridizing from the full double helix and the altered tertiary structure of the aptamer brought the ferrocene closer to the Au electrode, thus promoting the electron transfer in between. When monitored with square wave voltammetry (SQW), remarkable increase in the current was observed upon increasing the concentration of ATP (Panel B of Figure 1-6). The detection limit for the binding of adenosine was 10 nM, which is a substantial improvement over other methods reported previously.[20,27]

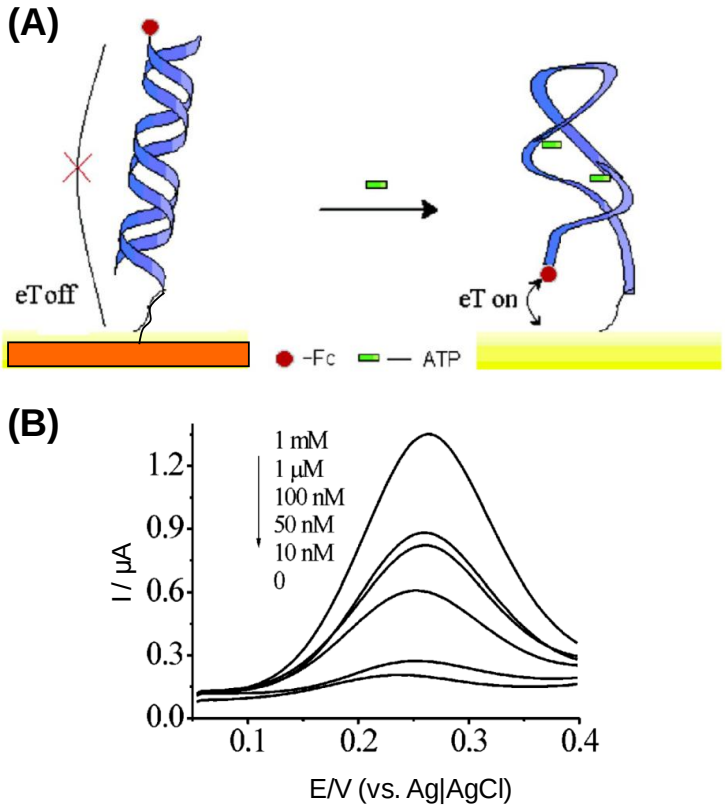

Figure 1-6. (a) Schematic representation of the TREAS (target-responsive electrochemical aptamer switch) strategy for ATP detection based on the alteration in the ferrocene electrochemistry. (b) Representative square-wave voltammograms for the duplex modified electrode after reaction with various concentrations of ATP, ranging from 10 nM to 1 mM, in 10 mM HEPES containing 50 mM $NaClO_4$. Adapted with permission from reference 29.

In 2008, Lu *et al.* demonstrated a new design of aptamer-based electrochemical sensors for thrombin, also based on the dissociation of complete DNA double helices.[30] As shown in Figure 1-7, they immobilized double-stranded constructs in which the aptameric strand was not labeled, but instead the complementary strand labeled with ferrocene at the distal end and thiol on the proximal end for self-assembly. In the presence of the analyte, the aptamer strand bound the analyte and dissociated from the

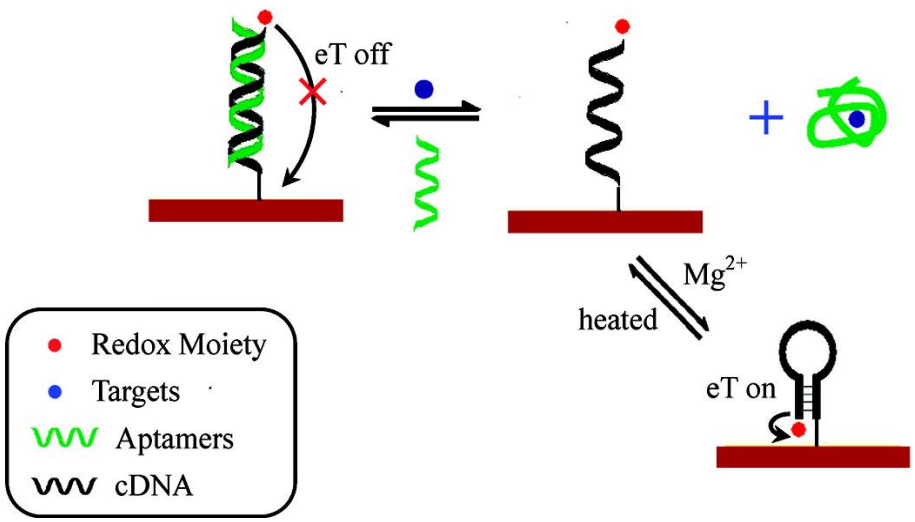

Figure 1-7. Schematic illustration of the strategy for an electrochemical "aptasensor" with aptamer-complementary DNA (cDNA) constructs as the probes; this is based on the formation of a hairpin structure of cDNA probes through the hybridization of the tailor-made complementary sequences at their both ends caused by the target binding-induced displacement of the aptamer strands. Adapted with permission from reference 30.

surface; the inherently designed sequence in the complementary strand then folded into a hairpin in the presence of Mg^{2+}, bringing the ferrocene closer to the electrode surface to promote the electron transfer in between. Lu *et al.* demonstrated the feasibility of this methodology for the detection of both adenosine and thrombin, with detection limits of 10 nM and 2 nM respectively. Later, Lu *et al.* reported a variation of this method, in which the aptamer strand was immobilized on the Au electrode and formed a double helix with a complementary strand labeled with ferrocene on its gold-proximal end.[31] In this case, efficient electron transfer between ferrocene and the electrode was observed prior to introduction of analyte into the system. Upon analyte binding (in this case, thrombin), the aptamer folded into the G-quartet structure and the complementary strand

was released, along with its tethered redox tag (ferrocene). A decrease in the electrical current was observed with increasing analyte concentration, with a detection limit of 2.5 nM. This sensor was also reusable, with regeneration following successive exposures to thrombin by repeating the on-chip hybridization of the ferrocene-labeled DNA strand (Figure 1-8).

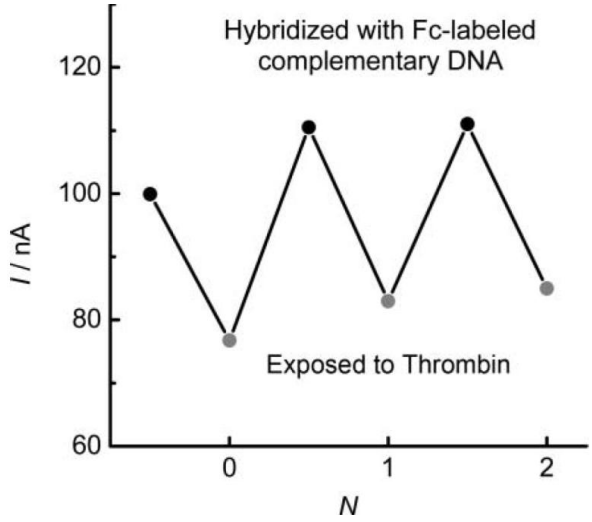

Figure 1-8. Typical profiles for the regeneration of the prepared electrochemical aptasensors first exposed to thrombin and then hybridized with the ferrocene (Fc)-labeled complementary DNA oligonucleotide. The concentration of thrombin was 100 nM. The concentration of the complementary DNA oligonucleotide used for the hybridization was 10 μM. *N* represents the number of sensor regeneration times. Reproduced with permission from reference 31.

Disassembly of a Preformed Aptamer-Analyte Construct

In a recent study by Hansen *et al.*, a dual-analyte biosensor was made by immobilizing two aptamers corresponding to two analytes onto a Au electrode.[32]

Proteins were then incubated in the system, each labeled with a different kind of quantum dot (Figure 1-9). Specifically, anti-lysozyme and anti-thrombin aptamers were immobilized, followed by incubation with CdS-modified thrombin molecules and PbS-modified lysozyme molecules. For the detection, the sensors were incubated with unlabeled analytes (thrombin and/or lysozyme); by displacement, the quantum dot-tagged proteins were released into the solution. Voltammetric measurements were then performed to assess the amount of quantum dots still retained on the surface by measuring the oxidation signal corresponding to the oxidation of Cd^{2+} and Pb^{2+} ions. Successive decreases in the signal (less material retained on the surface) corresponded to increasing concentrations of the analyte. A remarkable sensitivity was reported for this sensor design, with a detection limit of thrombin of 0.5 pM. The specificity for thrombin was confirmed as the sensor did not respond to unrelated proteins such as BSA and IgG. This protocol is promising for the simultaneous detection of multiple analytes for which aptamers have been selected. In principle, up to five or six proteins can be measured simultaneously based on the number of non-overlapping metal peaks in a defined voltage window.

1.2.1.2 Analyte-Induced Assembly of the Aptamer Construct

We now describe the other variation of configuration change-based electrochemical aptamer biosensors via an analyte-induced assembly scheme, in which the binding of the analyte to the (often immobilized) aptamer strand leads to the formation of the sensing construct. Aptamer-analyte-aptamer sandwich structures have epitomized this type of design in recent literature.[33–36] These aptamer sensing constructs often involve nanoparticle or enzyme-labeling to enhance the signal.

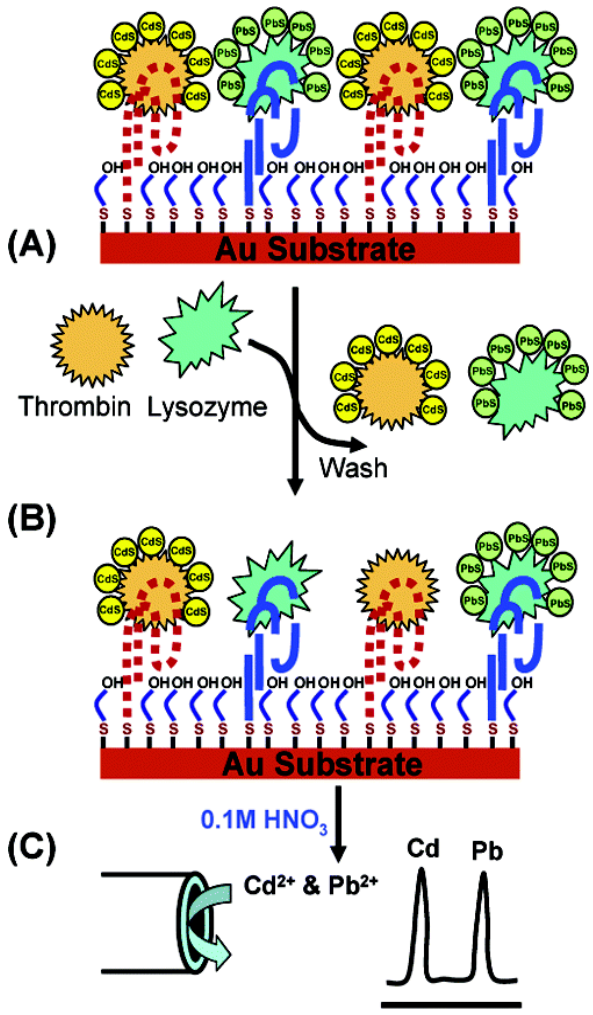

Figure 1-9. Operation of the aptamer/quantum-dot-based dual-analyte biosensor, involving displacement of the tagged proteins by the target analytes. (A) Mixed monolayer of thiolated aptamers on the gold substrate with the bound protein-QD conjugates; (B) sample addition and displacement of the tagged proteins; (C) dissolution of the remaining captured QDs followed by their electrochemical-stripping detection at a coated glassy carbon electrode. Reproduced with permission from reference 32.

Numnuam *et al.* performed aptamer-based potentiometric measurements of thrombin using ion-selective microelectrodes to measure levels of Cd^{2+} that corresponded to the concentration of thrombin (the analyte).[33] Anti-thrombin aptamers were first

immobilized on a Au electrode, followed by the incubation with thrombin (Figure 1-10). The authors took advantage of the fact that there are two aptamer-recognition sites on thrombin which interacts with the G-quadruplex forming aptamer selected by Bock *et al.*[37] A CdS-modified secondary aptamer was added to form an aptamer-thrombin-aptamer sandwich assay. Cd^{2+} from CdS-modified aptamers was then dissolved in aqueous H_2O_2 producing a dilute solution that was suitable for potentiometric measurements with a Cd^{2+} ion-selective microelectrode. The detection limit in a 200 μL reaction volume was 0.l4 nM, which is equivalent to 28 fmol of protein.

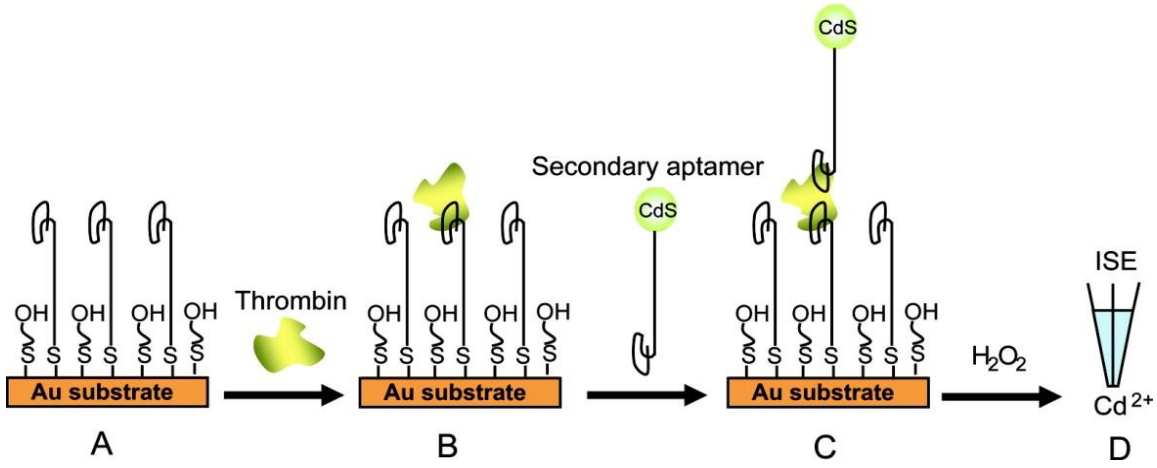

Figure 1-10. Representation of the analytical protocol of the aptamer-based potentiometric measurements of proteins using ion-selective microelectrodes. (A) Formation of a mixed monolayer of thiolated aptamers on gold substrate; (B) thrombin addition and binding with aptamers; (C) binding with CdS-labeled secondary aptamer; (D) dissolution of CdS labels followed by detection using a solid-contact Cd^{2+}-selective microelectrode. Reproduced with permission from reference 33.

In the study of Polsky *et al.*, nanoparticles were used not for direct measurements, but as catalysts for external electrochemical reactions.[34] Thiolated anti-thrombin aptamers were assembled on a Au electrode followed by incubation with thrombin-

containing samples (Figure 1-11). Secondary aptamer strands functionalized with Pt nanoparticles were then bound to form a sandwich structure. The resulting Pt-containing construct on the electrode surface then catalyzed the electrochemical reduction of H_2O_2 to H_2O, and the catalytic current was directly dependent on the concentration of thrombin in the analyte sample.

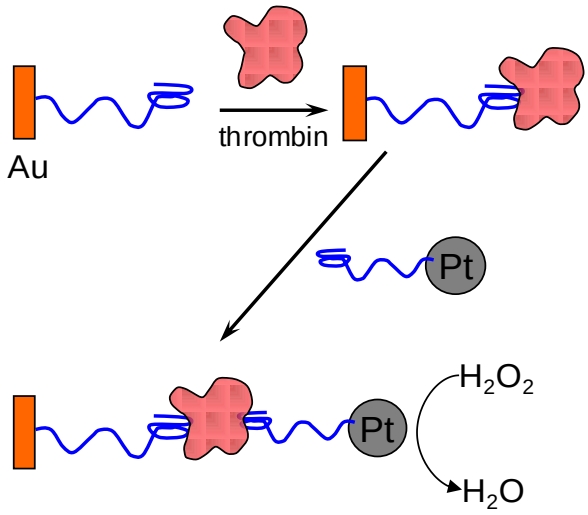

Figure 1-11. Schematic representation of the procedure for using Pt nanoparticles in the aptamer-based electrocatalytic detection of thrombin. Adapted with permission from reference 34.

Enzymatic assays were also developed in parallel with the aptamer-analyte-aptamer sensor design. Mir *et al.* developed a thrombin detection methodology in which anti-thrombin aptamers were first immobilized on a Au surface.[36] Upon binding thrombin, the sensor was incubated with a solution containing a secondary aptamer conjugated to HRP (horseradish peroxidase, which also catalyzed the reduction of H_2O_2 to H_2O). Ikebukuro *et al.* also devised a similar scheme,[36] with the secondary aptamer tethered with glucose oxidase, the enzyme used in the glucose sensor.

A recent report for Kang *et al.* showed the feasibility of using an antibody-analyte-aptamer sandwich as opposed to an aptamer-analyte-aptamer sandwich. This methodology was demonstrated for thrombin detection using methylene blue as the redox probes which intercalated to the "extended" double-helical protrusion from the G-quartet structure (the aptamer).[38]

1.2.2 Conformational Change

Probably one of the simplest types of aptamer-based biosensors is one that translates the analyte binding-induced conformational change (no release or attachment of DNA/RNA strands) directly into a measurable signal. Not only does this eliminate the necessity for multiple steps in the transduction event, it allows the production of simple biosensors that can easily repeat measurements (reusable). However, this type of aptamer-based biosensor only succeeds providing the aptamer undergoes a significant conformational change upon binding the analyte molecules (as discussed below). A plethora of literature can be found in this area of research, so much that the term "electronic aptamer-based sensors" or "E-AB sensors" is epitomized by these types of sensors.[39–42] We will briefly describe a few representative examples of such biosensors, with the redox markers covalently tethered, electrostatically associated, or freely diffused in solution.

1.2.2.1 Covalently-Tethered Redox Markers

In 2005, Plaxco, Heeger and coworkers described their first design of aptamer-based electrochemical biosensors, namely the electronic aptamer-based (E-AB) sensor, based on the alteration in the distance between a covalently-tethered redox marker on the aptamer strand and the Au electrode on which it is immobilized (Panel A of Figure 1-12). Their initial work was for the detection of thrombin,[39] and their E-AB sensor was constructed by covalently linking a methylene blue moiety to one end of the aptamer sequence, while the other end was modified with a thiol group for surface immobilization. In the absence of thrombin, the aptamer sequence remained unfolded – the randomized, unstructured aptamer thus had the flexibility to bring the methylene blue marker (at least transiently) close to the electrode surface, thus facilitating electron transfer between the methylene blue and the Au electrode. Upon binding thrombin, the aptamer folded into its inherent tertiary structure – namely the G-quadruplex[37] – thus relocating the redox marker away from the Au electrode. The electron transfer process was thus inhibited, and a decrease in the electrochemical current could be measured (Panel B of Figure 1-12). Regeneration of the original signal was possible with a wash using 6 M guanidine hydrochloride, making this type of biosensor reusable. The detection of thrombin in serum was also demonstrated, augmenting the possibility of the application of these E-AB sensors for clinical purposes.

A similar methodology was used by the same group for the detection of the BB variant of PDGF (platelet-derived growth factor) with a detection limit of 1 nM in undiluted serum and 50 pM in 50% serum.[38] This PDGF sensor design was different from the above thrombin counterpart in that sensing corresponded to a "signal-on"

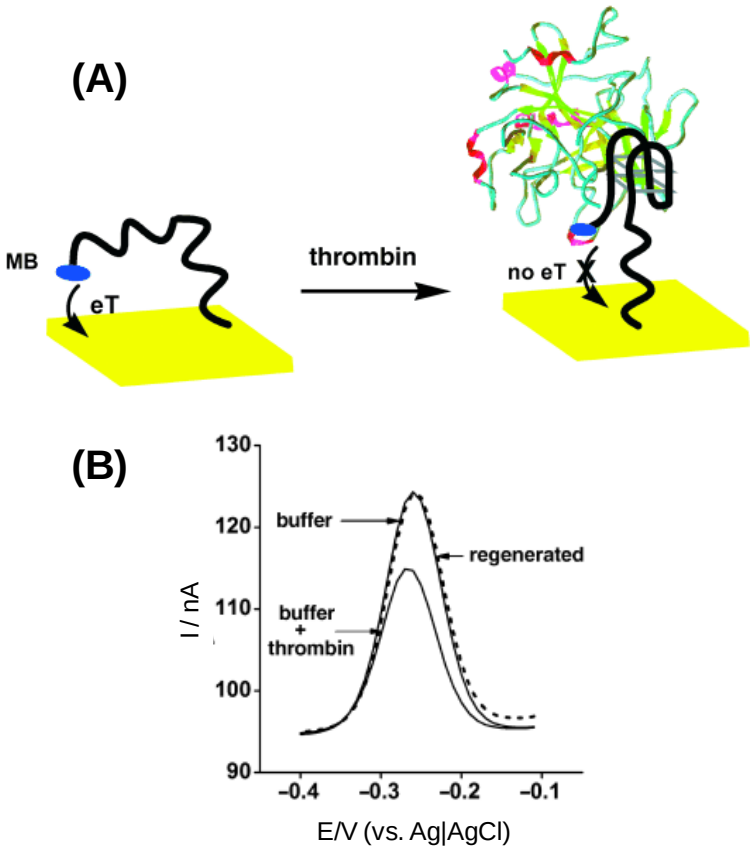

Figure 1-12. (a) A schematic view of the E-AB sensor based on the change in electron transfer efficiency of MB upon the binding of analyte to the aptamer. (b) The response of the E-AB sensor to 64 nM thrombin in buffered saline and its regeneration (by an eight-minute, room-temperature wash with 6 M guanidine hydrochloride). Adapted with permission from reference 39.

mechanism whereas in the thrombin study, it was "signal-off". These are due to subtleties in how the aptamer binds its analyte, particularly the induced changes in its conformation. A similar system was used for the detection of cocaine.[39] Efforts were also placed on the optimization of probe packing density and surface chemistry.[40] In 2008, Gothelf and coworkers designed their "E-AB" sensor for the detection theophylline

in serum with an RNA aptamer.[41] A 0.2 μM detection limit was reported based on a "signal-on" sensing scheme depicted in Figure 1-13.

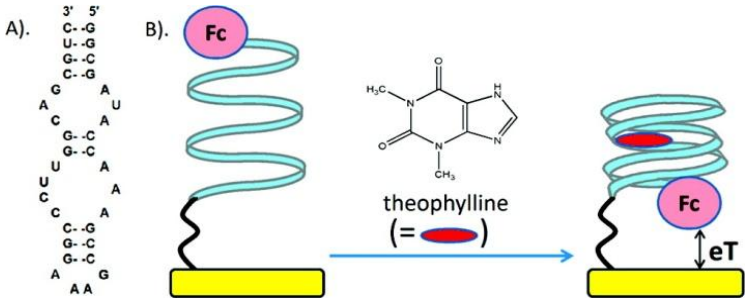

Figure 1-13. (A) Theophylline-binding RNA aptamer sequence and (B) schematic representation of the electrochemical RNA aptamer-based sensor for theophylline (Fc = ferrocene). Reproduced with permission from reference 43.

1.2.2.2 Solution-Diffused Redox Markers

One requirement for conformational change-based E-AB sensors described above is the covalent attachment of a redox marker to the aptamer strand. Yet, there are alternative ways to make conformational change-based aptamer biosensors "label-free" – that is, no covalent linkage of redox markers to the aptamer is necessary. The redox markers are either freely diffusing in solution, or are electrostatically associated with the surface-bound DNA strands.

In the former, electrochemical impedance spectroscopy was employed for studying recognition-induced switching of surface charge upon incubation with positively charged proteins.[44] In 2005, Rodriguez *et al.* developed a scheme that used an indium tin oxide (ITO) electrode covered with streptavidin to allow the conjugation of biotin-labeled

anti-lysozyme aptamers to the surface (Figure 1-14).[44] Before incubation with lysozyme, $[Fe(CN)_6]^{3-}$/$[Fe(CN)_6]^{4-}$ ions in solution could not physically get into close proximity with the electrode owing to electrostatic repulsion with the negatively-charged DNA phosphate backbone. A high electron transfer resistance was recorded. Lysozyme has a pI value > 7, which means that at physiological pH, the protein is positively charged. Upon incubation of the system with lysozyme, there is a nearly complete reversal of the surface charge due to the introduction of positive charges. For the $[Fe(CN)_6]^{3-}$/$[Fe(CN)_6]^{4-}$ ions in solution, their diffusion towards the ITO surface was facilitated and a decrease in the electron transfer resistance expected. The successive decreases in the electron transfer resistance were tabulated for increasing concentrations of lysozyme, and a detection limit of 0.2 μg/mL of lysozyme was reported.[44]

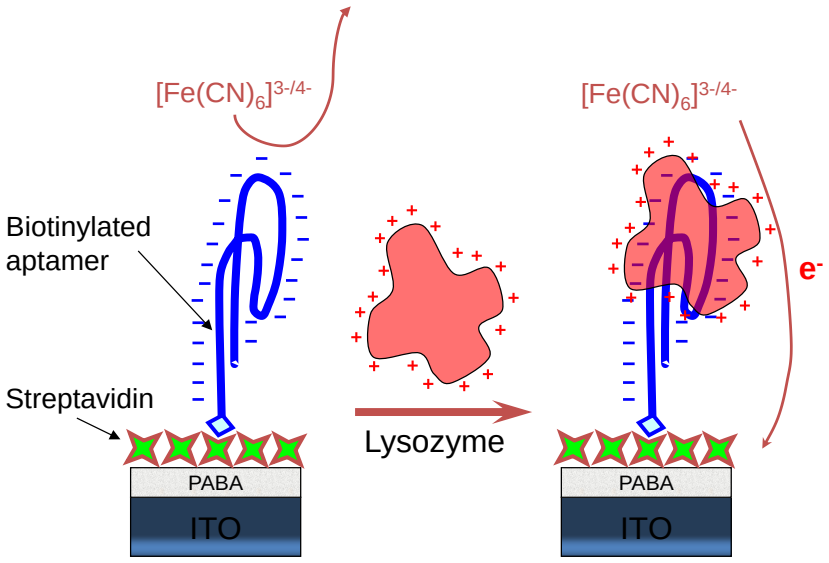

Figure 1-14. A schematic representation of an anti-lysozyme biosensor on an ITO (indium tin oxide) surface based on analyte-induced surface charge density changes with freely-diffusive redox markers. In the presence of lysozyme, a positively charged protein, electron transfer from solution-based $[Fe(CN)_6]^{3-/4-}$ is facilitated, resulting in a decrease in electron transfer resistance. Reproduced and modified with permission from reference 44.

A similar methodology was used for the detection of other proteins: Lee *et al.* used anti-thrombin aptamer-modified pyrolyzed carbon electrodes for the label-free detection of thrombin.[45] Thrombin has a pI value between 7.0 and 7.6, so detection carried at pH = 8.0 would render thrombin to be negatively charged. After incubation of the sensor with thrombin (> 0.5 nM), an increase in the electron transfer resistance of the $[Fe(CN)_6]^{3-}/[Fe(CN)_6]^{4-}$ redox couple at the carbon electrode was observed. The same group also demonstrated that the use of BSA (bovine serum albumin) and a non-ionic detergent (Triton X-100) helped prevent non-specific binding of the protein to the electrode surface.[45] A similar detection scheme for thrombin, but with ferrocene as the redox marker, was proposed by Cai *et al.*[46] This type of detection scheme was also performed with methylene blue as a diffusive redox label, in which the interaction of methylene blue with DNA may rely on the intercalation in between base pairs.[47–49]

1.2.2.3 Electrostatically-Bound Redox Markers

Our efforts[50] in the development of conformation sensors based on electrostatically-bound redox markers using lysozyme as model protein are provided in detail in Chapter 2 of this thesis.

1.2.3 Conductivity Change

The question of the inherent conductivity of the DNA double helix was and is still a debate to some extent since the discovery of its structure by Watson and Crick.[51] Typically, conductivity through base-pair stacks in the double helix has been studied through oxidative charge transfer, in which sequencing gel electrophoresis can be used to determine the pattern of guanine oxidation product formation (since guanine is the

nucleobase with the lowest oxidative potential) as a guanine radical cation (G+•) in double-helical DNA tethered to anthraquinone (AQ).[52–56] One requirement for efficient charge transfer to occur is that there should be substantial stacking of base pairs to allow for substantial π-orbital overlap between them. Sen and coworkers have developed aptamer-based biosensors based on the fact that the presence of an analyte will alter the conductivity of a DNA construct by promoting/disrupting base-stacking upon the occurrence of aptamer/analyte binding.[57,58] Two types of sensor designed were reported, namely the integrated-ligand sensor and the coupled-ligand sensor;[57] in both cases adenosine was used as a trial analyte. In the former, the presence of analyte resulted in stacking between two other previously separated double helical sections, leading to efficient charge transfer from an AQ end-tethered to one of the helices (the proximal helix) to the distal helix. The integrated-ligand sensor places the aptamer in the conduction path itself, while in the coupled-ligand sensor, the receptor (aptamer) is placed adjacent to an otherwise distorted conduction path (Panel A of Figure 1-15). The success of the concept of coupled-ligand sensors was also demonstrated with the detection of L-arginimide.[58]

It became interesting to consider whether it was possible to extend the idea of these "deoxyribosensors" to the world of electrochemical biosensors. Barton and coworkers showed that electrochemistry was suitable for sensing single-base pair mismatches in DNA double helices: by incorporating intercalating daunomycin molecules into a double-stranded DNA construct immobilized on a Au electrode, they observed that significant current was recorded for the reduction of daunomycin.[59] If the double-stranded DNA contained a CA mismatch, the daunomycin electrochemistry was

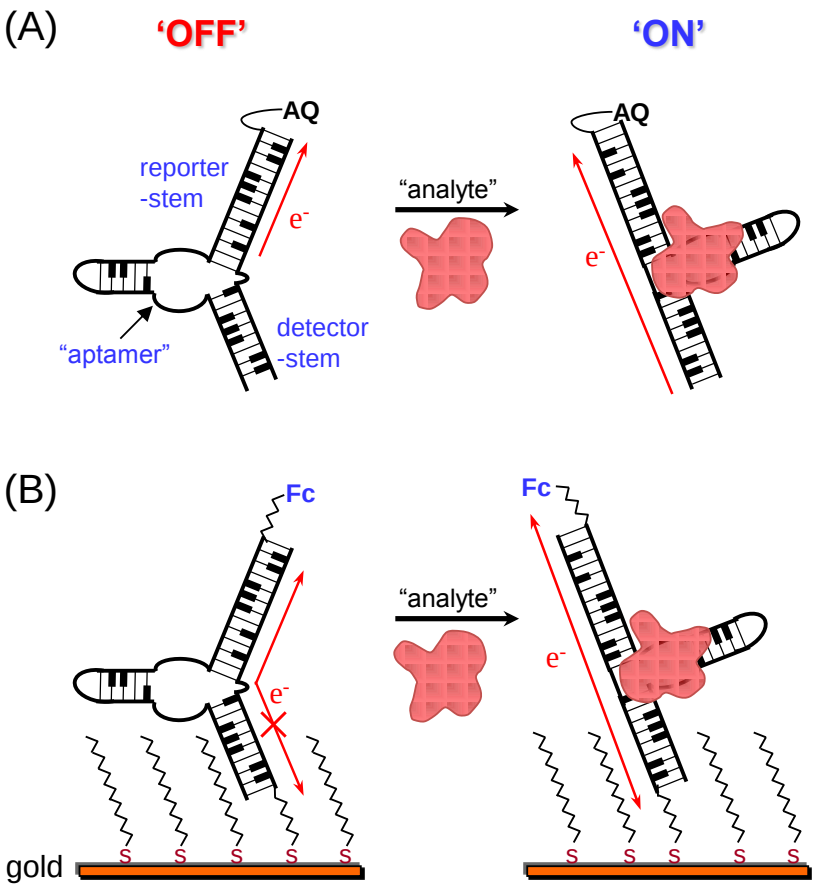

Figure 1-15. Design of DNA conformational switches as electronic sensors (deoxyribosensors) for specific detection of molecular analytes, and illustration of the conduction path change upon analyte binding. (a) Biochemical mode of ligand/analyte detection. (b) Modification and immobilization of the deoxyribosensor constructs onto a gold chip for direct electronic detection of analyte. Reproduced with permission from reference 59.

disrupted of optimal base stacking. Furthermore, it was shown by Wong and Gooding that perturbations of base stacking result in the decrease in the conductivity of DNA double helices. For instance, the incubation of the system with *cis*-platin, an anti-cancer agent that is known to cause perturbations in a double-helical structure,[60] will significantly affect the electrochemical response of the intercalated AQMS (anthraquinonemonosulfonic acid) moieties.

Huang *et al.* recently demonstrated the immobilization of "deoxyribosensors" on Au electrodes for the detection of plasma proteins, for which an DNA aptamer is available.[61] A coupled-ligand sensor was designed for electrochemical measurements for thrombin (Panel B of Figure 1-15). Where the DNA strand was originally modified with AQ in biochemical measurements, it was now modified with ferrocene as the redox marker. The other end of the construct was derivatized with a thiol moiety to allow for self-assembly on the Au surface. Upon the incubation with thrombin, notable increase in the current was recorded (Panel A of Figure 1-16), resulting from the rectified conduction path brought about by binding of thrombin to the adjacent receptor (aptamer loop). A dramatic improvement in the electrochemical sensitivity of this sensor was observed compared to its biochemical performance, i.e., a low-pM range thrombin could be detected (Panel B of Figure 1-16). At a concentration of thrombin near binding saturation, the same concentration of non-related proteins resulted in a negligible increase in the electrical current, suggesting that the sensor was highly specific for thrombin. Challenging the system with diluted serum still resulted in a quantitative response, which demonstrated the utility of such a sensor for biomedical or clinical purposes. Owing to the generic and modular nature of the design of deoxyribosensors (coupling a DNA conduction path and an aptamer loop) and the established surface chemistry used to construct the biochip that utilizes the deoxyribosensor, we envision that this methodology will be widely applicable to the development of rapid, DNA-based electronic sensors for any number of small and macromolecular analytes of biomedical and/or environmental importance.

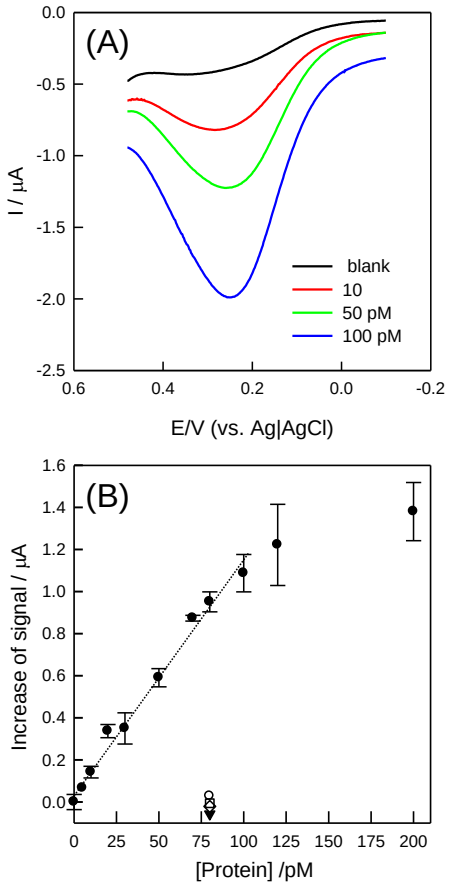

Figure 1-16. (a) Square wave voltammetry (SQW) responses of deoxyribosensor-modified electrodes in the presence of different concentrations of thrombin. The experiments were carried out in 50 mM Tris, pH 7.4 and 50 mM NaCl. (b) The increase in the reduction current is presented as a function of the thrombin concentration; the sensor response in the presence of 80 pM BSA (○), Avidin (□), IgA (◇) or IgG (▼) is also shown in this plot. Reproduced with permission from reference 61.

1.3 Conclusion and Future Outlooks

We summarize in this chapter three types of designs for the aptamer-based electrochemical biosensors published in the literature in the past few years. In comparison to aptamer-based optical sensors, electrochemical sensors offer many

advantages. One major advantage is the requirement of less sophisticated instrumentation and less power: this is an important factor for the design of portable, point-of-care (POC) diagnostic devices that may be suitable for use in the environment of the clinic. One major outlook for the use of aptamer-based electrochemical sensors is in the development of diagnostic tools for tumour markers in blood samples. For many types of carcinomas, substantial complications in both economic management and diagnostic procedures limit the overall efficiency and accuracy of early screening. Hence, the necessity arises for the development of portable, inexpensive, fast, and reliable technologies geared towards the specific early screening of cancers. While aptamer-based biosensor technology is still at a rather early stage compared to ELISA or antibody-based assays, we have summarized in this review that scientific development in this area is still ongoing and the repertoire of available DNA or RNA aptamers are also growing rapidly. We are convinced that the field of aptamer-based electrochemical sensors will grow even faster in the near future, and that these sensors will contribute to the advancement of analytical science as a whole, and, hopefully, benefit the health of individuals.

1.4 References

1. Cardosi, M. F.; Turner, A. P. F. The realization of electron transfer from biological molecules to electrodes. In *Biosensors: Fundamentals and Applications*; Turner, A. P. F.; Karube, I.; Wilson, G. S., Eds.; Oxford University Press: London and New York, 1990; pp. 257-275.
2. Blake, C.; Gould, B. J. *Analyst* **1984**, *109*, 533-547.
3. Ellington, A. D.; Szostak, J. W. *Nature* **1990**, *346*, 818-822.
4. Tuerk, C.; Gold, L. *Science* **1990**, *249*, 505-510.

5. O'Sullivan, C. K. *Anal. Bioanal. Chem.* **2002**, *372*, 44-48.

6. Liu, J.; Lu, Y. *Angew. Chem. Int. Ed.* **2006**, *45*, 90-94.

7. Nutiu, R.; Lu, Y. *Chem. Eur. J.* **2004**, *10*, 1868-1876.

8. Nutiu, R.; Lu, Y. *Methods* **2005**, *37*, 16-25.

9. Nutiu, R.; Lu, Y. *J. Am. Chem. Soc.* **2003**, *125*, 4771-4778.

10. Mok, W.; Li, Y. *Sensors* **2008**, *8*, 7050-7084.

11. Strehlitz, B.; Nikolaus, N.; Stoltenburg, R. *Sensors* **2008**, *8*, 4296-4307.

12. Song, S.; Wang, L.; Li, J.; Zhao, J; Fan, C. *TrAc, Trends Anal. Chem.* **2008**, *27*, 108-117.

13. de-los-Santos-Álvarez, N.; Lobo-Castañón, M. J.; Miranda-Ordieres, A. T.; Tuñón-Blanco, P. *TrAc, Trends Anal. Chem.* **2008**, *27*, 437-446.

14. Willner, I.; Zayats, M. *Angew. Chem. Int. Ed.* **2007**, *46*, 6408-6418.

15. Herne, T. M.; Tarlov, M. J. *J. Am. Chem. Soc.* **1997**, *119*, 8916-8920.

16. Steel, A. B.; Herne, T. M.; Tarlov, M. J. *Anal. Chem.* **1998**, *70*, 4670-4677.

17. Levicky, R.; Herne, T. M.; Tarlov, M. J.; Satija, S. K. *J. Am. Chem. Soc.* **1998**, *120*, 9787-9792.

18. Huizenga, D. E.; Szostak, J. W. *J. Am. Chem. Soc.* **1995**, *34*, 656-665.

19. Lin, C. H.; Patel, D. J. *Chem. Biol.* **1997**, *4*, 817-832.

20. Shen, L.; Chen, Z.; Li, Y.; Jing, P.; Xie, S.; He, S.; He, P.; Shao, Y. *Chem. Commun.* **2007**, 2169-2171.

21. Yu, H.-Z.; Luo, C. Y.; Sankar, C. G.; Sen, D. *Anal. Chem.* **2003**, *75*, 3902-3907.

22. Su, L.; Sankar, C. G.; Sen, D.; Yu, H.-Z. *Anal. Chem.* **2004**, *76*, 5953-5959.

23. Ge, B.; Huang, Y.-C.; Sen, D.; Yu, H.Z. *J. Electroanal. Chem.* **2007**, *602*, 156-162.

24. Zayats, M.; Huang, Y.; Gill, R.; Ma, C. *J. Am. Chem. Soc.* **2006**, *128*, 13666-13667.

25. Wu, Z.-S.; Guo, M.-M.; Zhang, S.-B.; Chen, C.-R.; Jiang, J.-H.; Shen, G.-L.; Yu, R.-Q. *Anal. Chem.* **2007**, *79*, 2933-2939.

26. Ihara, T.; Maruo, Y.; Takenaka, S.; Takagi, M. *Nucleic Acids Res.* **1996**, *24*, 4273-4280.

27. Li, B.; Du. Y.; Wei, H.; Song, S. *Chem. Commun.* **2007**, 3780-3782.

28. Xiao, Y.; Piorek, B. D.; Plaxco, K. W.; Heeger, A. J. *J. Am. Chem. Soc.* **2005**, *127*, 17990-17991.

29. Zuo, X.; Song, S; Zhang, J.; Pan, D.; Wang, L.; Fan, C. *J. Am. Chem. Soc.* **2007**, *129*, 1042-1043.

30. Lu, Y.; Li, X.; Zhang, L.; Yu, P.; Su, L.; Mao, L. *Anal. Chem.* **2008**, *80*, 1883-1890.

31. Lu, Y.; Zhu, N.; Yu, P.; Mao, L. *Analyst* **2008**, *133*, 1256-1260.

32. Hansen, J. A.; Wang, J.; Kawde, A.-N.; Xiang, Y.; Gothelf, K. V.; Collins, G. *J. Am. Chem. Soc.* **2006**, *128*, 2228-2229.

33. Numnuam, A.; Chumbimuni-Torres, K. Y.; Xiang, Y.; Bash, R.; Thavarungkul, P.; Kanatharana, P.; Pretsch, E.; Wang, J.; Bakker, E. *Anal. Chem.* **2008**, *80*, 707-712.

34. Polsky, R.; Gill, R.; Kaganovsky, L.; Willner, I. *Anal Chem.* **2006**, *78*, 2268-2271.

35. Mir, M.; Vreeke, M.; Katakis, I. *Electrochem. Commun.* **2006**, *8*, 505-511.

36. Ikebukuro, K.; Kiyohara, C.; Sode, K. *Biosens. Bioelectron.* **2005**, *20*, 2168-2172.

37. Bock, L. C.; Griffin, L. C.; Latham, J. A.; Vermaas, E. H.; Toole, J. J. *Nature* **1992**, *335*, 564-566.

38. Kang, Y.; Feng, K.-J.; Chen, J.-W.; Jiang, J.-H.; Shen, G. L.; Yu, R.-Q. *Bioelectrochem.* **2008**, *73*, 76-81.

39. Xiao, Y.; Lubin, A. A.; Heeger, A. J.; Plaxco, K. W. *Angew. Chem. Int. Ed.* **2005**, *44*, 5456-5459.

40. Lai, R. Y.; Plaxco, K. W.; Heeger, A. J. *Anal. Chem.* **2007**, *79*, 229-233.

41. Baker, B. R.; Lai, R. Y.; Wood, M. S.; Doctor, E. H.; Heeger, A. J.; Plaxco, K. W. *J. Am. Chem. Soc.* **2006**, *128*, 3138-3139.

42. White, R. J.; Phares, N.; Lubin, A. A.; Xiao, Y.; Plaxco, K. W. *Langmuir* **2008**, *24*, 10513-10518.

43. Ferapontova, E. E.; Olsen, E. M.; Gothelf, K. V. *J. Am. Chem. Soc.* **2008**, *130*, 4256-4258.

44. Rodriguez, M. C.; Kawde, A.-N.; Wang, J. *Chem. Commun.* **2005**, *4267-4269.*

45. Lee, J. A.; Hwang, S.; Kwak, J.; Park, S. I.; Lee, S. S.; Lee, K.-C. *Sens. Actuators, B* **2008**, *129*, 372-379.

46. Cai, H.; Lee, T. M.-H.; Hsing, I.-M. *Sens. Actuators, B* **2006**, *114*, 433-437.

47. Hianik, T.; Ostatná, V; Sonlajtnerova, M.; Grman, I. *Bioelectrochemistry* **2007**, *70*, 127-133.

48. Hianik, T.; Ostatná, V.; Zajacová, Z.; Stoikova, E.; Evtugyn, G. *Bioorg. Med. Chem. Lett.* **2005**, *15*, 281-295.

49. Evtugyn, G.; Porfireva, A.; Ryabova, M.; Hianik, T. *Electroanal.* **2008**, *21*, 2310-2316.

50. Cheng, A. K. H.; Ge, B.; Yu, H.-Z. *Anal. Chem.* **2007**, *79*, 5158-5164.

51. Watson, J. D.; Crick, F. H. C. *Nature* **1953**, *171*, 737-738.

52. Eley, D. D.; Spivey, D. I. *Trans. Faraday Soc.* **1962**, *58*, 411-415.

53. Turro, N.; Barton, J. K. *J. Biol. Inorg. Chem.* **1998**, *3*, 201-209.

54. Núñez, M.; Hall, D. B.; Barton, J. K. *Chem. Biol.* **1999**, *6*, 85-97.

55. Henderson, P. T.; Jones, D.; Hampikian, G.; Kan, Y.; Shuster, G. B. *Proc. Natl. Acad. Sci. USA* **1999**, *96*, 8353-8358.

56. Meggers, E.; Michel-Beyerle, M. E.; Giese, B. *J. Am. Chem. Soc.* **1998**, *120*, 12950-12955.

57. Fahlman, R. P.; Sen, D. *J. Am. Chem. Soc.* **2002**, *124*, 14610-14616.

58. Sankar, C. G.; Sen, D. *J. Mol. Biol.* **2004**, *340*, 459-467.

59. Kelley, S. O.; Jackson, N. M.; Hill, M. G.; Barton, J. K. *Angew. Chem. Int. Ed.* **1999**, *38*, 941-945.

60. Wong, E. L. S.; Gooding, J. J. *Anal. Chem.* **2006**, *78*, 2138-2144.

61. Huang, Y.-C.; Ge, B.; Sen, D.; Yu, H.-Z. *J. Am. Chem. Soc.* **2008**, *130*, 8023-8029.

CHAPTER 2

APTAMER-BASED BIOSENSORS FOR LABEL-FREE VOLTAMMETRIC DETECTION OF LYSOZYME*

This chapter reports a simple electrochemical approach for the detection of the ubiquitous protein lysozyme using aptamer-modified electrodes. Anti-lysozyme DNA aptamers were immobilized on gold surfaces by means of self-assembly, for which the surface density of aptamers was determined by cyclic voltammetric (CV) studies of redox cations (e.g., $[Ru(NH_3)_6]^{3+}$) bound to the surface via electrostatic interaction with the DNA phosphate backbone. Upon incubation of the electrode with a solution containing lysozyme, the CV response of surface-bound $[Ru(NH_3)_6]^{3+}$ changed substantially, and the relative decrease in the integrated charge of the reduction peak can be tabulated as a quantitative measure of the protein concentration. It is significant that the on-chip protein / aptamer binding constant and the optimized surface density to achieve the best detection limit can be evaluated. This biosensor is label-free, and offers an alternative, sensitive, and versatile method for protein detection, which is beneficial to the ever-growing interests of fabricating portable bioanalytical devices with electrical read-out protocols.

* Reproduced in part with permission from Cheng, A. K. H.; Ge, B.; Yu, H. Z. (2007) Label-free voltammetric detection of lysozyme with aptamer-modified gold electrodes. *Anal. Chem.* 79: 5158–5164.

2.1 Introduction

Lysozyme is a ubiquitous protein in mammals and is often termed "body's own antibiotic". *In vivo*, lysozyme catalyzes the hydrolysis of 1,4-beta-linkages in the peptidoglycan found in the cell wall of gram positive bacteria, thus serving as a natural "drug".[1] Its primary sequence contains 129 amino acids and it has a molecular weight of 14.4 kDa.[1c] It has an isoelectric point of 11.0 and constitutes 3.5% of egg white protein.[2] At neutral pH, lysozyme is positively-charged: only taking into account the charge distribution in amino acid side chains, the variant of lysozyme from hen egg white has 17 positive charges and 9 negative charges, resulting in a net +8 charge.[3] It is clear that lysozyme's relatively small size and simplicity makes it an excellent model analyte for novel methods in protein detection. It has been discovered recently that antibodies against citrullinated variants of lysozyme are present in patients with rheumatoid arthritis,[4] which highlights the potential of lysozyme as a clinical index of these diseases.

As mentioned in Chapter 1, biosensors are powerful analytical tools capable of detecting biological macromolecules using electrical or optical read-out protocols;[5–8] recently the type that has received much interest is aptamer-based sensors,[9–11] based on nucleic acid (both DNA and RNA) receptors that have been selected *in vitro* from large combinatorial pools to bind to specific target molecules such as proteins, organic dyes, or other nucleic acids.[12–13] The advantages of aptamers over antibodies (especially in the variation of elicitation of immunological response if used in an *in vivo* system[14]) have prompted us to develop an aptamer-based voltammetric detection method for ubiquitous glycanhydrolase lysozyme.

Previous research has shown considerably the potential applications of aptamer-based biosensors;[9–11,15] efforts have been placed toward lysozyme recently. The positive nature of lysozyme renders the protein favourable for specific binding on DNA aptamers and thus detectable in the proposed analytical method. Notable publications are from Ellington and co-workers[16–18] for the development of anti-lysozyme aptamers with dissociation constants (K_D) as low as 31 nM.[16,18] Kirby et al. have developed a reusable bead-based electronic tongue sensor array of anti-lysozyme aptamers for the detection of proteins, where fluorescent labeling is involved.[18] Recently, Rodriguez et al. have used the electrochemistry of solution-diffused $[Fe(CN)_6]^{3-}$ to explore an aptamer-based detection scheme.[19] In brief, biotinylated anti-lysozyme aptamers were immobilized on a surface containing streptavidin, exploiting the high affinity interaction between the two biologically relevant moieties for immobilization. Before lysozyme incubation, electron transfer rate of $[Fe(CN)_6]^{3-}$ to the surface was slow due to the electrically-repellent nature of the redox-species with the negatively-charged aptamer. Upon lysozyme incubation in varying concentrations, the less negative environment allows $[Fe(CN)_6]^{3-}$ to be less repelled, which facilitates electron transfer to the gold surface.[19]

Our protocol exploits the electrostatic interaction between redox-active cations (e.g., $[Ru(NH_3)_6]^{3+}$) and the negatively-charged phosphate backbone of DNA.[20–22] Upon saturation of the DNA-modified surface with $[Ru(NH_3)_6]^{3+}$ (based on the adsorption isotherm), one molecule of $[Ru(NH_3)_6]^{3+}$ compensates the charges from three phosphate residues at physiological pH, assuming that only electrostatic interactions are involved and mass-transport is not a limiting factor.[20-21] This approach allowed an easy and accurate determination of surface density of DNA strands,[20] and permitted us to directly

assess differences in the charge densities of aptamer-modified electrodes by monitoring the CV response of surface-bound $[Ru(NH_3)_6]^{3+}$, before and after lysozyme binding (Figure 2-1).

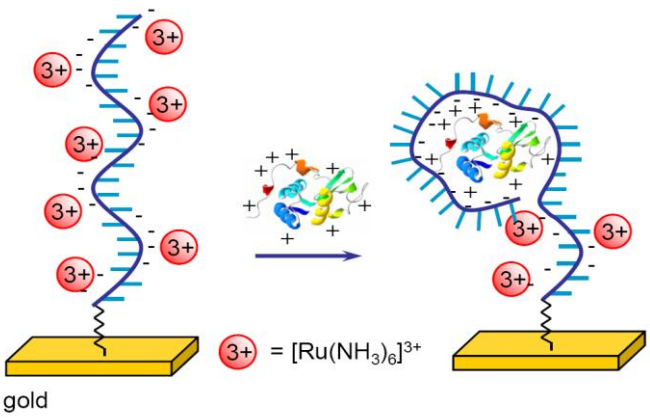

Figure 2-1. A schematic representation of the overall detection scheme of lysozyme with anti-lysozyme aptamers immobilized on gold electrodes via self-assembly. Binding of lysozyme to aptamer-modified surface reduces the electrostatic interaction between $[Ru(NH_3)_6]^{3+}$ and the DNA-modified surface, resulting in a decrease in the reduction peak in the cyclic voltammogram.

2.2 Results and Discussion

2.2.1 Detection of Lysozyme Using $[Fe(CN)_6]^{3-}$ as a Redox Marker in Solution

Figure 2-2 depicts representative cyclic voltammograms of 0.1 mM $[Fe(CN)_6]^{3-}$ on the aptamer-modified gold electrodes before and after incubation with 20 μg/mL lysozyme solution, and on a bare gold surface. Prior to lysozyme incubation, $[Fe(CN)_6]^{3-}$ can barely diffuse close to the DNA backbone due to electrostatic repulsion – thus, electron transfer from $[Fe(CN)_6]^{3-}$ to the aptamer-modified gold surface was severely blocked with respect to that from the redox anion to the bare gold surface (Figure 2-2).

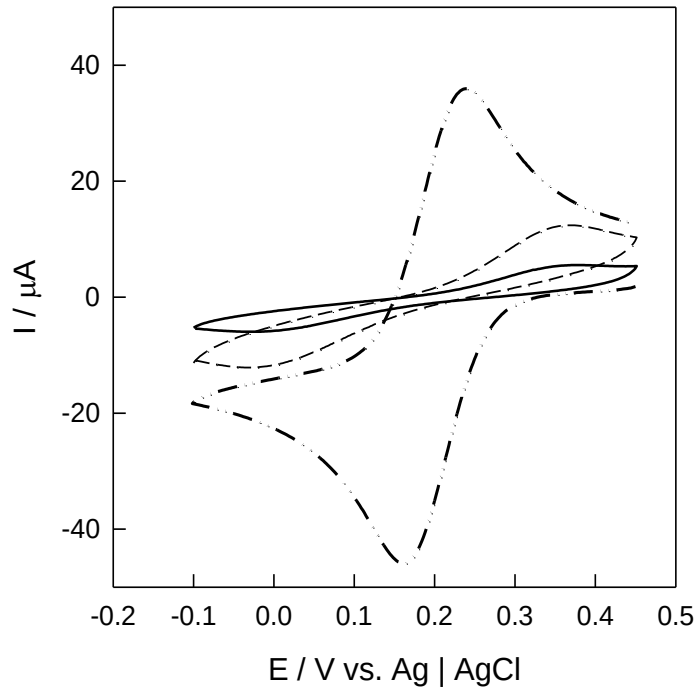

Figure 2-2. Cyclic voltammograms of 0.1 mM $[Fe(CN)_6]^{3-}$ on bare gold surface (dash and dotted line) and on aptamer-modified gold surface before (solid line) and after (dashed line) incubation with 20 μg/mL lysozyme in 20 mM Tris, 0.1 mM NaCl, 5 mM $MgCl_2$ at pH 7.4. The scan rate was 100 mV/s.

The formal potential (E°′) was determined to be 0.171 ± 0.003 V and the peak separation (ΔEp) 0.411 ± 0.004 V for $[Fe(CN)_6]^{3-}$ on the aptamer-modified surface (no lysozyme). Binding of lysozyme to the aptamer-modified gold electrode (with their inherently-designed abilities to bind in a 1:1 ratio[16]) should reduce the negative surface charge (contributed by the DNA backbone) since lysozyme has a net charge of +8. We believe that a complete reversal of surface charge (i.e., from negative to positive) may not be possible due to the length of the oligonucleotide (42-mer) in comparison with the number of positive charges of the protein. In other words, upon binding of lysozyme to the

aptamer-modified electrode, there is not enough positive charge from bound lysozyme to create excess positive charges on the surface. Nevertheless, there should be a substantial decrease in the overall density of negative charges on the surface. Therefore, upon lysozyme incubation, the positive charge of lysozyme serves to reduce the repulsion of $[Fe(CN)_6]^{3-}$ to the surface, promoting the interfacial electron transfer between the redox anions in solution and the electrode. This is reflected by a significant increase in redox current and a discernible decrease in peak separation ΔE_p (from 0.411 V to 0.404 V) upon binding of lysozyme (Figure 2-2).

The results obtained from our CV measurements are in good agreement with those described by Rodriguez et al., who also used $[Fe(CN)_6]^{3-}$ as a redox-active marker.[19] Difference in the two cases was demonstrated by measuring electron transfer resistance in the latter, which decreases upon the binding of lysozyme.[19] Our results showed that the method presented by Rodriguez et al. would also work on gold electrodes – not only will this prove the versatility of self-assembly of thiolated-aptamer sensors on gold, but also confirm the feasibility of simple voltammetric methods as analytical tools to study protein-aptamer interactions. However, we found that the reproducibility of this experiment was low, partially because the redox peaks of diffused species in solution we are looking for are not well defined as compared with those obtained on a bare gold electrode (Figure 2-2, dashed-dotted line); therefore, a quantitative detection of lysozyme may not be practical based on voltammetric responses of redox anions in solution.

2.2.2 Detection of Lysozyme Using $[Ru(NH_3)_6]^{3+}$ as a Redox Marker on Surface

The major drawback of the $[Fe(CN)_6]^{3-}$ experiment directed us to use a different redox system to study the binding process of lysozyme to aptamer-modified gold

electrodes. When the aptamer-modified surface was exposed to a solution containing $[Ru(NH_3)_6]^{3+}$, the redox cations bind electrostatically to the negatively charged phosphate backbone by replacing the native charge compensation ions (Na^+), and reach an ion exchange equilibrium.[20] In choosing a concentration of $[Ru(NH_3)_6]^{3+}$ for the CV measurements, caution was taken to not choose a concentration that was too high as this would result in the detection of solution $[Ru(NH_3)_6]^{3+}$ (which occurs at more negative reduction potentials). Our laboratory has previously experimentally determined, based on adsorption isotherms of $[Ru(NH_3)_6]^{3+}$, that 5.0 μM $[Ru(NH_3)_6]^{3+}$ is suitable for the experiments performed in the present study and will ensure saturation of the DNA-modified surface with the redox-active complex.[20] Before lysozyme binding, 5.0 μM $[Ru(NH_3)_6]Cl_3$ was incubated to allow binding to the aptamers via their negatively-charged phosphate backbones. The subsequent CV measurement allows an easy and straight-forward calculation of the surface density of the DNA strands on the surface with the charge integrated from the reduction peak from $[Ru(NH_3)_6]^{3+}$ to $[Ru(NH_3)_6]^{2+}$.[20]

The surface concentration of $[Ru(NH_3)_6]^{3+}$, Γ_{Ru}, can be calculated using Eq. (1)::

$$\Gamma_{Ru} = \frac{Q}{nFA} \qquad (1)$$

where Q is the charge obtained by integrating the reduction peak area of surface-bound $[Ru(NH_3)_6]^{3+}$, n is the number of electrons involved in the redox reaction, F is Faraday's constant, and A is the electrode area. This equation assumes the following: the interaction between $[Ru(NH_3)_6]^{3+}$ is *purely* electrostatic; there is complete exchange of $[Ru(NH_3)_6]^{3+}$ with compensation Na^+ ions; full saturation of the DNA-modified surface with $[Ru(NH_3)_6]^{3+}$ occurs at 5.0 μM; the cation exists and binds in the 3+ form [i.e., the cation

is (electro)chemically stable]; and every phosphate molecule is accessible for electrostatic binding with the cations.

Under saturation conditions (i.e., the highest possible concentration of surface bound $[Ru(NH_3)_6]^{3+}$ was achieved), the measured value can be converted to the surface density of DNA, Γ'_{DNA}, using the following equation:

$$\Gamma'_{DNA} = \Gamma_{Ru}(\frac{z}{m})N_A \qquad (2)$$

where *z* is the valence of the redox cation and *m* the number of nucleotides in the DNA. This equation has the same assumptions and conditions as Eq. (1).

Upon incubation in a solution containing lysozyme, there are significant changes in the exposed charged surface. Most notably, due to the positive nature of lysozyme, there is neutralization of the negatively-charged phosphate backbone as mentioned above, thus allowing $[Ru(NH_3)_6]^{3+}$ to bind where lysozyme does not. This results in a substantial decrease in the signal observed by CV measurements, which measures the redox behaviour exhibited by surface-bound $[Ru(NH_3)_6]^{3+}$. This decrease in CV response can be quantified using Eq. (1) with varying concentrations of lysozyme (all of which immobilized on surfaces with similar surface densities of aptamer) and thus the system can be used to quantify the amount of lysozyme in an unknown sample.

A well defined redox process of surface-bound cations can be observed, as shown in Figure 2-3, which depicts the CV responses of surface-bound $[Ru(NH_3)_6]^{3+}$ before and after incubation in 10 μg/mL lysozyme. The formal potential (E°′) was determined to be -0.249 ± 0.008 V and the peak separation (ΔEp) 0.037 ± 0.012 V. The quantity of

surface-bound cations (before adding lysozyme) can be determined by integration of the redox peaks, which can be used to determine the surface density of DNA on the surface as described above by Eqs. (1) and (2).

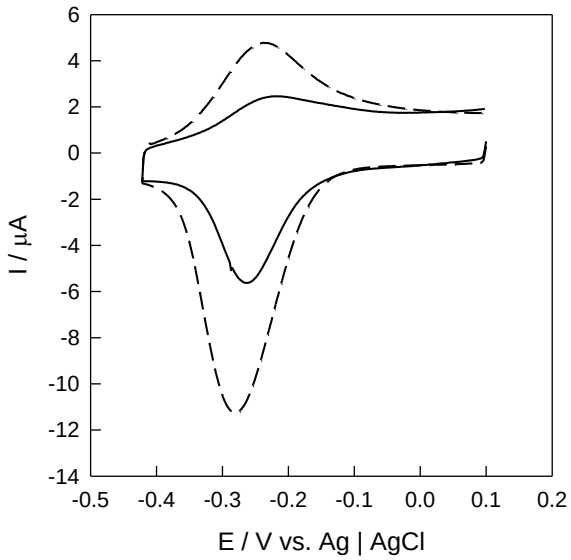

Figure 2-3. Cyclic voltammograms of 5.0 μM $[Ru(NH_3)_6]^{3+}$ on an aptamer-modified gold surface in 10 mM Tris buffer at pH 7.4 before (dashed line) and after (solid line) incubation with 10 μg/mL lysozyme. The scan rate was 500 mV/s.

Not only does a biosensor have to be sensitive to different **c**oncentrations of the analyte, it must also be specific. Experiments were thus conducted on another protein, cytochrome c, to serve as a control. Cytochrome c has very similar properties to lysozyme (it has an isoelectric point of approximately 11 and its size is 12 kDa);[24–25] thus, it serves as an excellent control to assess the specificity of aptamer-modified gold electrodes for the detection of lysozyme. As shown in Figure 2-4, incubation of the aptamer-modified gold electrodes with cytochrome c at a concentration of 10 μg/mL does

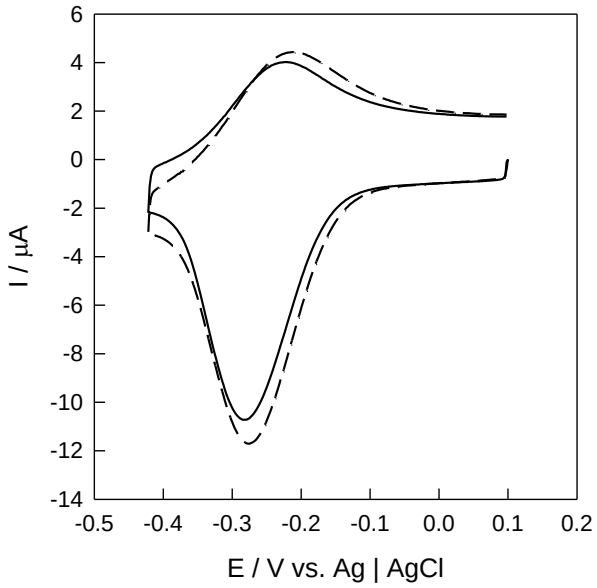

Figure 2-4. Cyclic voltammograms of 5.0 μM $[Ru(NH_3)_6]^{3+}$ on an aptamer-modified gold surface in 10 mM Tris buffer at pH 7.4 before (dashed line) and after (solid line) incubation with 10 μg/mL cytochrome c. The scan rate was 500 mV/s.

not produce any significant changes in the CV response as compared to the case of lysozyme (Figure 2-3). The apparent alteration in the reduction peak for surface-bound $[Ru(NH_3)_6]^{3+}$ in the presence of cytochrome c is merely a consequence of differences in background, shown by slight changes in the peak current (at -0.4 V) before and after protein incubation. Integration of the peak area before (2.5 μC) and after (2.4 μC) protein incubation gives the same charge within experimental uncertainty. These results indicate that cytochrome c does not bind to the anti-lysozyme aptamer-modified gold electrode in an aptamer-ligand fashion.

Another control has been performed by using a random sequence instead of anti-lysozyme aptamers immobilized on the gold surface. In contrast to anti-lysozyme

aptamer-modified electrodes, no significant change in $[Ru(NH_3)_6]^{3+}$ signal has been found upon the incubation of these gold electrodes in lysozyme under the same experimental conditions (data not shown). This once more confirms that the $[Ru(NH_3)_6]^{3+}$ system is applicable to sense the specific interaction between lysozyme and the anti-lysozyme aptamers immobilized on gold surfaces.

To prevent the potential influence of residual $[Ru(NH_3)_6]^{3+}$ on the surface, additional control experiments were performed to prove adequate removal of $[Ru(NH_3)_6]^{3+}$ prior to lysozyme exposure. Following the first exposure of the cell with $[Ru(NH_3)_6]^{3+}$, it was found that upon rinsing the cell with 10 mM Tris pH 7.4 then by small amounts of H_2O, followed by a CV measurement, the reduction peak observed for surface-bound $[Ru(NH_3)_6]^{3+}$ was in the order of 10^{-7} A (the same rinsing procedure was carried out for the actual experiments). The reduction peak observed for surface-bound $[Ru(NH_3)_6]^{3+}$ prior to the wash was in the order of 10^{-5} A. This 100-fold difference in current ensures that $[Ru(NH_3)_6]^{3+}$ cations are mostly removed prior to lysozyme exposure, and thus any influence of residual cations in the system will be negligible.

2.2.3 Quantitative Analysis of Lysozyme Using the $[Ru(NH_3)_6]^{3+}$ System

To quantitatively characterize the detection limit and response range of the lysozyme biosensor, we take the relative decrease in the integrated charge of the reduction peak (Figure 2-3). In particular, we show the dependence of the relative decrease in the charges obtained by integration of the reduction peak of $[Ru(NH_3)_6]^{3+}$ in the cyclic voltammograms before and after incubation with lysozyme, $\frac{\Delta Q}{Q_i} = \frac{(Q_i - Q)}{Q_i}$

(where Q_i and Q refer to the charges obtained before and after incubation respectively), with the concentration of lysozyme.

As shown in Figure 2-5 (one representative set of data), there is a rapid increase in the relative decrease in reduction signal as the concentration of lysozyme increases, where the error bar is an absolute value of uncertainty (standard deviation) in the charge from cyclic voltammetry determined from previous experimentation. The "dip" at 20 μg/mL may be due to this experimental uncertainty. In particular, the signal appears to saturate at 50 μg/mL lysozyme. An estimation of surface densities of lysozyme and the anti-lysozyme aptamer (with a DNA surface density of approximately 1.65×10^{12} molecules/cm^2) can easily justify this. It is important to note that we have consistently used the aforementioned aptamer surface density for all experiments conducted to determine the dependence of $\frac{\Delta Q}{Q_i}$ on the concentration of lysozyme. At a lysozyme concentration of 50 μg/mL and with an incubation volume of 20 μL, the number of lysozyme molecules in the cell is 4.16×10^{12}. However, a surface density of aptamer of approximately 1.65×10^{12} molecules/cm^2 immobilized on the electrodes gives a value of 1.09×10^{12} anti-lysozyme aptamers. Clearly, the number of molecules of lysozyme at a lysozyme concentration of 50 μg/mL exceeds the number of aptamer molecules available for binding by a factor of approximately 5. Thus, it would make sense that the ratio between the number of molecules of protein and the number of molecules of aptamer be 1:1 if the lysozyme concentration were 10 μg/mL. This optimized ratio indicates a very small dissociation constant of the aptamer-ligand complex. Figure 2-5 illustrates that as

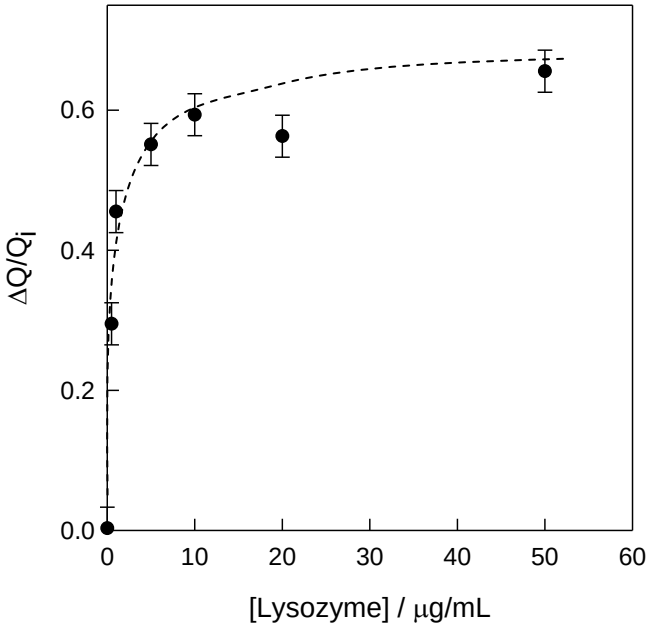

Figure 2-5. (A) Decrease in the integrated charge (reduction peak) as a function of concentration of lysozyme (experimental conditions as Figure 2-4). Aptamer-modified electrodes with surface density between $1.6 – 1.8 \times 10^{12}$ molecules/cm^2 were used. The dotted line serves to guide the eye.

the concentration increases from 10 μg/mL to higher concentrations, the signal no longer increases significantly. On the other hand, when the concentration of lysozyme was below 10 μg/mL, there is a steeper increase in the $\frac{\Delta Q}{Q_i}$ ratio, which signifies the sensitivity of this voltammetric method. In fact, the detection is shown to be sensitive to concentrations as low as 0.5 μg/mL, for which very reproducible changes in the CV response of surface bound $[Ru(NH_3)_6]^{3+}$ can be observed.

It is also important to note that at higher concentrations (e.g. 50-200 μg/mL), quantification of the reduction charge was not reproducible (data not shown), indicating

that the response mechanism likely becomes more complex (involving non-specific, electrostatic interactions between the positively charged protein and the anionic DNA backbone), and thus not suitable for practical applications. Nevertheless, we have shown experimentally that this aptamer-based biosensor is capable of detecting physiological concentrations (between 0.5 μg/mL to 50 μg/mL) of lysozyme in an analyte sample, which is comparable with that reported by Rodriguez et al.[19] (i.e., a well defined response for a 0.2 μg/mL protein solution can be obtained).

For a better understanding of the protein-aptamer interaction on surfaces, we further considered the adsorption isotherm of lysozyme binding to anti-lysozyme aptamers on gold electrodes. Based on the classical Langmuir model,[26] we assume that every binding site is equivalent and that the ability of the molecule to bind is independent on whether adjacent sites are occupied since DNA aptamer monolayers rarely form islands of very dense aggregates due to electrostatic repulsion of phosphate backbones (although slight alterations in the salt concentration in the immobilization buffer may render island formation). A linearized form of the adsorption isotherm is shown:

$$\frac{C}{\Delta Q / Q_{\mathrm{i}}} = \frac{C}{(\Delta Q / Q_{\mathrm{i}})_{\mathrm{sat}}} + \frac{K_D}{(\Delta Q / Q_{\mathrm{i}})_{\mathrm{sat}}} \qquad (3)$$

where C is the concentration of lysozyme in solution, $\frac{\Delta Q}{Q_i}$ is the sensor signal, $(\frac{\Delta Q}{Q_i})_{\mathrm{sat}}$ is the saturated sensor signal and K_D is the dissociation constant. Based on the linear fit in Figure 2-6, the K_D of the lysozyme-aptamer complex dissociating into free lysozyme in solution and aptamer strands on gold surfaces (with a DNA surface density between 1.6 – 1.8×10^{12} molecules/cm^2) is 610 ± 46 nM.

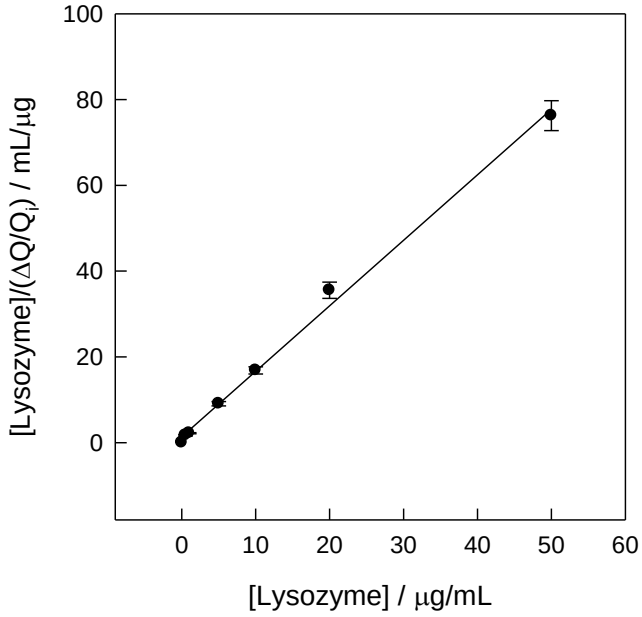

Figure 2-6. Linearized adsorption isotherm of lysozyme binding to anti-lysozyme aptamers on gold electrodes based on the Langmuir model. The line is the best linear fit to the experimental data (method of least-squares) from which the dissociation constant K_D was determined.

This larger dissociation constant compared to that obtained by Ellington and co-workers (31 nM)[16,18] may be understood as the differences between binding in solution and on surface. Firstly, binding on the surface may be hindered by the inability for all available aptamer molecules to fold into the correct secondary structure – this will render some of the aptamers on surface unavailable for binding to lysozyme. Secondly, binding of lysozyme to an aptamer should induce a change of the surface charges, which may interfere with the binding of another lysozyme molecule to an adjacent aptamer due to electrostatic repulsions. It is clear that these two factors would not impose any restrictions for lysozyme binding to anti-lysozyme aptamers in solution.

In comparison with measurements by Rodriguez et al.,[19] our work presents an alternative and simpler preparation and detection protocol for lysozyme. Our aptamers were immobilized on gold surfaces via self-assembly, a fast process that ensures a homogenous distribution of aptamer molecules on the surface. As mentioned earlier, the chance of aptamer island formation on gold is low. Rodriguez et al.[19], on the other hand, used an ITO (indium tin oxide) electrode by taking the advantage of the high affinity biological interaction between streptavidin and biotin to immobilize the anti-lysozyme aptamer on the surface. We note here that monolayers formed with such biological interactions also ensure adequate spacing between biotinylated aptamer molecules on the surface; we present our approach as merely an alternative method for the formation of aptamer-modified surfaces. This method is also advantageous over optical methods[18] in terms of sensor preparation as no fluorescent labeling of protein is necessary.

2.2.4 Effect of Surface density of Aptamer on Sensor Signal

It is possible that different surface densities may affect the kinetics and thermodynamics of binding of the analyte, most likely due to conformational effects. For example, on-chip DNA hybridization efficiency is significantly influenced by the probe strand density.[8,11] Thus, different gold electrodes modified with aptamers of different surface densities were prepared. This was achieved by allowing self-assembly in deposition solutions with a range of aptamer concentrations (0.5 – 5.0 μM). Other methods of modifying the surface density of aptamer molecules on a surface include varying immobilization time, treatment with MCH at high concentrations for different time periods, or varying the concentration of salt in **I-B**.

Figure 2-7 depicts a correlation between the sensor signal $\frac{\Delta Q}{Q_i}$ as a function of the surface density of the aptamers, Γ'_{DNA}, when the aptamer-modified electrodes were incubated with the same concentration of lysozyme (10 μg/mL). The error bars in both the sensor signal and the surface density (from charge determined by cyclic voltammetry) are the absolute values of the experimental uncertainty, or standard deviation, determined from previous experimentation. This plot allowed us to determine an optimal surface density for the experiments conducted previously. From the bell-shape plot, it is indicative that the sensor sensitivity is clearly dependent on the aptamer surface density: as the surface density increases, the $\frac{\Delta Q}{Q_i}$ ratio increases to a maximum, then decreases

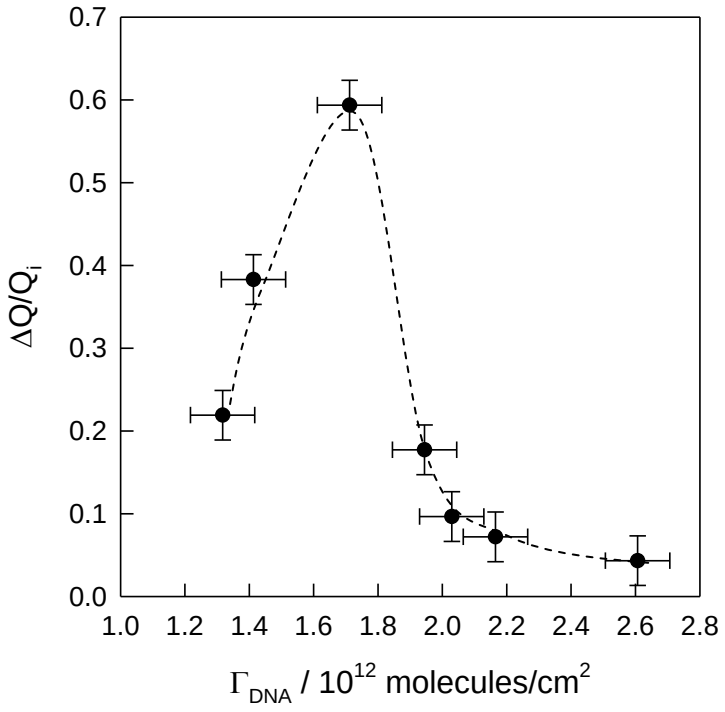

Figure 2-7. Sensor signal versus surface density of aptamers on gold electrode surface (experimental conditions as **Figure 2-5**). The dotted line serves to guide the eye.

substantially. We attribute the initial increase in the sensor signal to the difficulty to obtain well-defined CV curves of $[Ru(NH_3)_6]^{3+}$ for integration. Due to low molecular coverage of DNA on the surface, the contribution of redox signal of solution-diffused $[Ru(NH_3)_6]^{3+}$ is significant; it is difficult to accurately determine the surface density of $[Ru(NH_3)_6]^{3+}$ (i.e., electrostatically bound) from the very weak CV peaks. In comparison, the subsequent decrease in the sensor signal is more apparent, i.e., it is likely due to the steric / conformational effects as mentioned above. At higher surface densities, we believe binding of lysozyme to the aptamer is hindered due to spatial restriction for the DNA strand to fold into the aptamer configuration to bind to the fairly large lysozyme protein (4 nm in diameter). For lower surface densities, this is no longer a concern. Therefore, we believe that the ideal surface density for this aptamer sensor is between 1.6 – 1.8×10^{12} molecules/cm^2. In this case, there is the largest magnitude in the sensor signal ($\frac{\Delta Q}{Q_i}$), thus allowing easy quantification at various concentrations of lysozyme. Lower surface densities will result in interferences with solution $[Ru(NH_3)_6]^{3+}$, while higher surface densities would result in the steric restriction for the aptamer to fold correctly to bind lysozyme. It is important to note that these generalizations will have to be substantiated for other bio-recognition events, thus future experiments are warranted in this area.

2.3 Conclusion

The present study demonstrates that simple electrochemical methods are capable of monitoring the binding of a protein to an aptamer-modified surface. The binding event can be detected as a decrease in the integrated charge of the surface-bound $[Ru(NH_3)_6]^{3+}$

cations. The magnitude of decrease in the reduction signal of $[Ru(NH_3)_6]^{3+}$ on the surface can be used as a quantitative measure of the concentration of lysozyme in an analyte sample. The K_D of lysozyme-aptamer complex on the electrode surface was determined to be 610 ± 46 nM. A correlation between the sensor sensitivity and the aptamer surface density has also been evaluated, and the optimal surface density for the voltammetric sensing of lysozyme with aptamer-modified gold electrodes is $1.6 – 1.8 \times 10^{12}$ molecules/cm^2.

2.4 Experimental Section

2.4.1 Materials

The synthetic anti-lysozyme oligonucleotide (sequence designed by Ellington et al.[18]) HO-$(CH_2)_6$-S-S-$(CH_2)_6$-O-5′-ATC TAC GAA TTC ATC AGG GCT AAA GAG TGC AGA GTT ACT TAG-3′, control oligonucleotide HO-$(CH_2)_6$-S-S-$(CH_2)_6$-O-5′-ATC AAG GTG GGG GAT GGC TAA A-3′ and its complementary strand 5′-TTT AGC CAT CCC CCA CCT TGA T-3′ were purchased from Core DNA Services, Inc. (Calgary, AB). The 5′-thiol modifier was obtained from Glen Research (Sterling, VA). Gold substrates (regular glass slides first covered with 5-nm Cr, followed by 100-nm Au) were purchased from Evaporated Metal Films (EMF) Inc. (Ithaca, NY); and 6-mercapto-1-hexanol (MCH), hexaammine ruthenium (III) chloride (98%), potassium ferricyanide (98%), hen egg white lysozyme (95%), equine heart cytochrome c (95%) and Tween-20 from Sigma-Aldrich (Milwaukee, WI). Deionized water (> 18.3 Ω cm) was produced from a Barnstead EasyPure UV/UF compact water system (Dubuque, IA).

2.4.2 DNA Purification and Preparation

The disulfide-modified oligonucleotide was purified by reverse-phase HPLC on a Gemini 5-μm C18/110 Å column (Phenomenex, Torrance, CA), eluting with a gradient of 0.1 M triethylammonium acetate (TEAA) / CH_3CN (20:1) and CH_3CN at 1.0 mL/min. The sample was then treated with 10 mM TCEP (triscarboxyethylphosphine) in 100 mM Tris at pH 7.4 overnight and desalted through a MicroSpin G-50 column (G-50 Sephadex) to yield in single-stranded (ss) thiol-terminated DNA (e.g. HS-$(CH_2)_6$-O-5′ ATC TAC GAA TTC ATC AGG GCT AAA GAG TGC AGA GTT ACT TAG-3′). The purified anti-lysozyme aptamer was then heated to 80 ℃ and allowed to slowly cool to room temperature in Immobilization Buffer (**I-B**: 20 mM Tris-HCl / 0.1 M NaCl / 5 mM $MgCl_2$ at pH 7.41). This heating and cooling step is a necessary step (based on thermodynamics) to maintain the structural flexibility of the aptamers (for binding lysozyme).[19] The purified control oligonucleotide was hybridized with its complementary strand by heating and cooling in the same way.

2.4.3 Electrode/Substrate Preparation and Immobilization

The gold slides were cleaned by immersion in "piranha" solution (3:1 mixture of concentrated H_2SO_4 and 30% H_2O_2) for 5 minutes at 90 ℃, followed by a rinse with copious amounts of deionized water. *CAUTION: piranha reacts violently with organic solvents, and should be handled with extreme caution.* The gold chips were then dried with N_2. The thiol-terminated ssDNA strands were immobilized on the cleaned gold substrate by spreading a 20 μL droplet of aptamer in **I-B** for 12 hours at 100% humidity. After modification, the gold slides were rinsed with **I-B** again, followed by incubation for 1 hour in 1 mM MCH (in **I-B**) to remove non-specific DNA adsorption on the gold

surface. The gold slides were rinsed again with **I-B** then with deionized water, followed by drying with a stream of N_2 before electrochemical characterization.

The immobilization of aptamer strands on gold differs from our previous protocol,[20] for which we first immobilize dsDNA, followed by denaturing the non-thiolated strand. By control the concentration of thiolated ssDNA for self-assembly (from 0.5 to 5.0 μM), we hope to prepare a well-spaced monolayer of ssDNA that is capable of interacting with targets (e.g. lysozyme). Our rationale for this change is that we are immobilizing a monolayer of aptamer strands, not just merely a monolayer of ssDNA strands (no stable secondary structures anticipated). The anti-lysozyme aptamers need to fold to the correct secondary structure[19] (hence the heating and cooling step before immobilization), and dehybridization of a dsDNA monolayer cannot guarantee the aptamer molecules to fold correctly on the surface.

For the detection procedure, a 20 μL droplet of lysozyme of various concentrations in **I-B** were deposited onto the DNA-modified gold electrode and kept for 1 hour. This was followed by a 20-minute wash in Wash Buffer (**W-B**: 20 mM Tris-HCl / 0.1 M NaCl / 5 mM $MgCl_2$ / 1.0% (v/v) Tween-20 at pH 7.41) to remove non-specifically bound lysozyme. The sample was then rinsed in 10 mM Tris-HCl buffer at pH 7.41 before electrochemical characterization. A 1:1 lysozyme : aptamer complex was not formed prior to immobilization to optimize spacing for subsequent lysozyme interaction because it is likely unfavorable to immobilize this complex via the Au-S bond. Once the aptamer folds with lysozyme, the thiol moiety is possibly buried within the complex.

2.4.4 Electrochemical Measurements

CV measurements was performed with a μAutolab II potentiostat / galvanostat (EcoChemie B.V., Utrecht, Netherlands) using a single-compartment, three-electrode Teflon cell. The working electrodes, DNA-modified gold slides, were pressed against an O-ring seal at the cell bottom (with an exposed area of 0.66 cm^2). A Ag | AgCl | 3 M NaCl electrode was used as the reference, and a Pt wire as the counter electrode.

Electrochemical measurements of DNA-modified electrodes were performed in degassed 5 μM $[Ru(NH_3)_6]Cl_3$ in 10 mM Tris-HCl buffer at pH 7.41 (after incubation in the same solution for 15 min) and in 100 μM $K_3[Fe(CN)_6]$ in 20 mM Tris-HCl / 0.1 M NaCl / 5 mM $MgCl_2$ at pH 7.41, respectively.

2.5 References

1. (a) Vocadlo, D. J.; Davies, G. J.; Laine, R.; Withers, S. G. *Nature* **2001**, *412*, 835 – 838.; (b) Liu, J.; Lu, Y. *Anal. Chem.* **2004**, *76*, 1627 – 1632.; (c) Jollès, J.; Schoentgen, F.; Jollès, P.; Prager, E. M.; Wilson, A. C. *J. Mol. Evol.* **1976**, *8*, 59 – 78.
2. Hoober, K. L.; Sheasley, S. L.; Gilbert, H. F.; Thorpe, C. *J. Biol. Chem.* **1999**, *274*, 22147-22150.
3. Blake, C. C.; Koenig, D. F.; Mair, G. A.; North, A. C.; Phillips, D. C.; Sarma, V. R. *Nature* **1965**, *206*, 757 – 761.
4. Ireland, J.; Herzog, J.; Unanue, E. R. *J. Immunol.* **2006**, *177*, 1421 – 1425.
5. Kelley, S. O.; Jackson, N. M.; Hill, M. G.; Barton, J. K. *Angew. Chem Int. Ed.* **1999**, *38*, 941 – 943.

6. Kelley, S. O.; Barton, J. K.; Jackson, N. M.; Hill, M. G. *Bioconjugate Chem.* **1997**, *8*, 31 – 37.

7. Pang, D. W.; Abruňa, H. D. *Anal. Chem.* **1998**, *70*, 3162 – 3169.

8. Herne, T. M.; Tarlov, M. J. *J. Am. Chem. Soc.* **1997**, *119*, 8916 – 8920.

9. Nutiu, R.; Li, Y. *J. Am. Chem. Soc.* **2003**, *125*, 4771 – 4778.

10. Stojanovic, M. N.; Kolpashchikov, D. M. *J. Am. Chem. Soc.* **2004**, *126*, 9266 – 9270.

11. Fahlman, R. P.; Sen, D. *J. Am. Chem. Soc.* **2002**, *124*, 4610 – 4616.

12. Tuerk, G.; Gold, L.; *Science* **1990**, *249*, 505 – 510.

13. Ellington, A. D.; Szostak, J. W. *Nature* **1990**, *346*, 818 – 822.

14. O'Sullivan, C. K. *Anal. Bioanal. Chem.* **2002**, *372*, 44 – 48.

15. (a) Balamurugan S.; Obubuafo, A.; Soper, S. A.; McCarley, R. L.; Spivak, D. A. *Langmuir* **2006**, *22*, 6446 – 6453; (b) Savran, C.A.; Knudsen, S.M.; Ellington, A.D.; Manalis, S.R. *Anal. Chem.* **2004**, 76, 3194 – 3198.

16. Cox, J. C.; Ellington, A. D. *Bioorg. Med. Chem.* **2001**, *9*, 2525 – 2531.

17. Cox, J. C.; Hayhurst, A.; Hesselberth, J.; Bayer, T. S.; Georgiou, G.; Ellington, A. D. *Nucleic Acids Res.* **2002**, *30*, e108.

18. Kirby, R.; Cho, E. J.; Gehrke, B.; Bayer, T.; Park, Y. S.; Neikirk, D. P.; McDevitt, J. T.; Ellington A. D.; *Anal. Chem.* **2004**, *76*, 4066 – 4075.

19. Rodriguez, M.; Kawde, A-N.; Wang, J. *Chem. Commun.* **2005**, 4267 – 4269.

20. Yu, H.-Z.; Luo, C-Y; Sankar, C. G.; Sen, D. *Anal. Chem.* **2003**, *75*, 3902 – 3907.

21. Su, L.; Sankar, C. G.; Sen, D.; Yu, H.-Z. *Anal. Chem.* **2004**, *76*, 5953 – 5959.

22. Su, L.; Sen, D.; Yu, H.-Z. *Analyst* **2006**, *131*, 317 – 322.

23. Steel, A. B.; Herne, T. M.; Tarlov, M. J. *Anal. Chem.* **1998**, *70*, 4670 – 4677.

24. Margoliash, E.; Smith, E. L. *J. Biol. Chem.* **1962**, *237*, 2151 – 2160.

25. Margoliash, E.; Smith, E. L.; Kreil, G.; Tuppy, H. *Nature* **1961**, *192*, 1121 – 1127.

26. Steel, A. B.; Herne, T. M.; Tarlov, M. J. *Bioconjugate Chem.* **1999**, *10*, 419 – 423.

CHAPTER 3

APTAMER-BASED DETECTION OF EPITHELIAL TUMOUR MARKER MUCIN 1 WITH QUANTUM DOT-BASED FLUORESCENCE READOUT[*]

Mucin 1 (MUC1) is a glycoprotein expressed on most epithelial cell surfaces, which has been confirmed as one potentially useful biomarker for the diagnosis of early cancers. In this chapter, we report an aptamer-based, quantitative detection protocol for MUC1 using a 3-component DNA hybridization system with quantum dot (QD)-labeling: in the absence of MUC1 peptides, strong fluorescence is observed upon mixing the three specially designed DNA strands (quencher, QD-labeled reporter, and the MUC1 aptamer stem); in the presence of MUC1 peptides, a successive decrease in fluorescence intensity has been detected since the MUC1 peptide binds to the aptamer strand in such a way to allow the quencher and fluorescence reporter to be brought into close proximity (which leads to the occurrence of fluorescence resonance energy transfer, FRET, between the quencher and QD). The detection limit for MUC1 with this novel approach is in nanomolar (nM) level, and a linear response can be established for the approximate range found in blood serum. This study also provided further insight into the aptamer/analyte binding site/mode for MUC1, which augments the possibility to improve this detection methodology for early diagnostics of different epithelial cancers in large populations.

[*] Reproduced in part with permission from Cheng, A. K. H.; Su, H.; Wang, Y. A.; Yu, H. Z. (2009) Aptamer-based detection of epithelial tumor marker mucin 1 with quantum dot-based fluorescence readout. Anal. Chem. 81: In press.

3.1 Introduction

Mucins are cell-surface associated glycoproteins,[1] which are bound to cells by an integral transmembrane domain via the formation of a gel matrix.[2] The mucin 1 protein (MUC1) contains a hydrophobic membrane-spanning domain of 31 amino acids, a cytoplasmic domain of 69 amino acids,[1] and an extracellular domain consisting of a region of nearly identical repeats of 20 amino acids per repeat.[3] MUC1 has a protection function as its biological role by binding to pathogens[4] and possibly functions in a signal transduction pathway.[5] It is overexpressed in almost all human epithelial cell adenocarcinomas, including breast,[6,7] gastric,[8] colorectal,[9–11] lung,[12–14] prostate,[15] ovarian,[16,17] pancreatic,[18,19] and bladder carcinomas.[20,21] In addition, the expression of MUC1 in these adenocarcinomatous tissues lacks otherwise regular expression patterns, resulting in a ubiquitous, random expression of the protein all over the cell surface.[22] In many cases, the expression is increased so much that large amounts of the protein are found in serum,[23,24] which makes serum assays for MUC1 potentially useful for tumour detection.

The usefulness of MUC1 as a tumour marker has not been clinically overlooked, for which at least two assays using anti-MUC1 antibodies have been developed to monitor its concentration: the CA 15-3 assay and the CA 27.29 assay.[25–29] With the ultimate goal of developing practical and quantitative analytical tools for tumour markers, in this chapter we explore an aptamer-based detection methodology for MUC1. Aptamers are synthetic DNA or RNA molecules that have undergone rounds of *in vitro* selection to bind, with high affinity, to an analyte of choice.[30,31] As of today, many aptamers have been discovered that bind to proteins[32–36] and small molecules (such as organic dyes).[37,38]

Aptamers rival antibodies, the traditional recognition molecule, due to their ease of synthesis (*in vitro* rather than *in vivo*) and no need of elicitation of immunological response.[39] Recently, Ferreira *et al*. selected anti-MUC1 DNA aptamers that bind with high affinity to both a 9 amino acid immunogenic epitope of the 20 amino acid variable tandem repeat, and a 60 amino acid peptide corresponding to three copies of the 20 amino acid variable tandem repeat of MUC1.[40] The aptamer was characterized with competition ELISA. The group also demonstrated the application of using fluorescently-labeled aptamers to image MCF-7 breast cancer cells.[40]

The adaptation of aptamers for biosensing requires the transduction of the binding event to a measurable signal, either electrical or optical. The electrochemical detection of proteins or other biologically-relevant analytes through the measurement of electrical signals from redox markers covalently attached,[41–43] or electrostatically associated[4], with DNA (aptamer) strands immobilized on Au surfaces has been previously explored; for example, we have reported the aptamer-based voltammetric detection of the ubiquitous protein lysozyme (Chapter 2).[44] Optical signal transduction methods have relied on labeling with either gold nanoparticles (for which colourimetric differences are observed before and after analyte binding)[45] or organic dyes/quenchers (for which fluorescence resonance energy transfer (FRET) in between the two is expected).[46] In comparison, limited studies have been performed with aptamer-based detection with quantum dot-based fluorescence readout. Choi *et al.* used PbS QDs to specifically detect the protein thrombin; they attributed the decrease in fluorescence intensity to the charge transfer process (from the amine groups of the protein to the QD).[47] Korgel and co-workers conjugated prostate-specific membrane antigen (PSMA) aptamers to QD surfaces to

recognize and label prostate carcinoma cells.[48] More recently, Chen *et al.* used the anti-tenascin-C aptamer conjugated to QD surfaces to recognize human glioma cells.[49] Levy *et al.* reported an aptamer beacon-based detection scheme for the protein thrombin with quantum dot-based fluorescence readout, in which the detection limit was determined to be 1 μM.[50] In 2007, Bagalkot *et al.* also prepared QD-aptamer constructs that respond to the presence of prostate specific membrane antigen (PSMA); using a FRET system with intercalation of Dox (an antineoplastic anthracycline drug) on a double stranded region of the RNA aptamer, they developed an intricate system that could be used for cancer imaging, therapy and sensing of drug delivery.[51]

Compared to organic dyes, QDs typically have broader absorption spectra, narrower emission spectra, longer fluorescent lifetime, and better chemical-/photo-stability.[52] One of the most commonly used QD systems is CdSe/ZnS, in which an inner semiconductor CdSe core is coated with a ZnS shell. In this paper, we have designed a novel 3-component DNA system incorporating fluorescent QDs to selectively detect MUC1 peptides, a known tumour marker, at the nM level; component-deletion assays were performed to validate the sensor design.

3.2 Results and Discussion

3.2.1 Design and Preparation of the Sensor Constructs

The proposed sensor (Figure 3-1) is a 3-component DNA construct, where the hybridization events turn on or off, depending on the presence (or absence) of MUC1. We believe that in the absence of MUC1 (Figure 3-1(A), top), the MUC1 aptamer selected by Ferreira *et al.*[40] (the MUC1 S1.3 / MUC1 S2.2 sequence) folds into its

characteristic tertiary structure with a four base-pair stem and a loop formed by three consecutive thymine residues (on residue number 12–14 in the aptamer region, shown in blue) in the 5′ to 3′ direction. This has been further verified when we performed an *MFold bioinformatics* test, which predicts the secondary structure of DNA or RNA molecules under selected conditions. While RNA hairpin-loops are usually stable with the consensus sequences GNRA or UNCG in the loop region (where N = any base; R = any purine),[53] simple bioinformatics tests show that the formation of a three-thymine loop region is one of the most thermodynamically favorable structures under the given conditions for the anti-MUC1 DNA aptamer. In addition, there are other intermolecular interactions that we may be unaware of, e.g., ionic or other types of non-covalent interactions, which may stabilize the tertiary structure of the aptameric region, in addition to Watson-Crick base pairs. The immediate result upon the folding of the aptameric region (blue) is that the quantum dot-tethered strand, QD11F, which is covalently conjugated to a QD emitting at 530 nm, cannot Watson-Crick base-pair with the aptamer region, while the Iowa Black FQ quencher strand (Q13IB) that absorbs at 530 nm, is able to. We note that, in principle, multiple strands will be conjugated to the QD surface; here we show one for simplicity. Since the QD cannot get into close proximity with the Iowa Black FQ quencher, no FRET occurs, resulting in the observation of strong fluorescence. In the presence of MUC1 (Figure 3-1(A), bottom), we postulate that the binding of MUC1 to the aptameric region breaks the intramolecular Watson-Crick (and other) interactions to form the hairpin. This ultimately allows both QD11F and Q13IB to hybridize to the aptamer strand, hence bringing the quantum dot to close proximity with the Iowa Black quencher. FRET is allowed to occur, which quenches the fluorescence

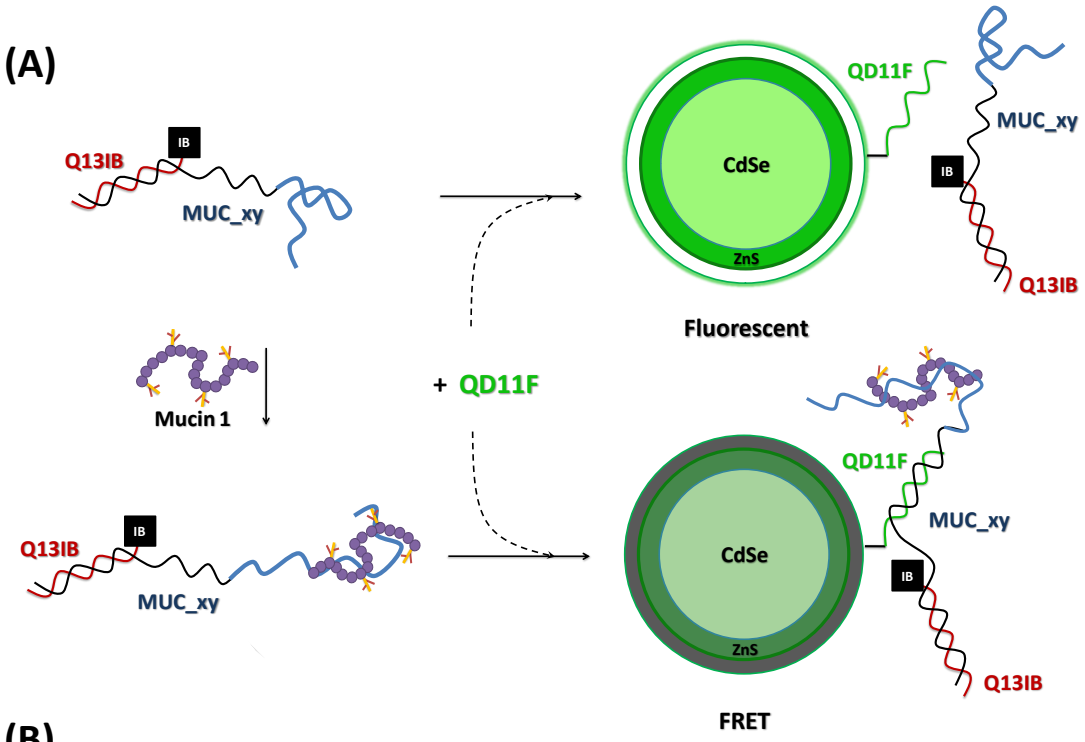

(B)

QD11F			5'-TCGATCCAGGG-3'
Q13IB	5'-CCATGTAGTAAGG-3'		
11F			5'-TCGATCCAGGG-3'
MUC1_45	3'-GGTACATCATTCC	*CA*	AGCTAGGTCCCATAGGTTTCCTAGTTGACG-5'
MUC1_47	3'-GGTACATCATTCC	*CATT*	AGCTAGGTCCCATAGGTTTCCTAGTTGACG-5'
MUC1_49	3'-GGTACATCATTCC	*CATTGT*	AGCTAGGTCCCATAGGTTTCCTAGTTGACG-5'
MUC1_49m	3'-GGTACATCATTCC	*CATTGT*	AGCTAGGTCCCATAGGTTTGGATGTTGACG-5'

Figure 3-1. *A schematic representation of the overall aptamer-based detection scheme of MUC1 peptides.* (A) In the absence of MUC1 peptides, the aptameric region (blue) will fold into its inherent secondary structure, which prevents the quantum dot-tethered DNA strand (QD11F, shown in green), to hybridize to MUC1_xy (black / blue). It should be noted that multiple strands may be conjugated to the QD surface; here we show one for simplicity. The hybridization of Q13IB (red), the quencher strand, to the aptamer strand (MUC1_xy) always happens. In the presence of MUC1 peptides, the aptameric region binds with the peptide, hence unfolding the aptameric region to a full single strand. This allows both QD11F and Q13IB to hybridize and FRET occurs, leading to a decrease in the fluorescence signal. (B) The sequences of the DNA strands used in the detection scheme are shown, with regions of intramolecular complimentary (in the absence of MUC1 peptides) denoted by underlining. We included the sequence of MUC1_49m which was used as a negative control.

emitted by the QD (upon excitation). In this case, successive decrease in fluorescence intensity is expected with increasing concentration of the MUC1 peptide. It is important to note that our detection scheme relies on the variation in the secondary structure of the aptamer strand upon analyte binding, which is inherent in the primary sequence. This is to say that, unlike previously studies,[54–56] the stem loop structure formed in the absence of analyte was not pre-engineered for the purpose of MUC1 detection.

Conjugation of the carboxy-terminated QDs to the amine-terminated DNA was done as per the procedure of Zhou *et al*.[57] with slight modifications. To verify successful coupling of the amine-terminated DNA to the QDs, a 3% agarose gel was prepared (Figure 3-2) which shows a retarded electrophoretic mobility of the QD-DNA conjugates compared to QDs alone. This can be explained by the increased formation of a highly convoluted and branched QD surface with multiple emanating DNA strands. Figure 3-2(A) shows a photograph of the ethidium bromide stained agarose gel upon illumination with a hand-held UV lamp. A 25 bp ladder was run for comparison purposes (Lane 1). The lane corresponding to QD alone (Lane 2) seems to exhibit two different mobilities (albeit pure): one that was not stained by ethidium bromide of lower mobility (green, as defined by the emission wavelength of the QD at 530 nm) and one that appeared to be non-specifically stained by ethidium bromide (through ionic interactions between positively-charged ethidium ions and negatively-charged quantum dot surfaces), which exhibited higher electrophoretic mobility (reddish-orange). To verify this, a second agarose gel was prepared without staining with ethidium bromide (Figure 3-2(B)). In this case, the band corresponding to ethidium-stained QD disappeared, which explains that the "unusual" mobility of pure QDs in Figure 3-2(A) is a result of non-specific ionic

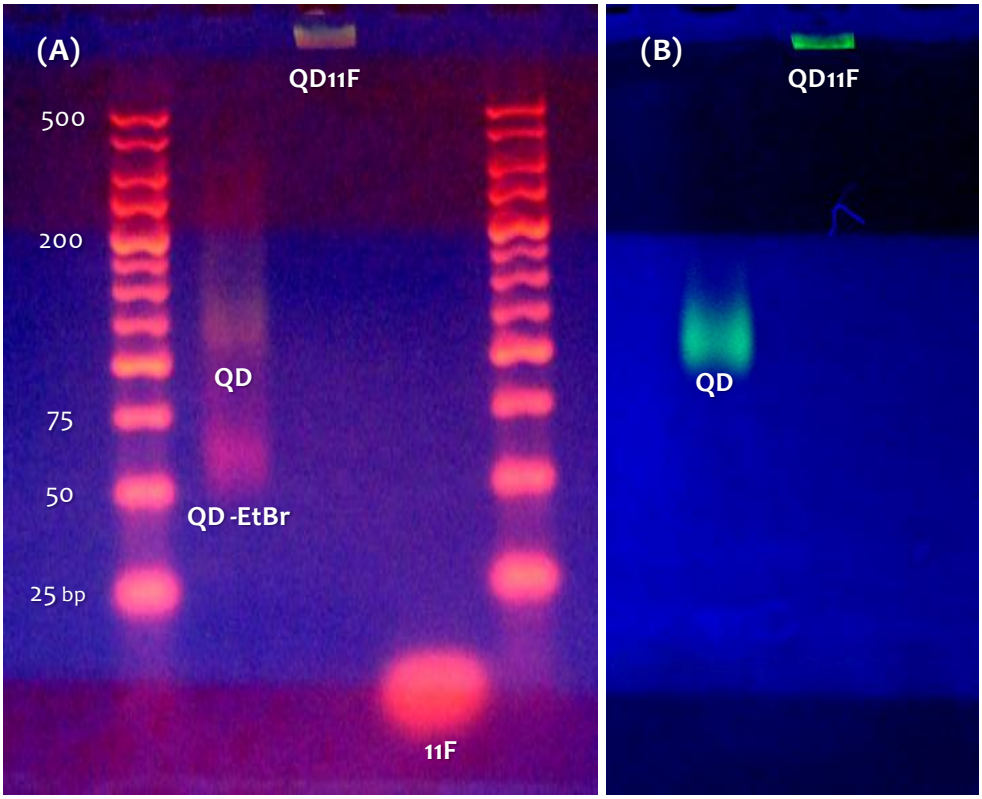

Figure 3-2. Verification of the amide coupling between the QD and 11F by observing a retarded mobility of QD-DNA versus QD alone in a 3% agarose gel with (A) and without (B) ethidium bromide staining. The optical images were taken under the irradiation with UV light.

interactions between ethidium cations and QD surfaces. In Lane 3 of Figure 3-2(A), the QD-DNA conjugates (QD11F) exhibited a very sluggish mobility. The differences in the mobility of QD versus QD-DNA indicate that the amide coupling chemistry was successful, i.e., amine-terminated DNA was indeed attached to the QD surface. We did not see a band of higher electrophoretic mobility corresponding to the uncoupled 11F DNA (control lane was ran in Lane 4), indicating that centrifugation is an effective

method for the purification of nanoparticles upon coupling with short DNA strands (see *Experimental Section*).

The mobility patterns of QD-DNA versus carboxy-terminated QDs are different from those reported previously by Chen *et al.*[49] In their work, an increased mobility of QD-DNA conjugates versus QDs alone was attributed to the increased charge-to-mass ratio upon conjugation to DNA. We attribute this discrepancy to the number of DNA molecules conjugated to the QD surface: in the work of Chen *et al.*, the DNA-to-QD ratio was 4:1; in our work the DNA-to-QD ratio was about 200:1, allowing for up to 50 times more DNA to be conjugated. We believe that the resulting conjugates are large and travel slowly through the 3% agarose matrix. However, the fact that we observe differences in mobility (with no remnants of the 11F strand and uncoupled QDs) suggest that the functionalization of DNA to QDs at high ratios was successful.

From the conjugation experiments, we estimate the coupling efficiency to be approximately 40% based on the amount of free 11F DNA measured in solution after the conjugation step (see *Experimental Section*). With an initial DNA:QD ratio of 200:1, approximately 80 11F strands were immobilized on each QD. We use this value as an initial guideline for the parameters used for FRET analysis.

3.2.2 Fluorescence Resonance Energy Transfer (FRET)

As part of the optimization process for the detection scheme, we seek to gain further insight on the basis by which FRET occurs between QDs and quenchers. FRET, in general, describes an energy transfer mechanism between two fluorophores (which serve as the donor and acceptor, respectively) that have substantial integral overlap in the

emission and absorption spectra. In the context of the present study, it does not refer to an energy transfer between two excitable fluorophores resulting in the observation of emission from the secondary one. We refer to the energy transfer from a QD to a quencher, which absorbs the energy emanated from the QD surface. One important factor in a thorough discussion of FRET is the Förster radius R_o, which is defined as the distance between the donor and acceptor for which the energy transfer efficiency is expected to be 50%.[58,59] Another important factor (E) is the energy transfer efficiency, which can be expressed in two ways (Eqs. 1 and 2), where I_{DA} and I_D are the donor fluorescence intensities with and without an acceptor, respectively, n_Q the number of quencher molecules (acceptor), and r the separation distance between the donor and acceptor:

$$E = 1 - \frac{I_{DA}}{I_D} \tag{1}$$

$$E = \frac{n_Q R_o^6}{n_Q R_o^6 + r^6} \tag{2}$$

All of these parameters can be measured or calculated trivially, except for the Förster radius:

$$R_o = 0.211 \, \mathrm{cm}^{1/2} \mathrm{M}^{1/6} \, [\kappa^2 n^4 Y J]^{1/6} \tag{3}$$

where κ is the orientation factor ($\kappa^2 = 2/3$ for random collisions), n the index of refraction ($n = 1.33$ in an aqueous medium), Y the quantum yield of the QDs (approximately 30%), and J the overlap integral, given by Eq. (4):

$$J = \frac{\int_0^\infty F_D(\lambda)\varepsilon_A(\lambda)\lambda^4 d\lambda}{\int_0^\infty F_D(\lambda)d\lambda} \qquad (4)$$

where F_D is the donor fluorescence intensity per unit wavelength interval, λ the wavelength, and ε_A the molar extinction coefficient of the acceptor. Typically J [M^{-1} cm^3] is computed on a program which overlays the normalized emission and absorption spectra of the donor and acceptor, respectively; for the 530 nm-emitting QDs and the Iowa Black FQ quencher, the value of J has been determined previously (and hence R_o) to be 2.62×10^{-13} M^{-1} cm^3 (R_o = 50.2 Å).[60]

According to Figure 3-1(A), we believe that the QD11F strand (containing the donor) and the Q13IB strand (containing the quencher) hybridize to an aptamer sequence to result in FRET. We started the optimization process by using three aptamer sequences, MUC1_45, MUC1_47 and MUC1_49 (sequences shown in Figure 3-1(B), along with the sequences of Q13IB, QD11F and 11F) with 2, 4, and 6 nucleotide gaps between the helices formed upon the hybridization of Q13IB and QD11F. We intended to check in which system do we obtain the highest efficiency of FRET upon the deliberate hybridization of the two solution-based strands (Q13IB and MUC1_xy) to QD11F by heating the samples to approximately 60 ℃ (a temperature that is not too high, in the hope of preserving the photostability in the QDs), followed by slowly cooling down the samples to room temperature. The initial hybridization experiment was performed with a 1:1:1 ratio of the three strands (addition of approximately 80 quencher and aptamer strands for each QD). We determine the efficiency of FRET by measuring the relative decrease in fluorescence intensity compared to a sample of QD11F alone (diluted to the

same concentration). For MUC1_45, which features a two-nucleotide gap between the IB helix (the double stranded region formed by hybridization of Q13IB) and the QD helix (the double stranded region formed by hybridization of QD11F), we observed a 5.2 ± 0.7% decrease in fluorescence; for MUC1_47, which features a 4-nucleotide gap between the IB helix and the QD helix, a 16.4 ± 1.2% decrease in fluorescence was recorded; for MUC1_49, which features a 6-nucleotide gap between the IB helix and the QD helix, the decrease in fluorescence was as high as 81.5 ± 2.6%. These remarkable differences indicated here merely show the effect of sterics: due to the size of the quantum dot (size of approximately 15 nm including inorganic core and organic polymer coating), hybridization is not possible if there is inadequate physical space for the hybridization. We have shown that a 6-nucleotide gap (approximately 0.33 nm × 6 = 1.98 nm) between the surface of the QD and the quencher can result in adequate FRET. Therefore, MUC1_49 was used in all subsequent experiments as the anti-MUC1 aptamer. Theoretically, the distance between the core of the QD to the quencher is more important. Based on the length of the flexible C6 linker on which the QD is tethered to the oligonucleotide and the radius of the nanoparticle, we estimate the separation distance to be approximately 8.3 nm. Given the Förster radius and this separation distance, we use Eqs. (1) and (2) to plot the relatively fluorescence intensity (from energy transfer efficiency) with the number of quencher molecules available in the system (solid line in Figure 3-3). A titration experiment was performed in which the QD11F conjugates were maintained at the same concentration and added with increasing concentrations (number of strands) of both Q13IB (quencher) and MUC1_49 (aptamer strand). The relative fluorescence intensity was recorded and the data are shown as filled circles on Figure 3-3.

It is clear that these data are consistent (within experimental uncertainty) with the theoretical prediction of the relative fluorescence intensity for the number of available strands of quencher oligonucleotides. It was determined that the addition of 80 quencher and aptamer strands per QD results in the highest decrease in fluorescence intensity (> 80%); we therefore continue further experiments with these optimized conditions using MUC1_49 as the "aptamer-containing platform" for the detection of MUC1.

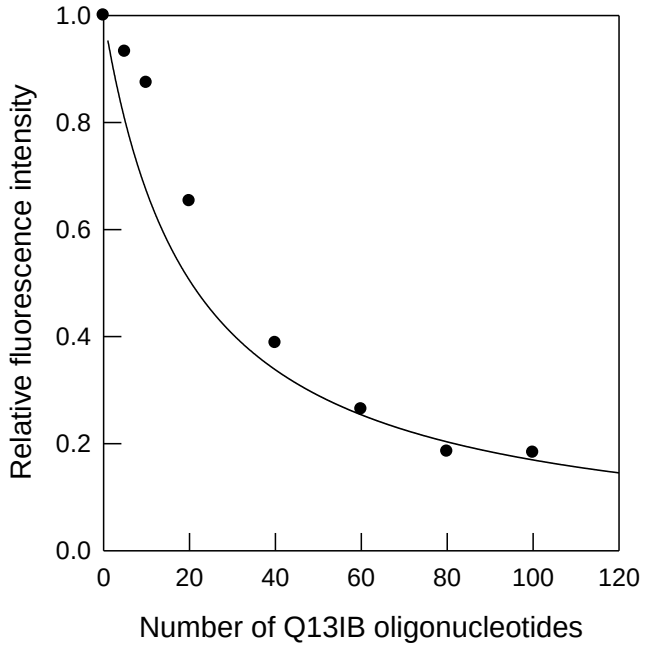

Figure 3-3. Decrease of the quantum dot (QD) fluorescence intensity upon increasing the number of Q13IB quencher strands based on theoretical estimation (solid line) and experimental titration data (filled circles).

3.2.3 Detection of MUC1 Based on the Decrease of Fluorescence Intensity

Briefly, the detection of MUC1 peptides occurred in two steps: MUC1 peptides were first incubated with the DNA aptamer MUC1_49 for 1 hour at room temperature to allow the equilibrium of the peptides binding to the aptamer. This was followed by the

addition of QD11F and Q13IB strands to the system; room temperature hybridization was allowed to occur for 30 min. Figure 3-4(A) depicts an optical image of two experimental samples, one without MUC1 and one with MUC1. These photos were taken using a digital camera, while exciting the QD with a hand-held ultraviolet lamp at 254 nm. As shown in Figure 3-4(A), the formation of the DNA sensing constructs occurred as expected (Figure 3-1). In the absence of MUC1 peptides, strong fluorescence is observed indicative of an inability for FRET to occur due to the fact that the QD11F strand cannot hybridize with MUC1_49. This is a direct consequence of the inherent folding of the aptamer sequence into its unique secondary structure, thus inhibiting the QD11F strand for hybridization. In other words, a folded secondary structure is thermodynamically more favourable than the hybridization of an 11-mer (QD11F). In the presence of MUC1 peptides (5.0 μM), a significant decrease in fluorescence intensity was observed as shown in Figure 3-4(A). We attribute this to the occurrence of FRET, in which case QD11F can hybridize to MUC1_49, thus bringing the quencher to close proximity with the QD. The binding of MUC1 to the aptamer breaks the Watson-Crick intramolecular interactions to form the hairpin, which effectively "straightens out" the aptamer strand, thus allowing QD11F to bind with a much higher efficiency. However, inarguably the system that we are studying is not simple, partially due to the heterogeneity of each individual QD. We use 5.0 μM as a "critical concentration" because it, in fact, is very similar to the critical concentration used in commercially available ELISA assays for CA15-3 (MP Biomedicals, Orangeburg, NY; Panomics Inc., Redwood City, CA), the antigenic region of the MUC1 protein for which tests are traditionally done for the diagnostics of breast cancer. It is generally accepted by vendors of CA15-3 ELISA kits that the cut-off value

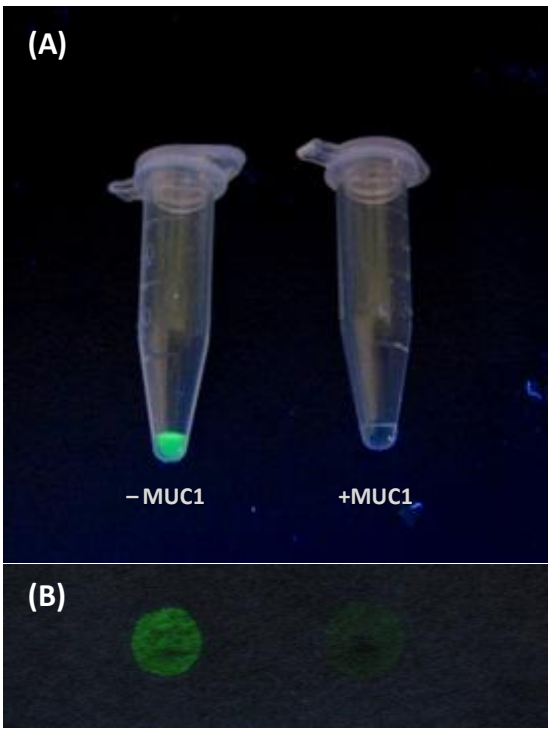

Figure 3-4. (A) Optical photos of two experimental samples with and without the presence of MUC1 peptides for the MUC1_49/QD11F/Q13IB construct. 5.0 μM MUC1 was used in this case; (B) 2 μL droplets of 5.0 μM MUC1 and a control sample deposited on filter paper. Both assays were checked under the irradiation of a handheld UV lamp.

of CA15-3 for normal healthy women is 35 U/mL. Using a purified breast tumour antigen stock of known units and the bicinchoninic acid (BCA) assay for protein concentration determination, we estimate that 1.0 μM of a 40 amino acid MUC1 peptide corresponds to approximately 6.3 U/mL of breast tumour antigen, from which CA 15-3 is derived. Therefore, 5.0 μM of MUC1 peptide corresponds to approximately 31.5 U/mL. The fact that we observe remarkable differences in fluorescence intensities between the experimental sample with or without MUC1 peptide at 5.0 μM (Figure 3-4(A)) highlights the aptitude of such a sensor for the immediate diagnostics of epithelial cancers by just

irradiating samples with a hand-held UV lamp. In Figure 3-4(B), we deposit 2 μL droplets of the same experimental samples (as used in Figure 3-4(A)) to a filter paper and show the feasibility of merely irradiating the sample with a hand-held UV lamp to distinguish between a blank and a solution containing 5.0 μM of MUC1 peptide (which is of approximate concentration to 35 U/mL of CA15-3). We demonstrate here the possibility of using this detection scheme/technique as a quick and easy assay for population screening. From the addition of MUC1 peptides for detection, followed by the addition of quencher and fluorescently (QD)-labeled strands, a total time of 90 min is used. In comparison to commercially available ELISA assays which take about 140 min, clearly we entitle advantages with the reported methodology in terms of timing and simplicity in sample handling.

We performed two simple experiments to initially verify the detection principle shown in Figure 3-1. In the first experiment, MUC1_49m was used rather than MUC1_49; MUC1_49m is a modified version of MUC1_49 with a mutation in the stem region of the stem-loop secondary structure of the aptamer region (blue), limiting the possibility of stem loop formation. The use of MUC1_49m resulted in the elimination of fluorescence either with or without MUC1 peptides due to FRET, which confirms the importance for the formation of the inherent stem loop structure of the aptamer stand. Another control experiment was performed with 598 nm-emitting QDs as opposed to 530 nm-emitting QDs; in this case FRET did not occur (due to insufficient spectral overlap) and thus the detection of MUC1 was not possible.

3.2.4 Verification of the Aptamer-Based Detection Scheme

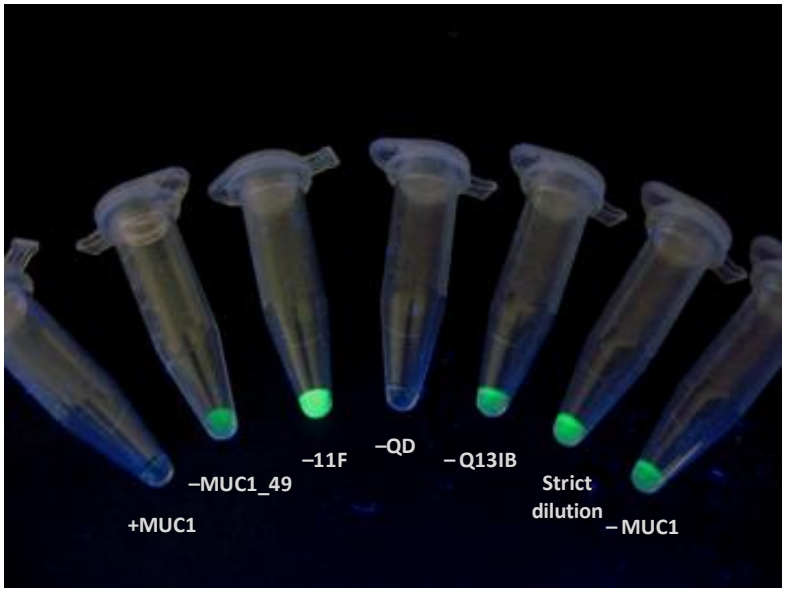

Figure 3-5. Optical photo of experimental controls to verify that FRET was the origin of the decreased fluorescence intensity. See text for details.

To verify that the detection occurred as predicted, a control experiment was performed in which various constituents of the system were removed systematically to examine the effect of that particular constituent on the sensor construct (Figure 3-5). The left- and right-most samples in Figure 3-5 are the same as those shown in Figure 3-4(A), which depicts the detection scheme (with all DNA constituents) with and without the presence of MUC1. As expected, there is decreased fluorescence intensity with the presence of MUC1. In the reaction sample labeled "strict dilution", the sample contains a water-diluted sample of the same concentration of the QD-DNA conjugate, but without the addition of any other strands. As expected, fluorescence is observed, and is very similar in intensity to that for the "-MUC1" sample. This shows that there is minimal

"background" signal in the absence of MUC1 peptides. All other reaction samples shown in Figure 3-5 contain 5.0 μM of MUC1. The reaction sample labeled "-Q13IB" lacks the Iowa Black quencher strand, which means that FRET should not occur since the energy acceptor is not present. This also proves that the decrease in intensity in the sample labeled "-MUC1" is due to FRET from the QD to the Iowa Black quencher. In the reaction sample labeled "-MUC1_49", no aptamer strand is present, which means that both Q13IB and QD11F do not have a "platform" strand for hybridization. The inability for these two strands to hybridize guarantees that no FRET can occur, which explains the observed fluorescence signal even with the presence of MUC1 peptides. The reaction sample labeled "-QD" features the full detection construct, but with the addition of 11F strands (i.e., the amine-terminated DNA) rather than QD conjugated amine-DNA (QD11F). Without the presence of quantum dots, no fluorescence should be observed, and thus the detection cannot be realized either. In the reaction sample labeled "-11F", the amine-DNA is not present, but the uncoupled carboxy-terminated QDs were added in the same concentration. Again no FRET was shown to occur, indicating that both quencher and fluorophore should be present and must be positioned in close proximity (with the aid of a hybridizing QD11F strand) to allow for FRET to occur. The above results confirm that the observed decrease in fluorescence intensity in the presence of MUC1 is ultimately due to FRET from the QD to the Iowa Black quencher, dissipating the observed fluorescence.

To further verify hybridized DNA constructs as the reason for FRET, we run a non-denaturing polyacrylamide gel to show the ability for Q13IB and 11F to hybridize to MUC1_49 with or without the presence of MUC1 peptides. For this control experiment,

we use the 11F strand (without QD) instead of QD11F. This is due to the fact that the QD11F strands that we produce are very heterogeneous in nature, in that individual QDs may have different numbers of 11F strands conjugated to them. To eliminate the possibility of seeing multiple native gel shifts as a result of hybridization of numerous QD structures (with different numbers of 11F strands conjugated to the QD) to MUC1_49, we use 11F instead, with a defined and regular structure and gel mobility. For the preparation of individual samples in each well of the gel, we follow the same two-step protocol, i.e., binding of MUC1 to aptamer, followed by addition of (QD)11F and Q13IB strands, but carry out the latter hybridization step at 4 ℃ as opposed to room temperature. Ultimately we hope to mimic the steric effects found in the QD system (thermodynamically making Watson-Crick hybridization of QD11F to MUC1_49 more difficult) by lowering the temperature which makes the same result if the platform MUC1_49 was folded into its inherent secondary structure. Figure 3-6 shows an optical image acquired by scanning a 15% non-denaturing polyacrylamide gel stained with "Stains All". In the lanes labeled "MUC1_49", we have the MUC1_49 strand only, and with the lane labeled "MUC1_49 + MUC1" we load the mixture of MUC1_49 and 5 μM MUC1 after being allowed to react. In principle, we should observe a gel shift, with "MUC1_49 + MUC1" having a lower mobility, which did not occur in the current system. In the absence of MUC1, the aptamer folds to form a 4 base pair hairpin (as shown in Figure 3-1(A)). In the presence of MUC1 we expect the aptamer strand to be lengthened and thus should exhibit a slightly higher electrophoretic mobility. However, the binding of the MUC1 peptide (with a molecular weight of 3775 g/mol – similar to that of a double stranded 5-mer) decreases the mobility of MUC1_49 slightly. We believe that

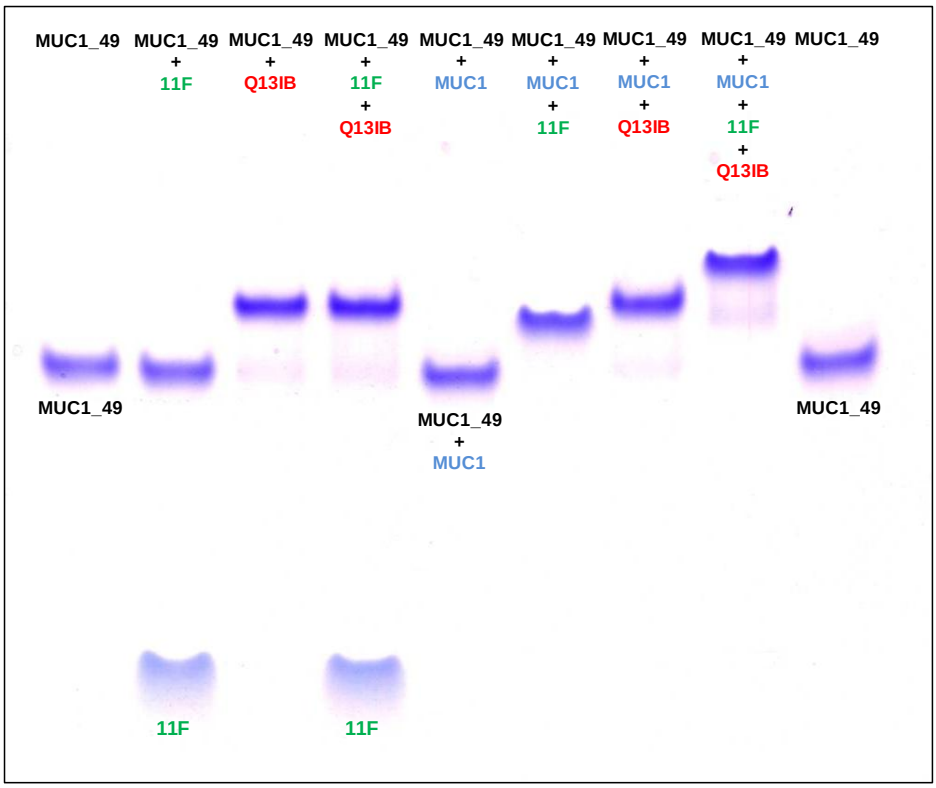

Figure 3-6. A digital scan of a 15% non-denaturing polyacrylamide gel stained with "Stains All". The hybridization of Q13IB to MUC_49 is independent of the presence of MUC1. 11F, on the other hand, can only hybridize to MUC1_49 in the presence of MUC1, thus providing direct support for the proposed detection scheme.

such an effect compensates for the changes in mobility due to differences in the folding structures in MUC1_49.

Figure 3-6 also indicates that the ability of Q13IB to hybridize to MUC1_49 is independent of the presence of MUC1; this is an interpretation from the gel shift upon hybridization of Q13IB to both the MUC1_49 alone or MUC1_49 with the presence of 5 μM MUC1 peptide. However, the hybridization of 11F to MUC1_49 is only successful in the presence of MUC1 peptides. In the absence of MUC1, we did not observe a gel shift

but rather an additional band of higher mobility corresponding to 11F as a single strand. In the presence of MUC1, a clear gel shift was observed without any residual 11F strands. These results indicate that the system functions as predicted from Figure 3-1. We further evaluate the ability for both Q13IB and 11F to hybridize together to MUC1_49 with or without MUC1 peptides. We have shown that both Q13IB and 11F can hybridize successfully to MUC1_49 in the presence of MUC1; however, in the absence of MUC1 only Q13IB hybridizes with the MUC1_49 strand.

It is evident that the binding mode of MUC1 peptides to anti-MUC1 aptamers is different from that of many other aptamers. In many cases such as the anti-thrombin aptamer,[36] the anti-PDGF (platelet-derived growth factor) aptamer,[35] the anti-cocaine aptamer,[34] or the anti-adenosine aptamer,[32] the DNA strand is initially in a random conformation but stabilizes with a defined secondary/tertiary structure upon binding with the analyte. A result of this type of conformational change was a plethora of literature studies on the design of "signal-on" electrochemical[41–43] or nanoparticle-based[45] biosensors for these molecules. Li and coworkers pioneered the design of systematic structure-switching aptamers, also based on a 3-component DNA hybridization system with organic fluorophores and quenchers.[46] Using adenosine and thrombin as model analytes, they demonstrated the production of signal-on devices upon analyte binding to the aptamer, which is accompanied by the release of a previously-hybridized quencher-strand involved in FRET with a fluorescently-labeled strand. The detection approach that we present herein demonstrates the other "end of the spectrum" in which the analyte-binding induced conformational change of the aptamer allows for the QD strand to bind in the presence of the analyte. We note several potential advantages of our design: firstly,

QDs were used instead of organic fluorophores, which exhibit superior photostability with higher fluorescence intensities; secondly, we demonstrate a system where diagnostics can be done without the use of complex instrumentation (*e.g.*, fluorospectrometer), since dichotomous answers ("yes" or "no") can be obtained by simply shining the samples with handheld UV lamp; thirdly, our method has the aptitude to extend to the simultaneous detection of multiple analytes, for which multiple aptamers are conjugated to QDs of different sizes (and hence emission wavelengths), which can be excited at the same UV wavelength.

3.2.5 Detection Limit and Dynamic Range

We established and proved the applicability of this aptamer-based tumour marker detection methodology as a direct "yes or no" screening assay by distinguishing the solution and filter paper-based samples under the irradiation of a handheld UV lamp. While dichotomous detection would have good applicability for qualitative analysis, it is also important to establish a quantitative protocol for more precise measurements. Figure 3-7 depicts the overlay of 5 representative fluorescence spectra (excited at 254 nm), with different concentrations of MUC1. It is clear that there is a sequential decrease in the fluorescence intensity upon increasing the concentration of MUC1 peptides. Figure 3-8(A) plots the relative decrease in fluorescence intensity as a function of the concentration of MUC1. This figure clearly shows saturation in the signal at higher concentrations of MUC1 (>15 μM). Assuming a Langmuir model to describe the aptamer/analyte binding event, we can obtain the dissociation constant (K_D) from the non-linear regression of the experimental data (Figure 3-8(A)):

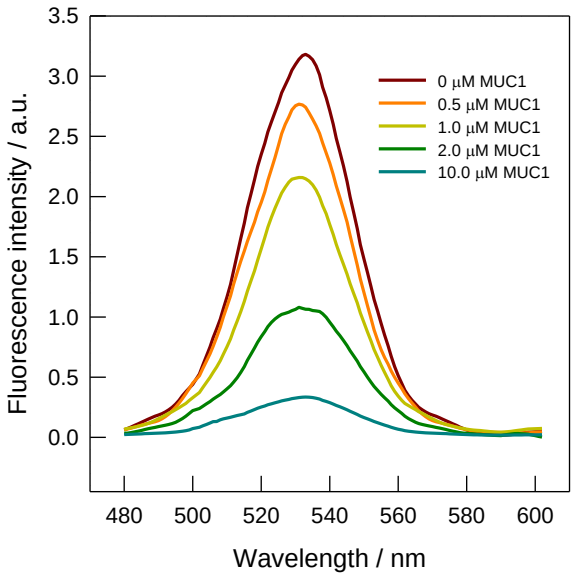

Figure 3-7. Representative fluorescence spectra (excitation at 254 nm) showing a sequential decrease in fluorescence intensity at 530 nm with increasing concentrations of MUC1.

$$\Delta I = \Delta I_{\max} \frac{[\mathrm{MUC1}]}{K_{\mathrm{D}} + [\mathrm{MUC1}]} \qquad (5)$$

where ΔI is the decrease in fluorescence intensity, ΔI_{max} is the maximum decrease in fluorescence, [MUC1] is the molar concentration of MUC1, and K_D is the aptamer-analyte dissociation constant. The K_D is calculated from the regression curve shown in Figure 3-8(A) to be 1.62 ± 0.28 μM. This K_D value is seemingly higher than that reported previously by Ferreira *et al.*;[40,61] the current system involves multiple binding/dissociation steps; in particular, the binding event and the room temperature hybridization can be appreciably difficult due to the size of the QD. Despite the fact that a larger K_D value was obtained, the detection limit we observed here indicates that our system is a promising methodology for the clinical detection of MUC1.

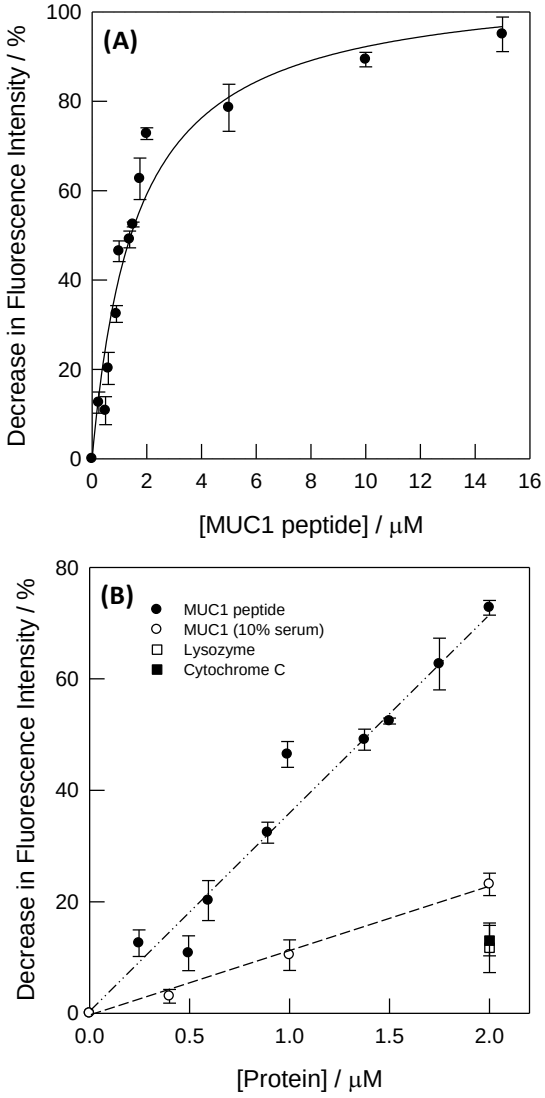

Figure 3-8. (A) The relative decrease in fluorescence intensity as a function of the MUC1 concentration. The solid line is a non-linear regression fit assuming a Langmuir type binding between the aptamer and MUC1, from which the dissociation constant (K_D) was calculated; (B) Working range of the detection, including the relative decrease in fluorescence signal for other proteins, lysozyme and cytochrome c, shown in open and filled squares, respectively. The open circles represent the signal for the sensor in the presence of 10% serum. The dotted lines serve to guide the eye.

From Figure 3-8(B), it can be observed that from the range of 0 to 2.0 μM of MUC1, the system follows a near linear relationship in which the relative decrease in fluorescence intensity is approximately proportional to the concentration of MUC1. At 2.0 μM, where the system reaches to an approximate 70% relative decrease in fluorescence intensity, two other proteins (cytochrome C and lysozyme) exhibit less than 10% decrease in fluorescence intensity. This result confirms the specificity of this aptamer-based MUC1 sensing methodology. Its potential for application in cancer early-diagnostics can be hinted from the ease of generation of a working curve from 250 nM to 2 μM. Ferreira *et al*. performed an aptamer-antibody sandwich ELISA in which a MUC1 peptide containing 5 variable tandem repeats was detected;[61] they observed a linear detection range from 8 μg/mL to 100 μg/mL. For a peptide containing 5 tandem repeats, this approximately corresponds to a linear range from 0.8 μM to 10 μM. It should be also noted that a different aptamer sequence for the 5 tandem repeat peptide was selected,[61] with similar dissociation constants compared to their initial aptamer sequence (as was adapted in this study).[40]

We also aspire to make systematic comparisons with presently used detection methods for MUC1. The names of the currently commercially available ELISA kits for the detection of MUC1 refer to the names of the antigenic epitope in MUC1 for which the monoclonal antibodies for each assay binds, as mentioned above. In the most popularly used CA 15-3 assay, two monoclonal antibodies (DF3 and 115D8.19.12) are used in a sandwich format.[25–27] The DF3 antibody recognizes an 8 amino acid sequence in the 20 amino acid tandem repeat,[28] and is the signal antibody. 115D8.19.12 is a solid-phase capture antibody, recognizing a peptide-carbohydrate epitope on the same repeat. For the

CA15-3 assay, the detection range is estimated to be from 5 U/mL to 250 U/mL with a detection limit of 5 U/mL. As discussed above, this is approximately from 0.8 μM to 39.7 μM of MUC1 peptide. We show here that the QD/aptamer-based detection method is not only rapid but also sensitive, with a detection limit of 250 nM.

To further evaluate the use of the sensor in biomedical systems, we also examined its performance in the presence of blood serum. In commercially available CA 15-3 ELISA kits (*e.g.*, MP Biomedicals, Orangeburg, NY), serum samples are first diluted 51 times (~2% serum) by placing 20 μL of undiluted serum in 1.0 mL of buffer. We decided to challenge our system with 10% calf serum, 5 times more serum compared to that of the ELISA assays. As shown by the open circle points in Figure 3-8(B), we still observe quantitative response to MUC1 peptides, with influence of the serum to the fluorescence signal to a manageable extent. Given the fact that we are using at least 5 times concentrated serum compared to that specified by the CA 15-3 ELISA kits, the presence of other plasma proteins may not a problem for diagnostic applications.

3.3 Conclusion

In conclusion, we have demonstrated the possibility of aptamer-based detection of tumour markers with quantum-dot based fluorescence readout. The specific detection of MUC1 exhibited a K_D of 1.62 ± 0.28 μM, with a detection limit of 250 nM and a dynamic range up to 10 μM. We have shown two types of detection approaches: (i) dichotomous, in which simple diagnostics tests ("has" or "does not have elevated MUC1 concentrations") can be performed by simple solution or filter paper-based assays (under irradiation with a handheld UV lamp); and (ii) quantitative, in which fluorescence spectra

were taken from samples of different concentration to construct a working curve. Component deletion assays were carried out to confirm that the decrease in fluorescence intensity was a result of a 3-component DNA hybridization event. Using non-denaturing gel electrophoresis, we showed that the binding of MUC1 peptides to its aptamer features a different conformational change from other aptamers: the binding of MUC1 peptides to the aptamer destabilizes the pre-formed tertiary interactions. These findings opens up avenues for the further optimization of the QD-based optical detection methods developed herein, as well as other tumour marker detection methodologies. Our group is currently underway with the development of electronic detection schemes of MUC1 (Chapter 4), as well as sensors using modular/allosteric regulation to achieve higher sensitivity (Chapter 5).

3.4 Experimental Section

3.4.1 Materials

The synthetic anti-MUC1 aptamer oligonucleotides MUC1_45, MUC1_47, MUC1_49, and MUC1_49m and the 11F strand for modification with quantum dots were purchased from Core DNA Services, Inc. (Calgary, AB). The quencher strand Q13IB was purchased from Integrated DNA Technologies (Coralville, IA). The MUC1 peptide with two repeats of the 20 amino acid variable tandem repeat region (from the N terminus to the C terminus: PDTRPAPGSTAPPAHGVTSAPDTRPAPGSTAPPAHGVTSA) was purchased as a custom synthetic peptide from the University of British Columbia Brain Research Centre (Vancouver, BC). Bovine serum albumin (BSA), α-cyano-4-hydroxycinnanic acid (CHCA), the bicinchoninic acid (BCA) assay kit, “Stains All”, 1-ethyl-3-(3-dimethylaminopropyl) carboiimide hydrochloride (EDC), N-

hydroxysuccinimide (NHS), hen egg white lysozyme (95%), equine heart cytochrome c (95%), breast tumour antigen (1000 U), and newborn calf serum were purchased from Sigma-Aldrich (Milwaukee, WI). All organic solvents were purchased from VWR (Bridgeport, NJ). 530 nm- and 598 nm-emitting carboxy-terminated quantum dots were from Ocean Nanotech, Llc (Springdale, AK). Deionized water (> 18.3 Ω cm) was produced from a Barnstead EasyPure UV/UF compact water system (Dubuque, IA).

3.4.2 DNA and Peptide Purification

Unmodified and amine-terminated DNA oligonucleotides were size-purified using denaturing (50% urea, w/v) polyacrylamide gel electrophoresis (PAGE) before use. The Q13IB quencher strand was purified with HPLC by Integrated DNA Technologies (Coralville, IA). The MUC1 peptide was purified by reverse-phase HPLC on a Gemini 5-μm C18/110 Å column (Phenomenex, Torrance, CA), eluting with a gradient of acetonitrile containing 0.1% trifluoroacetic acid:water (0 – 60%) at a flow rate of 1.0 mL/min. The peptide sample was lyophilized and dissolved in water. MALDI-TOF (matrix assisted laser desorption ionization, time of flight) spectroscopy was used to verify the molecular weight of the peptide. A saturated mixture of the CHCA matrix was made in a 1:1 mixture of acetonitrile:water containing 0.1% trifluoroacetic acid. Approximately 0.25 mg of purified peptide was dissolved in 5 μL of water and added to 5 μL of the aforementioned CHCA mixture. Peptide concentration was determined with the BCA assay using BSA as a standard.

3.4.3 DNA-Quantum Dot Coupling

The quantum dot-DNA coupling procedure was similar to that of Zhou *et al*,[57] with slight modifications. 6.9 mg of EDC and 4.1 mg of NHS were dissolved in 200 μL of 50% methanol in a glass vial, followed by the addition of 200 μL of 100 mM PBS buffer (including 100 mM of NaCl) at pH 6.0. 15 μL of 8 μM carboxy-terminated QDs (emitting at 530 nm) and an additional 235 μL of PBS buffer was added to bring the total volume to 650 μL. The mixture was sonicated for 2 min to allow the QDs to become homogenous. The mixture was left in the dark at room temperature for 1 hour to allow activation of the QD surface with EDC and NHS. It was then transferred to a 1.5 mL Eppendorf tube, and centrifuged at 13.2 krpm for 25 min, which resulted in a smear of green solid on one edge of the Eppendorf tube (visualized by a handheld UV lamp. The supernatant was carefully removed and checked with the UV lamp to make sure there was no QD fluorescence; it was then washed carefully twice with 200 μL of 50% methanol. 100 μL of 50 mM $NaHCO_3$ buffer (pH = 9.0) was added, followed by 175 μL of 50% methanol and 30 μL of 800 μM 11F amine-terminated DNA. This gives a QD:DNA ratio of 1:200. The mixture was then sonicated for 2 min to result in a fluorescently green solution, which was left at 4 ℃ overnight in the dark to allow the coupling of the amine-terminated DNA to the QD surface. It was then centrifuged for 25 min at 13.2 krpm to result in a yellow pellet (green when illuminated with a UV lamp). The supernatant was carefully removed and checked again to make sure that there was no green fluorescence. Upon washing twice with 200 μL of 50% methanol, the pellet was dried briefly in air for 5 min, followed by the addition of 15 μL of deionized H_2O to resuspend the pellet (sonication was performed for 2 min). The UV absorbance at 260 nm was taken on the combined supernatants to assess the amount of DNA *not* conjugated

to the QD surface, from which we can estimate the amount of DNA that was conjugated to the QDs. The pellet was stored at 4 ℃ in the dark prior to use and the sample was used within one week.

3.4.4 Analyte Binding and DNA Hybridization

5 pmol of DNA aptamer (MUC1_45, MUC1_47, MUC1_49 or MUC1_49m) was allowed to bind with the MUC1 peptide at various concentrations in 10 mM Tris (pH = 7.4), 100 mM NaCl, 5 mM $MgCl_2$, 0.2% BSA, or in 10% calf serum diluted in the same buffer. The aptamer binding event was allowed to take place for 1 hour at room temperature. A parallel control experiment was always performed with no MUC1 peptide added. After the binding event, 5 pmol each of Q13IB and QD11F (amount of DNA that was coupled on the QD surface, in the QD11F case) was added in the same buffer to the experimental samples. Room temperature hybridization was allowed to take place for 30 min.

3.4.5 Fluorescence Detection

Fluorescence spectra were obtained with a Cary Eclipse fluorescence spectrophotometer (Varian Inc. Palo Alto, CA, USA) using Nunc-96 microwell plates from Thermo Fisher Scientific (Rochester, NY). Excitation of the samples was at 254 nm and the spectra were scanned from 480 nm to 600 nm. Optical photos were taken with a Canon IXUS 950 IS digital camera, when the sample was irradiated with a handheld UV lamp.

3.4.6 Gel Electrophoresis

A 3% agarose gel was prepared to verify the amide coupling chemistry of the DNA to the QD. A 15% non-denaturing polyacrylamide gel was run in 4 ℃ to check the hybridization patterns of Q13IB and 11F to the aptamer strand with or without the presence of the MUC1 peptide. 1.0 μM of DNA (either ssDNA or dsDNA) was loaded per lane and the gel was ran in TAE buffer (4 mM Tris at pH = 7.4, 2 mM CH_3COOH, 20 μM EDTA) with 12.5 mM CH_3COOMg at 4 ℃ at 300 V for 3 hours. The gel was stained with "Stains All" for 30 min in the dark, and destained by illuminating the gel with a desk lamp for 1 hour at room temperature. The resulting gel was placed in between transparency sheets and was scanned with a commercial flatbed scanner.

3.5 References

1. Gendler, S. J.; Spicer, A. P. *Annu. Rev. Physiol.* **1997**, *57*, 607 – 634.
2. Hollingsworth, M. A.; Swanson, B. J. *Nature Rev. Cancer* **2004**, *4*, 45 – 60.
3. Muller, S.; Alving, K.; Peter-Katalinic, J.; Zachara, N.; Gooley, A. A.; Hanisch, F. G. *J. Biol. Chem.* **1999**, *274*, 18165 – 18172.
4. McAuley, J. L.; Linden, S. K.; Png, C. W.; King, R. M.; Pennington, H. L.; Gendler, S. J.; Florin, T. H.; Hill, G. R.; Korolik, V.; McGuckin, M. A. *J. Clin. Invest.* **2007**, *117*, 2313 – 2324.
5. Wang, H.; Lillehoj, E. P.; Kim, K. C. *Biochem. Biophys. Res. Commun.* **2004**, *321*, 448 – 454.
6. Hayes, D. F.; Mesa-Tejada, R.; Papsidero, L. D.; Croghan, G. A.; Korzun, A. H.; Norton, L.; Wood, W.; Strauchen, J. A.; Grimes, M.; Weiss, R. B. *J. Clin. Oncol.* **1991**, *9*, 1113 – 1123.

7. Perey, L.; Hayes, D. F.; Maimonis, P.; Abe, M.; O'Hara, C.; Kufe, D. W. *Cancer Res.* **1992**, *52*, 2563 – 2568.

8. Medina, M.; Vádez, D.; Asenjo, J. A.; Egea, G.; Real, F. X.; Gil, J.; Subiza, J. L. *Cancer Res.* **1999**, *59*, 1061 – 1070.

9. Aoki, R.; Tanaka, S.; Haruma, K.; Yoshihara, M.; Sumii, K.; Kajiyama, G.; Shimamoto, F.; Kohno, N. *Dis. Colon Rectum.* **1998**, *41*, 1262 – 1272.

10. Tanimoto, T.; Tanaka, S.; Haruma, K.; Yoshihara, M.; Sumii, K.; Kajiyama, G.; Shimamoto, F.; Kohno, N. *Oncology* **1999**, *56*, 223 – 231.

11. Kiraga, Y.; Tanaka, S.; Haruma, K.; Yoshihara, M.; Sumii, K.; Kajiyama, G.; Shimamoto, F.; Kohno, N. *Oncology* **1998**, *55*, 307 – 319.

12. Willsher, P. C.; Xing, P.-X.; Clarke, C. P.; Ho, D. W. M.; McKenzie, I. F. C. *Cancer* **1993**, *72*, 2936 – 2942.

13. Seregni, E.; Botti, C.; Lombardo, C. Cantoni, A.; Bogni, A.; Cataldo, I.; Bombardieri, E. *Anticancer Res.* **1996**, *16*, 2209 – 2213.

14. Maeshima, A.; Miyagi, A.; Hirai, T.; Nakajima, T. *Pathol. Int.* **1997**, *47*, 454 – 460.

15. Zhang, S.; Zhang, H. S.; Reuter, V. E.; Slovin, S. F.; Scher, H. I.; Livingston, P. O. *Clin. Cancer Res.* **1998**, *4*, 295 – 302.

16. Nacht, M.; Ferguson, A. T.; Zhang, W.; Petroziello, J. M.; Cook, B. P.; Gao, Y. H.; Maguire, S.; Riley, D.; Coppola, G.; Landes, G. M.; Madden, S. L.; Sukumar, S. *Cancer Res.* **1999**, *59*, 5464 – 5470.

17. Hough, C. D.; Sherman-Baust, C. A.; Pizer, E. S.; Montz, F. J.; Im, D. D.; Rosenshein, N. B.; Cho, K. R.; Riggins, G. J.; Morin, P. J. *Cancer Res.* **2000**, *60*, 6281 – 6287.

18. Burdick, M. D.; Harris, A.; Reid, C. J.; Iwamura, T.; Hollingsworth, M. A. *J. Biol. Chem.* **1997**, *272*, 24198 – 24202.

19. Masaki, Y.; Oka, M.; Ogura, Y.; Ueno, T.; Nishihara, K.; Tangoku, A.; Takahashi, M.; Yamamoto, M.; Irimura, T. *Hepatogastroenterology* **1999**, *46*, 2240 – 2245.

20. Walsh, M. D.; Hohn, B. G.; Thong, W.; Devine, P. L.; Gardiner, R. A.; Samaratunga, M. L.; McGuckin, M. A. *Br. J. Urol.* **1994**, *73*, 256 – 262.

21. Retz, M.; Lehmann, J.; Röder, C.; Plötz, B.; Harder, J.; Eggers, J.; Pauluschke, J.; Kalthoff, H.; Stöckle, M. *Cancer Res.* **1998**, *58*, 5662 – 5666.

22. Baratt-Boyes, S. M. *Cancer Immunol. Immunother.* **1996**, *43*, 142 – 151.

23. Beatty, P.; Hanisch, F.-G.; Stolz, D. B.; Finn, O. J.; Ciborowski, P. *Clin. Cancer Res.* **2001**, *7*, 781s – 787s.

24. Croce, M. V.; Isla-Larrain, M. T.; Demichelis, S. O.; Gori, J. R.; Price, M. R.; Segal-Eiras, A. *Breast Cancer Res. Treat.* **2003**, *81*, 195 – 207.

25. Bon. G. G.; Kenemans, P.; Yedama, C. A.; van Kamp, G. J.; Nijman, H. W.; Hilgers, J. *Clinical relevance of the tumour marker CA 15.3 in the management of cancer patients*, in: Crommelin, D.; Schelleken, H., Eds. *From Clone to Clinic*, Dordrecht, The Netherlands: Kluwer Academic Publishers, **1990**, 111 – 122.

26. Bon, G. G.; von Mensdorff-Pouilly, S.; Kenemans, P. van Kamp, G. J.; Verstraeten, R. A.; Hilgers, J.; Meijer, S.; Vermorken, J. B. *Clin. Chem.* **1997**, *43*, 585 – 593.

27. Jezersek, B.; Cervek, J.; Rudolf, Z.; Novakovic, S. *Cancer Letters* **1996**, *110*, 137 – 144.

28. Price, M. R.; Hudecz, F.; O'Sullivan, C.; Baldwin, R. W.; Edwards, P. M.; Tendler, S. J. B. *Mol. Immunol.* **1990**, *27*, 795 – 802.

29. Reddish, M. A.; Helbrecht, N.; Almeida, A. F.; Madiyalakan, R.; Suresh, M. R.; Longenecker, B. M.; *J. Tumor Marker Oncol.* **1992**, *7*, 19 – 27.

30. Tuerk, G.; Gold, L.; *Science* **1990**, *249*, 505 – 510.

31. Ellington, A. D.; Szostak, J. W. *Nature* **1990**, *346*, 818 – 822.

32. Huizenga, D. E.; Szostak, J. W. *Biochemistry* **1995**, *34*, 656 – 665.

33. (a) Cox, J. C.; Ellington, A. D. *Bioorg. Med. Chem.* **2001**, *9*, 2525 – 2531; (b) Cox, J. C.; Hayhurst, A.; Hesselberth, J.; Bayer, T. S.; Georgiou, G.; Ellington, A. D. *Nucleic Acids Res.* **2002**, *30*, e108; (c) Kirby, R.; Cho, E. J.; Gehrke, B.; Bayer, T.; Park, Y. S.; Neikirk, D. P.; McDevitt, J. T.; Ellington A. D.; *Anal. Chem.* **2004**, *76*, 4066 – 4075.

34. (a) Stojanovic, M. N.; Landry. D. W. *J. Am. Chem. Soc.* **2002**, *124*, 9678 – 9679; (b) Stojanovic, M. N.; de Prada, P.; Landry, D. W. *J. Am. Chem. Soc.* **2001**, *123*, 4928 – 4931.

35. Green, L. S.; Jellinek, D.; Jenison, R.; Östman, A.; Heldin, C.-H.; Janjic, N. *Biochemistry* **1996**, *35*, 14413 – 14424.

36. Bock, L. C.; Griffin, L. C.; Latham, J. A.; Vermaas, E. H.; Toole, J. L. *Nature* **1992**, *355*, 564 – 566.

37. Grate, D.; Wilson, C. *Proc. Natl. Acad. Sci. USA* **1999**, *96*, 6131 – 6136.

38. Ellington, A. E.; Szostak, J. W. *Nature* **1992**, *355*, 850 – 852.

39. O'Sullivan, C. K. *Anal. Bioanal. Chem.* **2002**, *372*, 44 – 48.

40. Ferreira, C. S. M.; Matthews, C. S.; Missailidis, S. *Tumor Biol.* **2006**, *27*, 289 – 301.

41. Xiao, Y.; Lubin, A. A.; Heeger, A. J.; Plaxco, K. W. *Angew. Chem. Int. Ed.* **2005**, *44*: 5456–5459.

42. Lai, R. Y.; Plaxco, K. W.; Heeger, A. J. *Anal. Chem.* **2007**, *79*, 229–233.

43. Ferapontova, E. E.; Olsen, E. M.; Gothelf, K. V. *J. Am. Chem. Soc.* **2008**, *130*, 4256 – 4258.

44. Cheng, A. K. H.; Ge, B.; Yu, H.-Z. *Anal. Chem.* **2007**, *79*, 5158 – 5164.

45. Liu, J.; Lu, Y. *Angew. Chem. Int. Ed.* **2005**, *45*, 90 – 94.

46. (a) Nutiu, R.; Li, Y. *Chem. Eur. J.* **2004**, *10*, 1868 – 1876; (b) Nutiu, R.; Li, Y. *Methods* **2005**, *37*, 16 – 25; (c) Nutiu, R.; Li. Y. *J. Am. Chem. Soc.* **2003**, *125*, 4771 – 4778.

47. Choi, J. H.; Chen, K. H.; Strano, M. S. *J. Am. Chem. Soc.* **2006**, *128*, 15584 – 15585.

48. Shieh, F.; Lavery, L.; Chu, C. T.; Richards-Kortum, R.; Ellington, A. D.; Korgel, B. A. *Proc. SPIE* **2005**, *5705*, 159 – 165.

49. Chen, X.-C.; Deng, Y.-L.; Lin, Y.; Pang, D.-W.; Qing, H.; Qu, F.; Xie H.-Y. *Nanotechnology* **2008**, *19*, 235105 – 235110.

50. Levy, M.; Cater, S. F.; Ellington, A. D. *ChemBioChem* **2005**, *6*, 2163–2166.

51. Bagalkot, V.; Zhang, L.; Levy-Nissenbaum, E.; Jon, S.; Kantoff, P. W.; Langer, R.; Farokhzad, O. C. *Nano Lett.* **2007**, *7*, 3065–3070.

52. Haugland, R. P. *The Handbook, A Guide to Fluorescent Probes and Labeling Technologies*; Tenth Edition, Invitrogen Corporation: San Diego, **2005**.

53. Leulliot, N.; Baumrik, V.; Abdelkafi, M.; Turpin, P. Y.; Namane, A.; Gouyette, C.; Huynh-Dinh, T.; Ghomi, M. *Nucleic Acids Res.* **1999**, *27*, 1398 – 1404.

54. Hamaguchi, N.; Ellington, A.; Stanton, M. *Anal. Biochem.* **2001**, 126–131.

55. Dirks, R. M.; Pierce, N. A. *Proc. Natl. Acad. Sci. U.S.A.* **2004**, *101*, 15275–15278.

56. Bayer, T. S.; Smolke, C. D. *Nat. Biotechnol.* **2005**, *23*, 337–343.

57. Zhou, D.; Ying, L; Hong, X.; Hall, E. A.; Abell, C.; Klenerman, D. *Langmuir* **2008**, *24*, 1659 – 1664.

58. Lakowicz, J. R. *Principles of Fluorescence Spectroscopy*, 2nd ed.; Kluwer Academic: New York, 1999.

59. Turro, N. J. *Modern Molecular Photochemistry*; University Science books: Mill Valley, CA, 1991.

60. Cady, N. C.; Strickland, A. D.; Batt, C. A. *Mol. Cell. Probes* **2007**, *21*, 116–124.

61. Ferreira, C. S. M.; Papamichael, K.; Guilbault, G.; Schwarzacher, T.; Gariepy, J.; Missailidis, S. *Anal. Bioanal. Chem.* **2008**, *390*, 1039 – 1050.

CHAPTER 4

ELECTROCHEMICAL APTAMER-BASED BIOSENSORS OF MUCIN 1 BASED ON METHYLENE BLUE-LABELING*

In this chapter, aptamer-based electrochemical detection methodologies for mucin 1 (MUC1) have been explored by using methylene blue as a redox probe. The alterations in the redox behaviour of methylene blue on anti-MUC1 aptamer-modified Au electrodes upon the addition of MUC1 peptides have been tested in two ways: (1) methylene blue was covalently tethered to one end of the thiolated aptamers and (2) methylene blue was used as a diffusive redox marker in solution for interaction with unlabeled aptamers. The detection specificity and concentration dependence (from which the dissociation constant of the aptamer/analyte complex was extracted) for MUC1 peptides were further evaluated using square-wave voltammetry. In addition, we systematically investigated the pH dependence of the redox behaviour of methylene blue, with the hope of not only gaining understanding on the electrochemistry of methylene blue, but also augmenting the applicability of methylene blue-labeling for the development of DNA (aptamer)-based electrochemical biosensors.

* Based on currently prepared manuscript: Cheng, A. K. H.; Yu, H. Z. (2009) Electrochemical aptamer-based biosensors of mucin 1 based on methylene blue-labeling.

4.1 Introduction

Methylene blue (MB) is a heterocyclic aromatic chemical compound that has been used not only as a dye for bacteriology[1] but also as a medicinal treatment (e.g. by acting as a monoamine oxidase inhibitor[2]) for various diseases and maladies such as malaria[3] and cyanide poisoning.[4] In chemistry, MB is a widely used redox indicator, with its reaction epitomized by the "blue bottle" stunt performed worldwide in the regular chemistry classroom.[5] At neutral pH, MB undergoes a two-electron reduction accompanied by protonation to become leucomethylene blue (LB),[6] as shown in Figure 4-1. The reaction can be monitored spectroscopically as MB is blue in colour (due to extensive redistribution of the positive charge by conjugation), whereas LB is colourless. The electrochemistry of the MB/LB redox couple is well understood,[7–20] thus heightening the use of its redox behaviour for the ongoing fabrication of novel, portable, electrical biosensors geared towards the detection of biologically-relevant analytes.

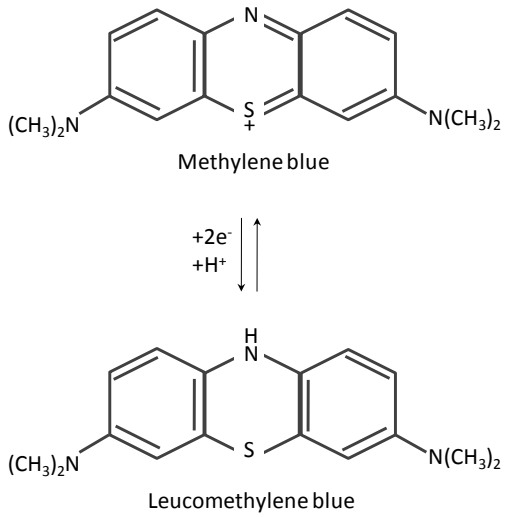

Figure 4-1. Redox property of methylene blue (MB) at neutral pH: the two-electron reduction of MB to leucomethylene blue (LB) is accompanied by a protonation step at the secondary amine position.

The idea to use the redox property of DNA-interacting MB for biosensing is not new: it was reported that MB can intercalate between the base pairs of dsDNA (double stranded DNA).[7–9] In 1997, Kelley *et al.* studied the electrochemistry of MB in the hope of gaining insight on the applicability of this redox probe for biosensing.[10] In their study, gold surfaces were derivatized with 15 base-pair (bp) dsDNA containing a 5′ hexanethiol linker for DNA SAM (self-assembled monolayer) formation. The electrochemistry of DNA-associated MB was studied with chronocoulometry and cyclic voltammetry; the surface coverage of DNA was examined by ellipsometry and ^{32}P-labeling. Since solution-diffused MB molecules have limited access to available sites in dsDNA near the electrode, intercalation of MB was predicted to be primarily on duplex sites far away from the alkanethiol linker, thus making MB separated from the electrode surface by both a σ-system of the aliphatic linker, in addition to a π-system of the base pairs. The general conclusion was that MB is capable of long-range electron transfer through the DNA base pairs. In 1999, the same group devised a single-base mismatch detection system based on the fact that long range electron transfer of intercalated MB on dsDNA will be disturbed by the existence of mismatches along the helix.[11] Further enhancement of signal was accomplished using a solution-based mediator, potassium ferricyanide.

The interaction of redox markers with ssDNA (single stranded DNA) started with the work of Mikkelsen and co-workers,[12–14] who showed that the affinity of $[Co(phen)_3]^{3+}$ for dsDNA was greater than for ssDNA – this was used to distinguish between ssDNA and dsDNA. Further studies were done with other redox indicators such as $[Ru(NH_3)_6]^{3+}$ with dsDNA and ssDNA,[15,16] with demonstrated applicability for biosensing.[17] In the study of the interaction of MB with ssDNA (versus dsDNA), Ozsoz's group observed

opposite trends in terms of the binding affinity of the redox marker for ssDNA and dsDNA.[18,19] It was found that the interaction of MB with ssDNA was on guanine residues, for which the signal becomes masked upon hybridization of the DNA with its complimentary strand. This results in a decrease in current measured by SQW (square wave voltammetry).[20,21] A linear relationship between the number of guanine residues and the surface density of absorbed MB was found by Gooding and coworkers, indicative of the specific interaction of MB with guanines.[20] They proposed that the binding mode of MB-guanine complexes exists in three ways: T-shaped, non-stacked and face-to-face.[20]

While the subject matter in which MB has been studied primarily resides within the realm of nucleic acid interactions, the last decade or so have shown the aptitude for both solution-diffused MB and nucleic acid-tagged MB as redox indicators in biosensors for proteins and small molecules. Studies were primarily on aptamers,[22,23] synthetic nucleic acid sequences that have been iteratively selected *in vitro* to bind with high specificity to an analyte of choice. For nucleic-acid tagged MB, detection was primarily based on the conformational changes of the aptamer strand upon analyte binding. The E-AB sensors (electronic aptamer-based sensors) pioneered by Plaxco, Heeger and co-workers started with the detection of thrombin, using MB-tagged anti-thrombin aptamers immobilized on a Au electrode.[24] In the absence of thrombin, the flexibility of the ssDNA brought the MB moiety close to the electrode surface, promoting electron transfer; in the presence of thrombin, folding of the aptamer to its secondary structure (namely, the G-quartet[25]) brought the MB moiety far from the electrode, resulting in a decrease in the measured electrochemical current. This research has been extended by the same group to the detection of PDGF (platelet-derived growth factor)[26] and cocaine.[27] Gothelf and

coworkers applied a similar concept for RNA aptamer-based detection of theophylline using ferrocene-redox labeling.[28] Recently, another detection scheme was devised by Dong and coworkers based on the interaction of solution-diffused MB with DNA aptamers.[29] A partial dsDNA was immobilized on a Au surface with the longer aptamer-containing strand capable of binding to adenosine. Before the addition of adenosine, MB molecules were allowed to interact along the ssDNA regimes (particularly at guanine-containing regions) since there is minimal interaction of MB at dsDNA regimes.[18-20,29] Upon the addition of adenosine, folding of the aptamer caused release of the aptamer-containing strand on the electrode. The signal from MB decreased with increasing concentrations of adenosine. An exemplary detection limit of 10 nM was obtained with a detection range from 2 nM to 2 μM.[29]

The purpose of this chapter is to develop aptamer-based electrochemical biosensors for protein biomarkers (e.g., MUC1) using MB redox labeling. In particular, we are interested in comparing side-by-side the electrochemical response of DNA-tagged and solution-diffused redox centres (e.g. MB/LB). We compared the two systems with anti-mucin 1 (MUC1) aptamers, which are specific to MUC1 peptides. As mentioned in the previous chapter, protein mucins are important cell surface-associated glycoproteins known to have elevated concentrations in patients with early epithelial adenocarcinomas.[30] Although the anti-MUC1 aptamer was selected in 2006,[31] this is the first time that MUC1 may be detected electrochemically. The hypothesized detection schemes for MUC1 are shown in Figure 4-2. In the absence of MUC1, the aptamer is predicted by *MFold* tests to assemble into a unique secondary structure featuring a 4 bp stem-loop motif. Figure 4-2(A) shows the modification of a gold electrode with MB-

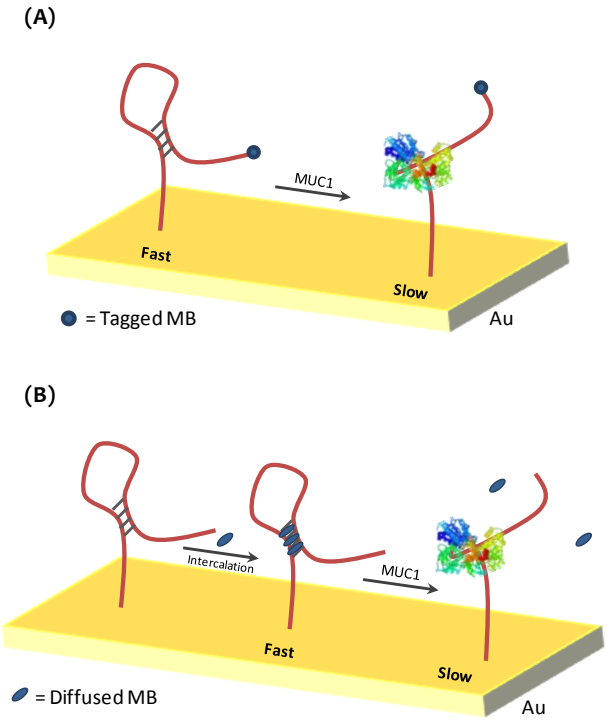

Figure 4-2. Schematic cartoon representing the aptamer-based electrochemical detection of mucin 1 (MUC1) on Au electrodes using nucleic acid-tagged MB (A) and solution-diffused MB (B). Decrease in current derived from MB is expected for both schemes.

tethered aptamers: the presence of MUC1 is expected to change the conformation of the aptamer as was shown in Chapter 3. Such a structural change, in turn, relocates the MB further away from the electrode surface, for which decrease in current is expected. The use of solution-diffused MB (as shown in Figure 4-2(B)) could be more intriguing. As mentioned above, while Ozsoz and Gooding speculated on the inability of MB to bind with dsDNA,[18–21] Barton and coworkers[10,11] suggested that the intercalation of MB into the dsDNA base stack forms the basis of long range electron transfer through the π-system.[32–35] The present scheme (Figure 4-2(B)) should help us elucidate the binding modes between solution-diffused MB molecules and DNA-modified electrodes, as the

preformed stem loop structure of the aptamer may be disrupted upon binding MUC1 via the elimination of base pairing (Chapter 3).[36]

4.2 Results and Discussion

4.2.1 Cyclic Voltammetric Study of Anti-MUC1 Aptamer-Modified Au Electrodes

Figure 4-3(A) shows a representative cyclic voltammogram of a Au electrode modified with MB-tethered anti-MUC1 aptamers. Reversible redox behaviour was observed as evident by similar catholic and anodic peak currents. The formal potential (E°′) was determined to be -0.308 ± 0.004 V (vs. Ag | AgCl | 3 M NaCl) and the peak separation (ΔEp) 0.021 ± 0.003 V. Shown in Figure 4-3(B) are cyclic voltammograms corresponding to 2.0 μM MB (as a chloride salt) in 10 mM Tris, 100 mM NaCl, 5 mM $MgCl_2$, pH = 7.4 on 1-mercapto-6-hexanol (MCH)-treated Au electrodes and on anti-MUC1 aptamer-modified Au electrodes. On MCH-treated electrodes (which is the passivation step used for the preparation of DNA-immobilized gold chips to ensure minimal physical adsorption[37,38]), no clear Faradaic current was observed in either the negative or positive reaction. The fact that appreciable Faradaic currents were observed upon the immobilization of anti-MUC1 aptamers suggests the specific interaction between MB and surface-bound DNA aptamers. From the cyclic voltammogram of MB on anti-MUC1 aptamer-modified electrodes, the formal potential (E°′) was determined to be -0.255 ± 0.011 (vs. Ag | AgCl | 3 M NaCl) and the peak separation (ΔEp) 0.103 ± 0.008 V. Compared to MB-tethered aptamers, the redox process occurs at a less negative potential suggesting that thermodynamically the redox process for free MB is more favoured compared to that of tagged-MB. However, the larger peak separation (0.103 V vs. 0.021 V) suggests that the electron transfer rate is slower.

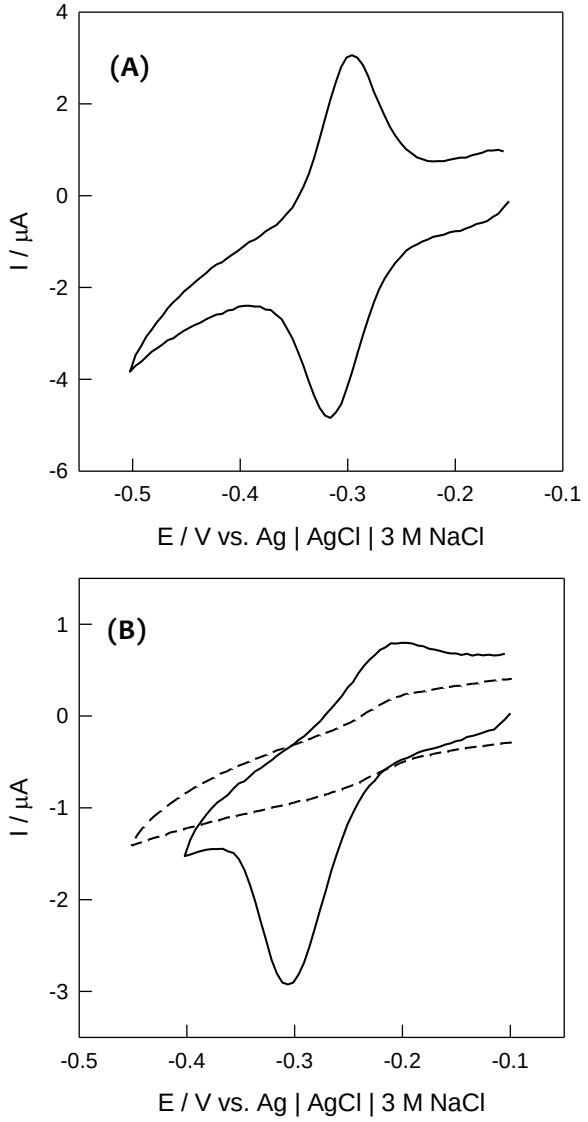

Figure 4-3. (A) Cyclic voltammogram of MB-tethered anti-MUC1 aptamers (HS-$(CH_2)_6$-O-5′-GCA GTT GAT CCT TTG GAT ACC CTG G-3′-C7-NHCO-$(CH_2)_3$-MB) on Au electrodes in 10 mM Tris, 100 mM NaCl, 5 mM $MgCl_2$, pH = 7.4. The scan rate was 500 mV/s; (B) Cyclic voltammogram of 2.0 μM MB on 1-mercapto-6-hexanol (MCH)-treated Au electrodes (dashed line) and on anti-MUC1 aptamer (HS-$(CH_2)_6$-O-5′-GCA GTT GAT CCT TTG GAT ACC CTG G-3′) modified Au electrodes in 10 mM Tris, 100 mM NaCl, 5 mM $MgCl_2$, pH = 7.4 (solid line). The scan rate was 500 mV/s.

Unlike the cyclic voltammogram of tagged-MB, solution-diffused MB does not exhibit reversible behaviour since the reduction peak current is much larger than that of the oxidation peak current. This very fact indicates that this system is far more complicated than the MB-tagged system, which may render it less useful to further pursue its applicability for biosensing. As mentioned earlier, two primary modes of interaction between MB and DNA have been formulated from literature: electrostatic interaction of positively-charged MB with DNA (mainly with guanine residues),[18–20] and the intercalation of MB between base pairs of dsDNA.[7–9] Three main conclusions can be made from the cyclic voltammograms shown in Figure 4-3(B): (1) the fact that the oxidation reaction has a smaller current suggests that a fraction of solution-diffused MB is interacting with DNA via electrostatic interactions. Based on Figure 4-1, it is clear that at physiological pH, MB is positively charged while LB is neutral (LB actually has two more ionization steps that are at much lower pH; a further study of the pH dependence will be presented in a later section). The fact that we observed a lower oxidation current suggests that neutral LB has a decreased ability to interact with DNA – this suggests that MB may be interacting with DNA via electrostatic interactions in single stranded regions; (2) the fact that we are observing residual signals from the oxidation of LB suggests that while LB has a decreased ability for electrostatic interactions, MB and LB may interact with DNA in a different mode – via intercalation; (3) the fact that we see minimal charge from the redox properties exhibited by MB on the alkanethiol-treated Au chip verifies that there is a definite interaction between MB/LB and DNA. At this point, it is clear that we do not fully understand the complex electrochemistry of solution-diffused MB on DNA-modified gold electrodes.

We were first interested in the verification that the current from MB was that of surface-bound MB, and not from solution-diffused MB. This can be viewed upon as a verification of a successful self-assembly process of thiol-derivatived MB-tagged aptamers on Au electrodes, as well as a verification that diffusive MB molecules are interacting with the surface-bound aptamers, and thus adsorbed on the electrode surface. To do this, the peak current was recorded as a function of both the scan rate (Figure 4-4) and the square root of the scan rate (data not shown) for the two systems. For diffusion-controlled redox processes, in which the current is limited by the diffusion of the electroactive species to the electrode surface, the peak current is proportional to the square root of the scan rate:[39]

$$I_p = (2.69 \times 10^5) n^{3/2} A C D^{1/2} \nu^{1/2} \qquad (1)$$

where I_p is the peak current (amperes), n is the number of electrons transferred, A is the electrode area (m^2), C is the bulk concentration of the redox active species (M), ν is the scan rate (V/s) and D is the diffusion coefficient (m^2/s). On the other hand, the peak current is proportional to the scan rate (as opposed to $\nu^{1/2}$) for surface immobilized cations:[39]

$$I_p = \frac{n^2 F^2}{4RT} \nu A \Gamma \qquad (2)$$

where Γ is the surface concentration of the electroactive species (mol/cm^2), F is Faraday's constant, and R and T have their regular meanings. According to Figure 4-4, the linear relationship found when the cathodic peak current was plotted as a function of the scan rate for both systems indicated that the signals were derived from surface-adsorbed electroactive MB species as opposed to solution-diffused MB.

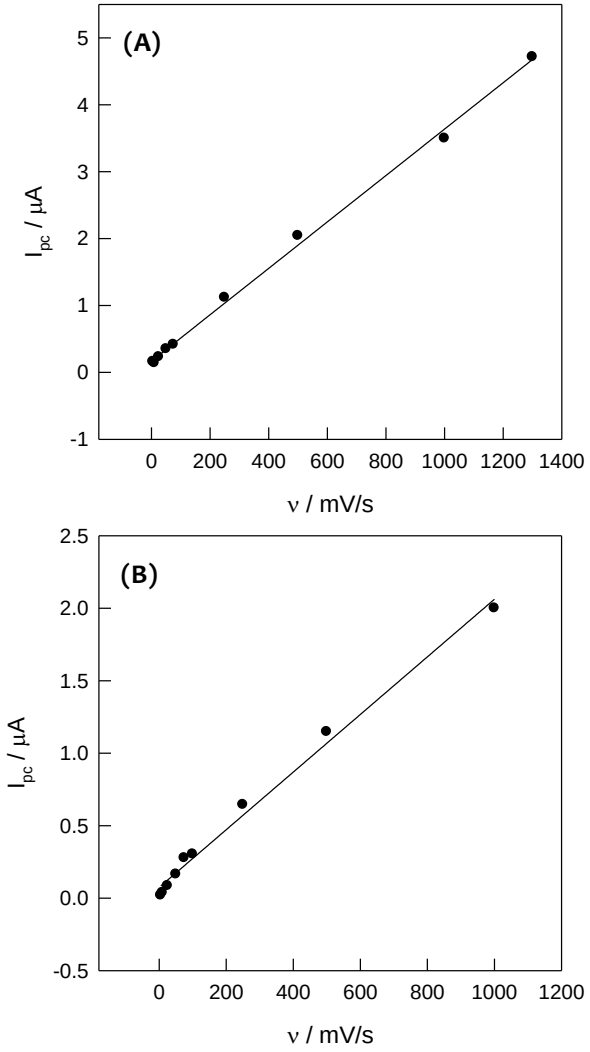

Figure 4-4. Plot of peak current as a function of the scan rate for (A) MB-tagged anti-MUC1 aptamer-modified Au electrodes, and (B) solution-diffused MB on anti-MUC1 aptamer-modified Au electrodes. The lines shown are least-squares linear regressions of the points in the two cases.

The results shown in Figure 4-4(A) also confirmed that the self-assembly process of MB-tethered aptamers was successful. Given this fact, we may use the cyclic voltammogram in Figure 4-3(A) to calculate the surface density of DNA, which should be equal to the surface density of MB since there is one MB per DNA strand immobilized

on the electrode. The fulfillment of the assumption that the MB species are surface-adsorbed allows one to consider the following equations (where Γ'_{MB} is the surface density of MB, Γ'_{DNA} is the surface density of DNA, N_A is Avogadro's constant), which may be used to calculate the surface coverage on the electrode:

$$\Gamma'_{MB} = \frac{Q_{MB}}{nFA} N_A \quad (3)$$

$$\Gamma'_{DNA} = \Gamma'_{MB} \quad (4)$$

We have determined the surface densities of several repeated samples and plotted a histogram (Figure 4-5(A)). It is evident that consistent surface densities can be obtained (with 1.0 μM DNA deposition solutions) for 20 chips, with a mean surface density of 1.24 × 10^{12} molecules/cm^2 and a standard deviation of 0.06 × 10^{12} molecules/cm^2. The Gaussian shape of the histogram is consistent with the nature of the self-assembly process, i.e., the spontaneous chemical adsorption of thiolated DNA strands on gold surfaces reaches equilibrium. We note that it is also possible to use the voltammetric signal of solution diffused $[Ru(NH_3)_6]^{3+}$, a typical redox marker used for surface density determination.[15,16] For the solution-diffused MB system, the surface density of the aptamer monolayer was also determined. By incubating Au electrodes in 1.0 μM DNA deposition solutions, relatively consistent surface densities were obtained using the $[Ru(NH_3)_6]^{3+}$ method,[15,16] as shown in Figure 4-5(B). A typical cyclic voltammogram of the system with 5.0 μM $[Ru(NH_3)_6]^{3+}$ in solution is shown in Figure 4-6. From 20 chips (1.0 μM DNA deposition solutions), the mean surface density was 2.69 × 10^{12} molecules/cm^2, with a standard deviation of 0.31 × 10^{12} molecules/cm^2. The

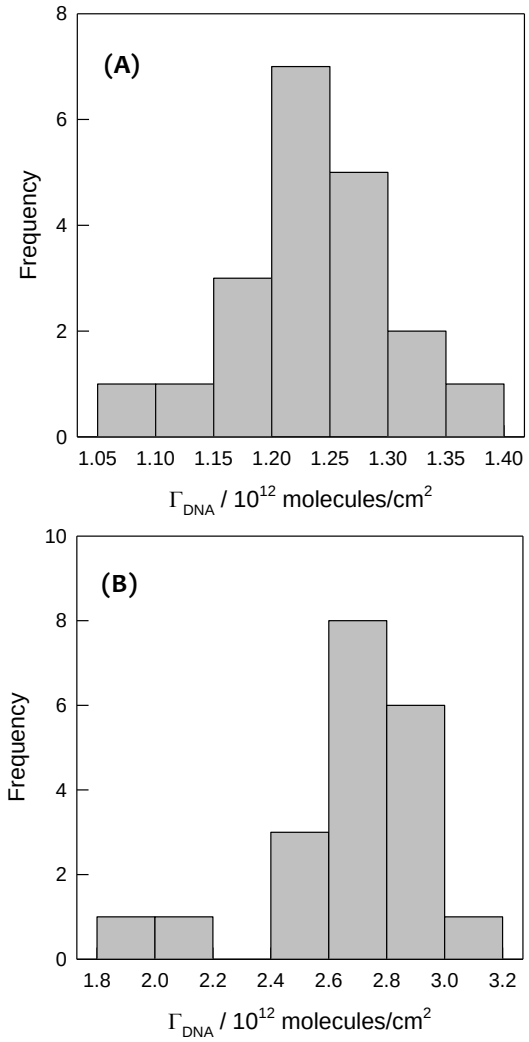

Figure 4-5. Histogram of the surface density of DNA in 20 different chips immobilized with (A) MB-tagged anti-MUC1 aptamers on Au electrodes and (B) anti-MUC1 aptamers on Au electrodes. The immobilization buffer was 10 mM Tris, 100 mM NaCl, 5 mM $MgCl_2$, pH = 7.4

solution-diffused system has a surface density approximately double of that compared to the MB-tagged system, which indicates that the derivatization of DNA with MB indeed influences its binding to the electrode surface. However, it is important to note that even though the MB-tagged system had a lower surface density, the MB signal exhibited (as

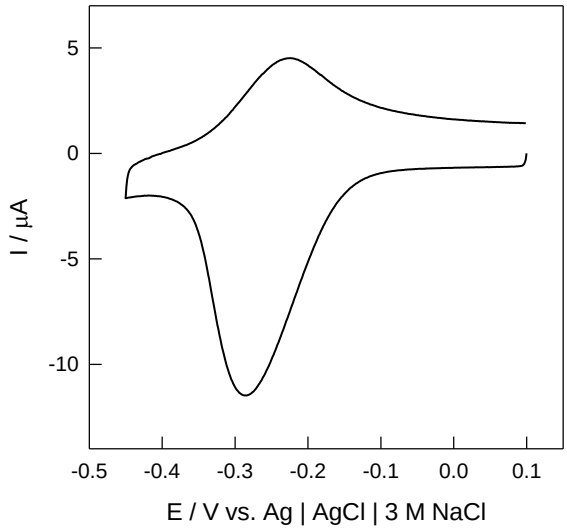

Figure 4-6. 5.0 μM $[Ru(NH_3)_6]Cl_3$ on anti-MUC1 aptamers on Au electrodes in 10 mM Tris, 100 mM NaCl, 5 mM $MgCl_2$, pH = 7.4. The scan rate was 500 mV/s.

shown by the cyclic voltammograms in Figure 4-3) was much stronger compared to the solution-diffused case, which means that the use of intercalative/electrostatically-bound MB molecules for biosensing may not be optimal.

4.2.2 The pH-Dependence on the Redox Behaviours of MB

According to Figure 4-1, the reduction of MB to LB is accompanied by the protonation of the secondary amine. The redox behaviour of MB (both on MB-tagged nucleic acids and solution-diffused MB) should therefore be affected by the pH of the electrolyte. Accordingly, cyclic voltammograms were recorded in a pH range from pH = 5.0 to pH = 10.0 (shown in Figure 4-7); the pH range was chosen to preserve the integrity of possible Watson Crick DNA base pairs (due to the pKa values of the four DNA

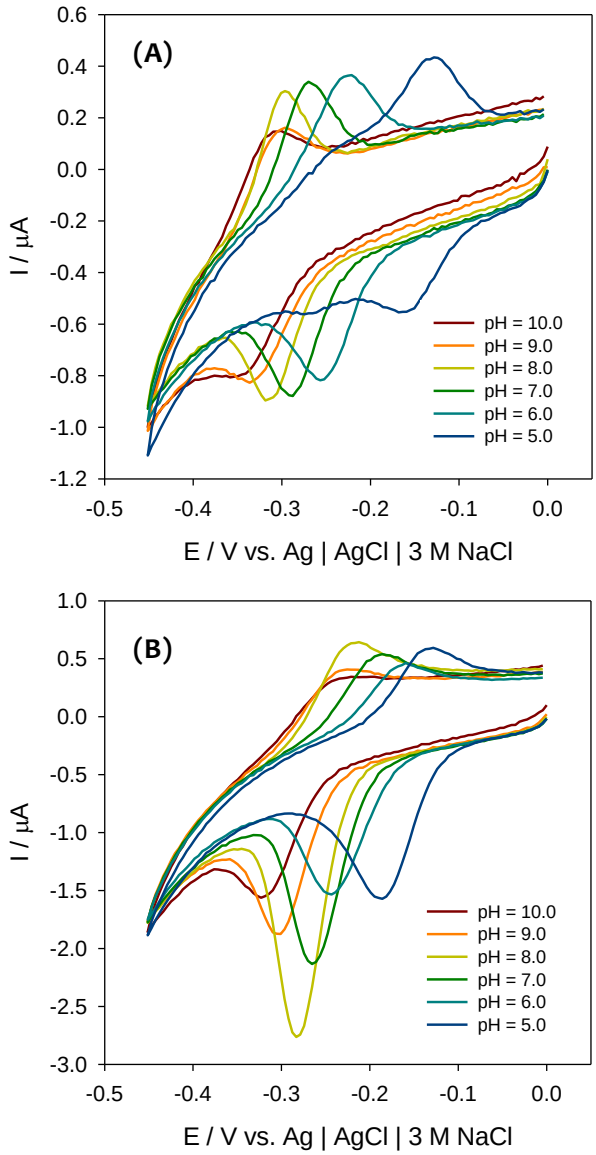

Figure 4-7. Overlay of cyclic voltammograms at various pH of (A) MB-tagged anti-MUC1 aptamers and (B) 2 µM MB on anti-MUC1 aptamers grafted on Au electrodes in 10 mM Tris, 100 mM NaCl, 5 mM $MgCl_2$, pH = 7.4. The scan rate was 500 mV/s.

nucleotides).[40] Presented in Figure 4-8(A) is the variation of anodic and cathodic peak potentials as a function of pH. The peak potentials shift positive upon decreasing the pH, which indicates that that the MB redox process is thermodynamically more favoured at

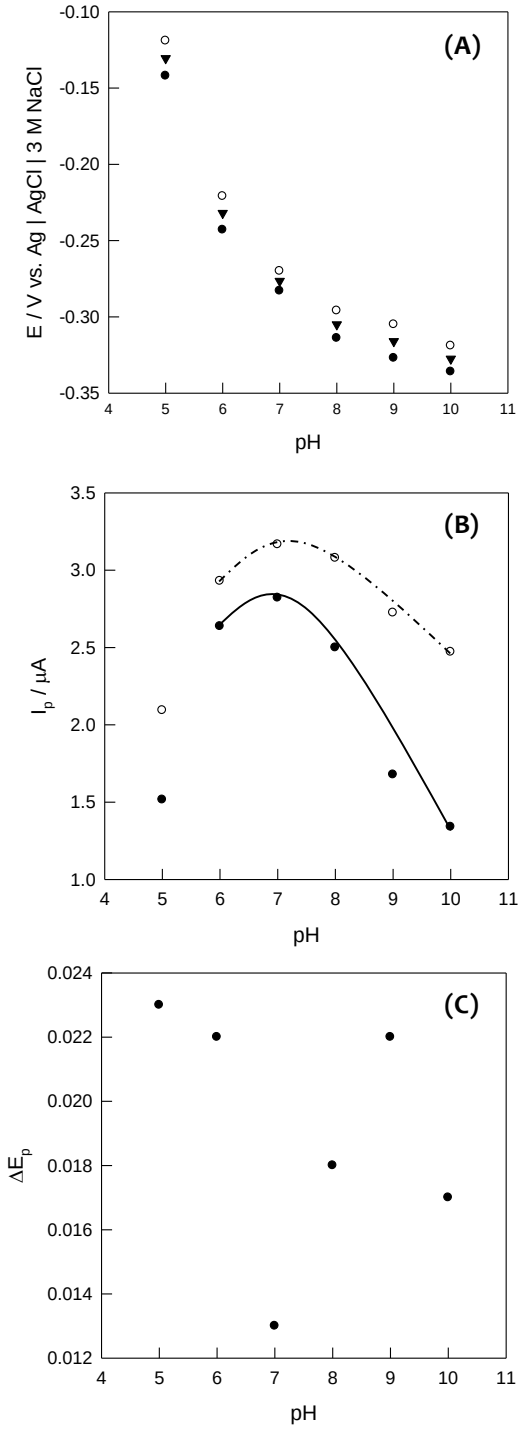

Figure 4-8. Plot of cathodic peak (closed circles), anodic peak (open circles), and formal (triangles) potentials (A), cathodic (closed circles) and anodic (open circles) peak currents (B), and peak potential separation (C) as a function of pH for MB-tagged anti-MUC1 aptamer-modified Au electrodes. The curves are drawn to guide the eye only.

lower pH [less negative E°(½ (E_{pc} + E_{pa})) at lower pH]. This can be derived from considering the variation of Gibb's free energy change ΔG on the peak potential (E) converted relative to SHE (standard hydrogen electrode) vs. $E^{\circ\prime}$ of SHE:

$$\Delta G = -nF(E - E^{\circ\prime}_{SHE}) \quad (5)$$

Since the Ag | AgCl | 3M NaCl electrode is roughly 0.209 V more positive compared to that of SHE, the peak potentials in the cyclic voltammograms under pH investigation do not have a reverted charge (from negative to positive) when converted to potentials relative to SHE. Therefore, as the pH decreases, the absolute difference between the standard potential of SHE and the peak potential position is less, resulting in a less negative [$E - E^{\circ\prime}_{SHE}$] value. According to Eq. (5), this results in a less positive ΔG, which means that the system is thermodynamically more favourable. The pH dependency on peak potential can also be proved from a derivation of the Nernst equation for the reduction half reaction, taking into consideration the pH. From the equation,

$$MB^+ + 2e^- + H^+ \rightleftharpoons LB \quad (6)$$

we may apply the Nernst equation for the reduction half reaction:

$$E = E^\circ - \frac{0.05916}{n}\log\left(\frac{[LB]}{[MB^+][H^+]}\right) \quad (7)$$

$$E = E^\circ - \frac{0.05916}{n}\log\left(\frac{[LB]}{[MB^+]}\right) + \frac{0.05916}{n}\log[H^+] \quad (8)$$

$$E = E^\circ - \frac{0.05916}{n}\log\left(\frac{[LB]}{[MB^+]}\right) - (pH)\left(\frac{0.05916}{n}\right) \quad (9)$$

According to Eq. (9), the peak potentials are lower (more negative) at higher pH, and therefore thermodynamically less favourable, which is consistent with the data presented in Figure 4-7, and the Gibb's free energy consideration from Eq. (5). The observed shifting of potential peaks can be understood by the altered availability of protons required for the reduction reaction from MB to LB. Similar trends were observed previously, which explained that the protonation of the heterocyclic nitrogen is less favourable at higher pH.[41]

We now consider the variation of the cathodic and anodic peak currents as a function of pH. While the effect of pH on thermodynamics was clearly observed with the peak potential versus pH dependency, we address the question whether pH has an effect on the kinetics as well. From Figure 4-8(B), the largest current was recorded when the pH was around physiological pH. It may be conceivable that there is specific interaction of tagged MB with the DNA backbone. Given the length of the linker between the MB moiety and the DNA backbone (C7 aliphatic linker) provided by the supplier, it is reasonable to believe that there may be direct association of MB with DNA via electrostatic interactions. Since the protonation state (and hence charge) of nucleotides varies as a function of pH, interaction of MB with DNA (if it occurred) would also vary as a function of pH. While this is merely a hypothesis, more evidence will follow in a later section in which the current was recorded for solution-diffused MB on an untagged aptamer system. The variation may also be understood on the integrity of the stem loop structure as a function of pH. Since the stem relies heavily on Watson Crick hydrogen bonding capability (which varies as a function of pH), decreasing or increasing the pH from neutrality would make these interactions less favourable, thus unfolding the aptamer

from its secondary structure: the unfolding of the aptamer would bring MB far from the electrode surface, translating to a decrease in peak current. More experiments are warranted to fully understand these variations in peak current. We also consider the variation of the peak separation ΔEp as a function of pH (Panel C of Figure 4-8). While the distribution is mostly random, a local minimum at pH = 7.0 suggests that the electron transfer rate was the fastest at neutral pH. Again, this may be explained by the largest structural integrity of the stem at neutrality. In all, these results emphasize the importance to work in physiological pH. For detection of MUC1 peptides, we employ detection in the pH = 7.0 to pH = 8.0 range, a typical range to preserve the proteins and peptides for which the test was designed.

Like the case of MB-tagged anti-MUC1 aptamers, we evaluate the effect of pH on the peak potential, peak current and peak separation for the MB-untagged system (Figure 4-9). The trend in Figure 4-9(A) is similar to that of Figure 4-8, which shows that as the pH of the system decreases, the peak potential shifts to more positive values, indicative of a thermodynamically more favoured redox process. Again, this trend may be understood by the ease of protonation in the reduction reaction from MB to LB at lower pH. We also consider the variation in the cathodic and anodic peak current as a function of pH. As shown in Figure 4-9(B), the same trend as the tagged-MB system was found in that the current peaks at around physiological pH, with the effect much prominent in the cathodic versus anodic peaks. From the discussion, since it was speculated that the cathodic peaks were from electrostatic interaction of DNA with MB, while anodic peaks were from intercalation of LB, this suggests that the effect of pH on electrostatically-associated MB is more significant compared to that on intercalated LB.

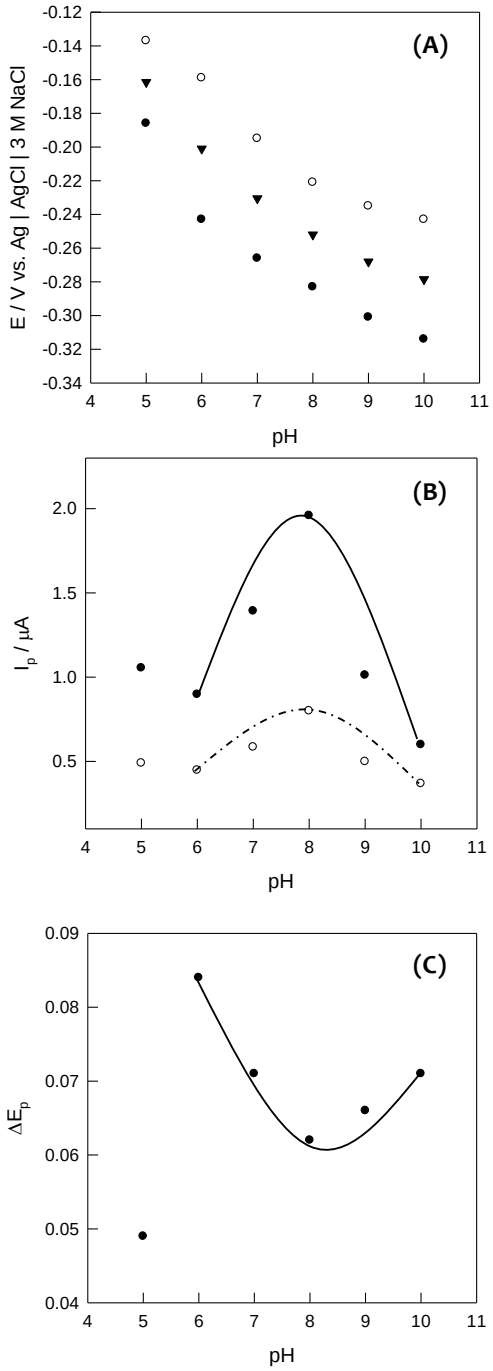

Figure 4-9. Plot of cathodic peak (closed circles), anodic peak (open circles), and formal (triangles) potentials (A), cathodic (closed circles) and anodic (open circles) peak currents (B), and peak potential separation (C) as a function of pH for solution-diffused MB on anti-MUC1 aptamer-immobilized Au electrodes. The curves are drawn to guide the eye only.

Here it is important to discuss the protonation states of LB. Unlike MB, LB ionizes in two steps at pH = 4.5 and pH = 5.9 respectively, corresponding to the protonation of the two tertiary exocyclic amines.[42,43] In a pH range from 4.0 to 6.0, LB is therefore expected to exist in three protonation/ionization states. Therefore, at pH = 5.0, LB is expected to be positively charged, allowing it to have electrostatic interactions with DNA as well. This is reflected by the sudden increase in cathodic peak current at pH = 5.0 versus pH = 6.0. The fact that we have generated another species of LB is shown by the plot of peak separation as a function of pH (Panel C of Figure 4-9). The pH in which the lowest peak separation was observed (pH = 8.0) corresponded to the pH in which the highest peak current was observed – this is reasonable given the fact that the high peak current corresponded to the fastest electron transfer. However, significantly faster electron transfer (smallest peak separation) was observed at pH = 5.0, out of the trend from the pH range from 6.0 to 10.0. This is indicative of an entirely different redox process in which a positively-charged LB is under consideration. These pH variation studies demonstrate that the electrochemistry of the MB/LB pair is highly dependent on the pH. This may have implications in the design of biosensors which utilizes MB as a redox indicator. While most biosensors will utilize pH values near neutrality (to preserve integrity of the analyte [often a protein or peptide]), the pH dependency studies herein demonstrate the importance to consider the protonation states of MB/LB as well for further understanding of the electrochemical behaviours observed.

We further investigate the pH profile of peak potentials compared to theory. From Eq. (9), the dependence of peak potentials on pH should be linear with a theoretical slope (dE/dpH) of -0.05916/n in the pH range where the 2-electron, 1-proton reduction

occurs (i.e. from pH = 6.0 to pH = 10.0). From the method of least-squares linear regression, it was found that perfect linearity was not realized in the MB-tagged system, with calculated coefficient of determinations (R^2) of 0.919, 0.896, and 0.909 for the cathodic, anodic, and formal peak potential variations respectively, as shown in Figure 4-8(A) in the pH range from 6.0 to 10.0. For a $2e^- + 2H^+$ reduction, d*E*/dpH is expected to be -29.58 mV/pH unit. In the cathodic, anodic, and formal peak potential variations with pH, d*E*/dpH was determined to be -23.0 mV/pH, -23.1 mV/pH and -23.0 mV/pH, respectively. This is fairly close to the theoretical value of -29.59 mV/pH. However, in the solution-diffused MB situation (Figure 4-9(A)), although linearity was observed in the pH range from 6.0 to 10.0 (R^2 = 0.991, 0.929, and 0.985 for the cathodic, anodic and peak potential variations with pH), non-optimal d*E*/dpH values were calculated: d*E*/dpH was determined to be -17.7 mV/pH, -20.8 mV/pH, and -18.2 mV/pH, respectively, for the cathodic, anodic and formal potential variations. Substantial deviations from ideality may hint at an inherent complexity in terms of interaction of solution-diffused MB with DNA grafted on Au electrodes. While experiments showed and confirmed the surface confinement of MB molecules on the surface (Figure 4-4), non-ideality from theoretical predictions may stem from the limitation of diffusing protons to the electrode at higher pH, demonstrated by the slight improvement in terms of reversibility at lower pH, as shown in Figure 4-7(B). In general, we may encounter intrinsic complications in the solution-diffused MB system that may limit its capacity for biosensing.

4.2.3 Detection of Mucin 1 by Methylene Blue-Tagged Aptamers

From the cyclic voltammetric considerations of MB-tagged aptamers and solution-diffused MB interacting with aptamers, the latter system is appreciably more

complicated since (1) irreversible redox behaviour was observed, and (2) we are not clear at this stage about the binding modes of free MB to DNA strands on an electrode surface. While both electrostatic and intercalative mechanisms have been popularized previously,[7–9,18–20] our results indicate that both could be possible. These complexities have prompted us to mainly focus on MUC1 detection with the MB-tagged aptamer system. Preliminary studies for the solution-diffused system have been also conducted, but data are not shown. We rationalize that the development of biosensors does not only encompass the art of analyte detection, but also full understanding of the mechanism in which the biosensor functions in order to extend the research efforts to other analytes.

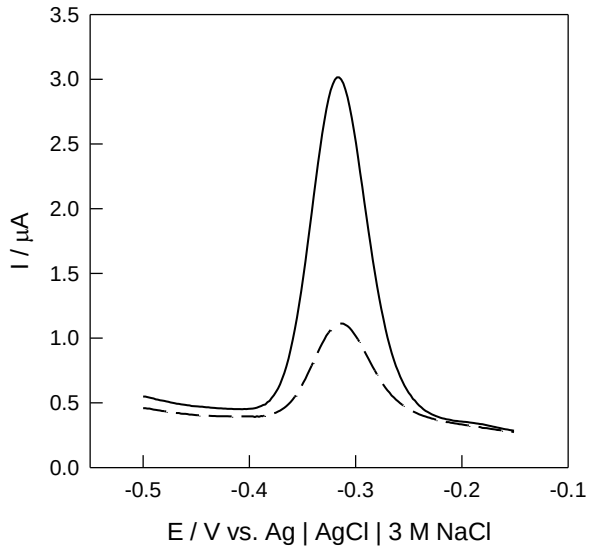

Figure 4-10. Square wave voltammograms of MB-tagged anti-MUC1 aptamers immobilized on a gold surface in 10 mM Tris, 100 mM NaCl, 5 mM $MgCl_2$ at pH 7.4 = before (solid line) and after (dashed line) incubation with 1.0 μM MUC1 peptide.

Shown in Figure 4-10 are square wave voltammograms corresponding to the oxidation process of MB-tethered anti-MUC1 aptamer monolayers on Au electrodes in the absence and presence of 1.0 μM MUC1. As predicted earlier, a decrease in the

current was recorded upon the incubation of MUC1. This can be explained by the altered conformation of the aptamer bringing MB farther from the electrode surface (Chapter 3), for which we expect that the electron transfer rate between MB and the electrode should change upon MUC1 binding. To calculate the electron transfer rate, we resort to Laviron's procedure,[44] where at higher scan rates, the transfer coefficient α and the electron transfer rate *k* can be extracted using the following equations:

$$E_{pa} = E^{\circ\prime} - \left(\frac{RT}{\alpha nF}\right)\ln\left(\frac{\alpha nF\nu}{RTk}\right) \tag{10}$$

$$E_{pc} = E^{\circ\prime} - \left(\frac{RT}{(1-\alpha)nF}\right)\ln\left(\frac{(1-\alpha)nF\nu}{RTk}\right) \tag{11}$$

where E_{pa} and E_{pc} are the anodic and cathodic peak potentials, respectively, $E^{\circ\prime}$ is the formal potential, *v* is the scan rate, and *n* is the number of electrons transferred. *R*, *T*, and *F* have their usual meanings. Eqs. (10) and (11) may be rearranged to Eqs. (12) and (13):

$$E^{\circ\prime} - E_{pa} = \frac{RT}{\alpha nF}\ln\nu + \frac{RT}{\alpha nF}\ln\left(\frac{\alpha nF}{RTk}\right) \tag{12}$$

$$E^{\circ\prime} - E_{pc} = \frac{RT}{(1-\alpha)nF}\ln\nu + \frac{RT}{(1-\alpha)nF}\ln\left(\frac{(1-\alpha)nF}{RTk}\right) \tag{13}$$

to reflect the relationship between $E^{\circ\prime} - E_{pa}$ or $E^{\circ\prime} - E_{pc}$ vs. ln*v*, which is a linear relationship at high scan rates.[44] As shown in Figure 4-11, which shows the Laviron plot of the system in the absence of MUC1, a near linear relationship exists for this plot of $E^{\circ\prime} - E_{pa}$ or $E^{\circ\prime} - E_{pc}$ vs. ln*v* at high scan rates. The slope and y-intercept of the linear region

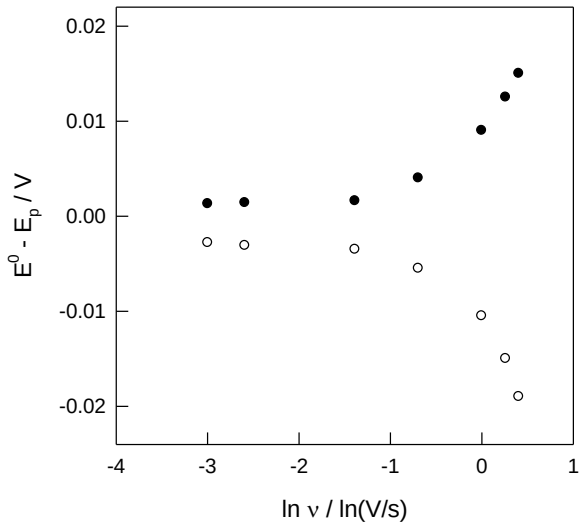

Figure 4-11. Laviron plot for MB-tagged anti-MUC1 aptamers immobilized on a gold surface in 10 mM Tris, 100 mM NaCl, 5 mM $MgCl_2$ at pH = 7.4 before incubation with MUC1. Filled circles represent anodic data, while opened circles represent cathodic data.

may be used to estimate the transfer coefficient α and the electron transfer rate *k*. From the Laviron plot shown in Figure 4-11, the electron transfer rate for the system in the absence of MUC1 construct was 25.5 $\pm$ 5.7 s^{-1}. The electron transfer rate for the system in the presence of 1.0 μM MUC1 was 19.3 $\pm$ 4.8 s^{-1} (Laviron plot not shown). The average value of α was 0.52 $\pm$ 0.09 before analyte binding and 0.49 $\pm$ 0.07 after analyte binding. The similarity in the electron transfer rates suggests similar electron transport mechanisms in the two states; this result is in accord with previous studies by Plaxco, Heeger and coworkers on the use of aptamer-tagged MB for monitoring analyte-induced conformational change.[24] It also explains that the residual signals observed after incubation with 1.0 μM MUC1 was due to the flexibility of the aptamer to transiently undergo electron transfer with the electrode.

The detection sensitivity and selectivity was evaluated by plotting the concentration of MUC1 peptides as a function of the sensor signal, given by $\Delta I/I_i$, the change in the oxidative current divided by the initial measured current before the addition of MUC1 peptides. This plot is shown in Figure 4-12(A). Saturation of the signal was observed at concentrations of MUC1 peptide higher than 0.5 μM. The signal decrease saturated at a sensor signal of approximately 0.7, indicative of residual current exhibited by MB. As mentioned, this can be understood by the inherent flexibility of ssDNA on Au electrodes. Addition of lysozyme, cytochrome c, and BSA (bovine serum albumin), at concentrations where the sensor signal for MUC1 was approximately 0.6, resulted in minimal responses. Another control experiment was performed in which a non-aptamer-containing bifunctional ssDNA (one end derivatized with -SH for SAM formation, the other end tagged with MB) was used. Negligible changes in oxidative current were observed before and after the addition of MUC1 (data not shown). The two current detection methodologies for MUC1 rely on ELISA (enzyme-linked immunosorbent assay) with samples diluted to a serum concentration of 2%.[45–48] As shown in Figure 4-12(A), diluting MUC1 peptides in 2% serum still resulted in quantitative response, demonstrating the potential of this sensor for biomedical and clinical testing. From the figure, a detection limit of 25 nM was observed, which guarantees a signal-to-noise ratio of at least 3.0. This is an improvement over both our previously reported quantum dot-based optical detection method (Chapter 3) with a detection limit of 250 nM,[36] as well as current ELISA methodologies with a detection limit of 0.8 μM.[45–48]

A linearized form of the Langmuir curve can be used to extract the dissociation constant K_D between the aptamer and the analyte:

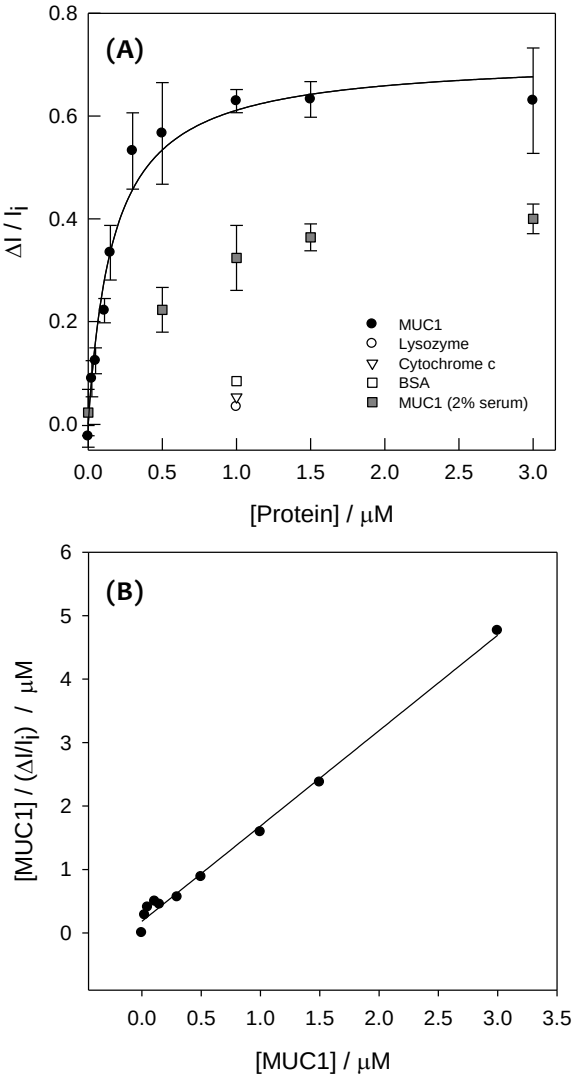

Figure 4-12. (A) The sensor signal by $\Delta I/I_i$ as a function of the concentration of MUC1 peptides. The solid line is a non-linear regression assuming a Langmuir isotherm. The sensor signal upon the addition of lysozyme (open circles), cytochrome c (open triangles), bovine serum albumin (open squares), as well as MUC1 peptides dissolved in 2% calf serum in 10 mM Tris, 100 mM NaCl, 5 mM $MgCl_2$, pH = 7.4 (filled squares) are shown. The uncertainty refers to the standard deviation in 5 representative trials each; (B) Linearized adsorption isotherm of MUC1 peptide binding to MB-tagged anti-MUC1 aptamers on gold electrodes based on the Langmuir model. The line is the best linear fit to the experimental data (method of least-squares) from which the dissociation constant K_D was determined.

$$\frac{C}{\Delta I / I_i} = \frac{C}{[\Delta I / I_i]_{sat}} + \frac{K_D}{[\Delta I / I_i]_{sat}} \quad (9)$$

where C is the concentration of MUC1 peptides, K_D is the dissociation constant, $\Delta I/I_i$ is the sensor signal, and $[\Delta I/I_i]_{sat}$ is the saturated or maximum sensor signal. The the concentration divided by the sensor signal $[C / (\Delta I/I_i)]$ may be plotted as a function of the concentration of MUC1 peptides (C). The linearized form of the Langmuir isotherm is shown on Panel B of Figure 4-12. From the y-intercept and the slope, the $[\Delta I/I_i]_{sat}$ term and the K_D was extracted to be 0.7145 and 168 $\pm$ 30 nM respectively. This dissociation constant is smaller than that for our previously reported optical-based detection method (1.62 ± 0.28 μM),[36] which is consistent with the fact that a lower detection limit was also observed (25 nM versus 250 nM).

While data are not shown, decrease in oxidation current was also observed when the solution-diffused MB system was added with MUC1 peptides. We indicate that the detection of MUC1 with the solution-diffused MB system is poorer compared to the MB-tagged system. A detection limit of 50 nM was observed with an aptamer-analyte dissociation constant of 428 $\pm$ 75 nM (data not shown). Detection was not possible in the presence of 2% serum which may indicate that the system responds strongly to adsorbed proteins on the working electrode. Response to lysozyme and cytochrome c (as negative controls) was also more prominent compared to the MB-tagged aptamer case. It definitely seems that this system is less useful for biosensing compared to the methylene blue-tethered aptamer-based system.

4.3 Conclusion

In summary, we have evaluated the applicability of two different MB labeling approaches (covalently tethered and electrostatic/intercalative bound) for biosensing. In the former variation of MB-based electrical biosensors, detection of MUC1 was observed by alteration in the redox properties of aptamer-tagged MB upon analyte binding-induced conformational change which brings the MB moiety farther away from the electrode. The pH dependency studies using cyclic voltammetry showed the possibility of association of tagged-MB directly with the backbone via the flexibility C7 linker. A detection limit of 25 nM was achieved with an aptamer-analyte dissociation constant of 168 ± 30 nM. In the latter variation of MB-based electrical biosensors, it was clear that the redox behaviour of MB/LB was influenced by the complex binding modes between the redox markers and the DNA strands on the Au surface. Further experiments are warranted to fully understand the interaction of MB with DNA in the hope of fully applying this system for other protein biomarkers for which aptamers are available.

4.4 Experimental Section

4.4.1 Materials

The synthetic anti-MUC1 oligonucleotides (sequence designed by Ferreira et al.[31]) HO-$(CH_2)_6$-S-S-$(CH_2)_6$-O-5′-GCA GTT GAT CCT TTG GAT ACC CTG G-3′-C7-NHCO-$(CH_2)_3$-MB, HO-$(CH_2)_6$-S-S-$(CH_2)_6$-O-5′-GCA GTT GAT CCT TTG GAT ACC CTG G-3′, and control oligonucleotides HO-$(CH_2)_6$-S-S-$(CH_2)_6$-O-5′-ATC AAG GTG GGG GAT GGC TAA A -3′-C7-NHCO-$(CH_2)_3$-MB, HO-$(CH_2)_6$-S-S-$(CH_2)_6$-O-5′-ATC AAG GTG GGG GAT GGC TAA A -3′ were purchased from Biosearch Technologies, Inc. (Novato, AB) and the Core DNA Services, Inc (Calgary, AB). The MUC1 peptide

with two repeats of the 20 amino acid variable tandem repeat region (from the N terminus to the C terminus: PDTRPAPGSTAPPAHG-VTSAPDTRPAPGSTAPPAHGVTSA) was purchased as a custom synthetic peptide from the University of British Columbia Brain Research Centre (Vancouver, BC). Gold substrates (regular glass slides first covered with 5-nm Cr, followed by 100-nm Au) were purchased from Evaporated Metal Films (EMF) Inc. (Ithaca, NY); calf serum, the bicinchoninic acid (BCA) assay kit, 6-mercapto-1-hexanol (MCH), hexaammine ruthenium (III) chloride (98%), methylene blue (98%), hen egg white lysozyme (95%), equine heart cytochrome c (95%) and bovine serum albumin (98%) were from Sigma-Aldrich (Milwaukee, WI). Deionized water (> 18.3 Ω cm) was produced from a Barnstead EasyPure UV/UF compact water system (Dubuque, IA).

4.4.2 DNA Preparation and Protein/Peptide Preparation

Disulfide-modified oligonucleotides were treated with 10 mM TCEP (triscarboxyethylphosphine) in 100 mM Tris at pH 7.4 overnight and desalted through a MicroSpin G-50 column (G-50 Sephadex) to yield in single-stranded (ss) thiol-terminated DNA. The purified anti-MUC1 aptamer was then heated to 80 ℃ and allowed to slowly cool to room temperature in immobilization buffer (10 mM Tris-HCl, 100 mM NaCl, 5 mM $MgCl_2$ at pH 7.4). This heating and cooling step is a necessary step (based on thermodynamics) to maintain the structural flexibility of the aptamers (for binding MUC1). The control oligonucleotide was immobilized by heating and cooling in the same way. The MUC1 peptide was purified by reverse-phase HPLC on a Gemini 5-μm C18/110 Å column (Phenomenex, Torrance, CA), eluting with a gradient of acetonitrile containing 0.1% trifluoroacetic acid:water (0 – 60%) at a flow rate of 1.0 mL/min. The

peptide sample was lyophilized and dissolved in water. MALDI-TOF (matrix assisted laser desorption ionization, time of flight) spectroscopy was used to verify the molecular weight of the peptide. A saturated mixture of the CHCA matrix was made in a 1:1 mixture of acetonitrile:water containing 0.1% trifluoroacetic acid. Approximately 0.25 mg of purified peptide was dissolved in 5 μL of water and added to 5 μL of the aforementioned CHCA mixture. Peptide/protein concentration was determined with the BCA assay using bovine serum albumin as a standard.

4.4.3 Electrode/Substrate Preparation and Immobilization

The gold slides were cleaned by immersion in "piranha" solution (3:1 mixture of concentrated H_2SO_4 and 30% H_2O_2) for 5 minutes at 90 ℃, followed by a rinse with copious amounts of deionized water. *CAUTION: piranha reacts violently with organic solvents, and should be handled with extreme caution.* The gold chips were then dried with N_2. The thiol-terminated ssDNA strands were immobilized on the cleaned gold substrate by spreading a 20 μL droplet of aptamer in immobilization buffer for 12 hours at 100% humidity. After modification, the gold slides were rinsed with immobilization buffer again, followed by incubation for 1 hour in 1 mM MCH (in immobilization buffer) to remove non-specific DNA adsorption on the gold surface. The gold slides were rinsed again with immobilization buffer then with deionized water, followed by drying with a stream of N_2 before electrochemical characterization.

For the detection procedure, a 20 μL droplet of MUC1 of various concentrations in immobilization buffer were deposited onto the DNA-modified gold electrode and kept for 1 hour. The sample was then rinsed in 10 mM Tris, 100 mM NaCl, 5 mM $MgCl_2$ at pH 7.4 before electrochemical characterization.

4.4.4 Electrochemical Measurements

Cyclic voltammetric and square wave voltammetric measurements were performed with a μAutolab II potentiostat / galvanostat (EcoChemie B.V., Utrecht, Netherlands) using a single-compartment, three-electrode Teflon cell. The working electrodes, DNA-modified gold slides, were pressed against an O-ring seal at the cell bottom (with an exposed area of 0.66 cm^2). A Ag | AgCl | 3 M NaCl electrode was used as the reference, and a Pt wire as the counter electrode.

Electrochemical measurements of DNA-modified electrodes were performed in 2.0 μM methylene blue in 10 mM Tris-HCl, 100 mM NaCl, 5 mM $MgCl_2$ at pH 7.4 for aptamer-modified Au electrodes, in 10 mM Tris-HCl, 100 mM NaCl, 5 mM $MgCl_2$ at pH 7.4 for methylene blue-tagged aptamer-modified Au electrodes, and in degassed 5 μM $[Ru(NH_3)_6]Cl_3$ in 10 mM Tris-HCl buffer at pH 7.41 (after incubation in the same solution for 15 min) for surface density measurements.

4.5 References

1. Forbes, B. A.; Sahm, D. F.; Weissfeld, A. S. *Bailey & Scott's Diagnostic Microbiology*; Eleventh Edition, Mosby: **2002**.
2. Gillman, P. K. *Can. J. Anaesth.* **2008**, *55*, 311 – 312.
3. Schirmer, H.; Coulibaly, B.; Stich, A. Scheiwein, M.; Merkle, H.; Eubel, J.; Becker, K.; Becher, H.; Muller, O.; Zich, T.; Schiek, W.; Kouyate, B. *Redox Rep.* **2003**, *8*, 272 – 276.
4. Brooks, M. M. *The Scientific Monthly* **1936**, *43*, 585 – 586.

5. (a) Campbell, J. A. *J. Chem. Educ.* **1963**, *40*, 578 – 583. (b) Vandaveer, W. R., IV, Mosher, M. *J. Chem. Educ.* **1997**, *74*, 402. (c) Cook, A. G.; Tolliver, R. M.; Williams, J. E. *J. Chem. Educ.* **1994**, *71*, 160 – 161.

6. Hulanicki, A.; Glab, S. *Pure Appl. Chem.* **1978**, *50*, 463 – 498.

7. Tuite, E.; Kelly, J. M. *Biopolymers* **1995**, *35*, 419 – 433.

8. Tuite, E.; Nordén, B. *J. Am. Chem. Soc.* **1994**, *116*, 7548 – 7556.

9. Nordén, B.; Tjerneld, F. *Biopolymers* **1982**, *21*, 1713 – 1734.

10. Kelley, S. O.; Barton, J. K. *Bioconjugate Chem.* **1997**, *8*, 31 – 37.

11. Kelley, S. O.; Boon, E. M.; Barton, J. K.; Jackson, N. M.; Hill, M. G. *Nucleic Acids Res.* **1999**, *27*, 4830 – 4837.

12. Millan, K. M.; Mikkelsen, S. R. *Anal. Chem.* **1993**, *65*, 2317 – 2323.

13. Millan, K. M.; Saraullo, A.; Mikkelsen, S. R. *Anal. Chem.***1994**, *66*, 2943 – 2948.

14. Mikkelsen, S. R.; Millan, K. M.; Spurmanis, A. J. *US5312527* **1994**.

15. Yu, H.-Z.; Luo, C-Y; Sankar, C. G.; Sen, D. *Anal. Chem.* **2003**, *75*, 3902 – 3907.

16. Su, L.; Sankar, C. G.; Sen, D.; Yu, H.-Z. *Anal. Chem.* **2004**, *76*, 5953 – 5959.

17. Cheng, A. K. H.; Ge, B.; Yu, H.-Z. *Anal. Chem.* **2007**, *79*, 5158 – 5164.

18. Erdem, A.; Kerman, K.; Meric, B.; Ozsoz, M. *Electroanalysis* **1999**, *11*, 586 – 587.

19. Erdem, A.; Kerman, K.; Meric, B.; Akarca, U. S.; Ozsoz, M. *Anal. Chim. Acta* **2000**, *422*, 139 – 149.

20. Yang, W.; Ozsoz, M.; Hibbert, D. B.; Gooding, J. J. *Electroanalysis* **2001**, *14*, 1299 – 1302.

21. Gooding, J. J. *Electroanalysis* **2002**, *14*, 1149 – 1156.

22. Ellington, A. D.; Szostak, J. W. *Nature* **1990**, *346*, 818 – 822.

23. Tuerk, C.; Gold, L. *Science* **1990**, *249*, 505 – 510.

24. Xiao, Y.; Piorek, B. D.; Plaxco, K. W.; Heeger, A. J. *J. Am. Chem. Soc.* **2005**, *127*, 17990 – 17991.

25. Bock, L. C.; Griffin, L. C.; Latham, J. A.; Vermaas, E. H.; Toole, J. J. *Nature* **1992**, *335*, 564 – 566.

26. Lai, R. Y.; Plaxco, K. W.; Heeger, A. J. *Anal. Chem.* **2007**, *79*, 229 – 223.

27. Baker, B. R.; Lai, R. Y.; M. S. Wood; Doctor, E. H. Heeger, A. J.; Plaxco, K. W. *J. Am. Chem. Soc.* **2006**, *128*, 3138 – 3139.

28. Ferapontova, E. E.; Olsen, E. M.; Gothelf, K. V. *J. Am. Chem. Soc.* **2008**, *130*, 4256 – 4258.

29. Wang, J.; Wang, F.; Dong, S. *J. Electroanal. Chem.* **2009**, *626*, 1 – 5.

30. (a) Beatty, P.; Hanisch, F.-G.; Stolz, D. B.; Finn, O. J.; Ciborowski, P. *Clin. Cancer Res.* **2001**, *7*, 781s – 787s. (b) Croce, M. V.; Isla-Larrain, M. T.; Demichelis, S. O.; Gori, J. R.; Price, M. R.; Segal-Eiras, A. *Breast Cancer Res. Treat.* **2003**, *81*, 195 – 207.

31. Ferreira, C. S. M.; Matthews, C. S.; Missailidis, S. *Tumor Biol.* **2006**, *27*, 289 – 301.

32. Turro, N.; Barton, J. K. *J. Biol. Inorg. Chem.* **1998**, *3*, 201 – 209.

33. Nunez, M.; Hall, D. B.; Barton, J. K. *Chem. Biol.* **1999**, *6*, 85 – 97.

34. Henderson, P. T.; Jones, D.; Hampikian, G.; Kan, Y.; Schuster, G. B. *Proc. Natl. Acad. Sci. USA* **1999**, *96*, 8353 – 8358.

35. Meggers, E.; Michel-Beyerle, M. E.; Giese, B. *J. Am. Chem. Soc.* **1998**, *120*, 12950 – 12955.

36. Cheng, A. K. H.; Su, H.; Wang, Y. A.; Yu, H.-Z. *Anal. Chem.* **2009**, *81*, In Press.

37. Herne, T. M.; Tarlov, M. J. *J. Am. Chem. Soc.* **1997**, *119*, 8916 – 8920.

38. Levicky, R.; Herne, T. M.; Tarlov, M. J.; Satija, S. K. *J. Am. Chem. Soc.* **1998**, *120*, 9787 – 9792.

39. Bard, A. J.; Faulkner, L. R. *Electrochemical Methods: Fundamentals and Applications*, Second edition; John Wiley & Sons: New York, **2001**.

40. Bloomfield, V. A.; Crothers, D. M.; Tinocco, I. J. *Nucleic Acids – Structures, Properties and Functions*, University Science Book: Sausalito, California, **2000**.

41. Murthy, A. S. N.; Reddy, K. S. *J. Chem. Soc., Faraday Trans. 1* **1984**, *80*, 2745 – 2750.

42. Obata, H. *Bull. Chem. Soc. Jpn.* **1961**, *34*, 1057 – 1063.

43. Hoffmann, A. A.; Dias, S. L. P.; Rodrigues, J. R.; Pavan, F. A.; Benvenutti, E. V.; Lima, E. C. *J. Braz. Chem. Soc.* **2008**, *19*, 943 – 949.

44. Laviron, E. *J. Electroanal. Chem.* **1979**, *101*: 19.

45. Bon, G. G.; von Mensdorff-Pouilly, S.; Kenemans, P. van Kamp, G. J.; Verstraeten, R. A.; Hilgers, J.; Meijer, S.; Vermorken, J. B. *Clin. Chem.* **1997**, *43*, 585 – 593.

46. Jezersek, B.; Cervek, J.; Rudolf, Z.; Novakovic, S. *Cancer Letters* **1996**, *110*, 137 – 144.

47. Price, M. R.; Hudecz, F.; O'Sullivan, C.; Baldwin, R. W.; Edwards, P. M.; Tendler, S. J. B. *Mol. Immunol.* **1990**, *27*, 795 – 802.

48. Reddish, M. A.; Helbrecht, N.; Almeida, A. F.; Madiyalakan, R.; Suresh, M. R.; Longenecker, B. M.; *J. Tumor Marker Oncol.* **1992**, *7*, 19 – 27.

CHAPTER 5

PRELIMINARY INVESTIGATIONS TOWARDS FUSION APTAMER-BASED ALLOSTERIC REGULATION FOR SOLUTION DETECTION OF MUCIN 1

In the last two chapters, we have shown the development of novel sensors for the specific detection of mucin 1 (MUC1) peptides via the binding affinity of anti-MUC1 DNA aptamers. Significant improvement in the detection limits was achieved when the detection was transformed from an optical system (Chapter 3) to an electrochemical approach using MB (methylene blue) labeling (Chapter 4). However, in neither case, the "ideal" detection limit inferred by the aptamer-analyte binding constant has been realized. The purpose of this chapter is to propose and provide experimental details-in-progress of an optical-based system for the detection of MUC1 with hopefully improved sensitivity with the aid of allosteric regulation. Briefly, allosteric regulation is the up- or down-regulation of a biological process (i.e. binding event, or protein activity) by a secondary molecule. By fusing anti-thrombin aptamer sequences with anti-MUC1 aptamer sequences, we hope to develop optical biosensors for MUC1 via the allosteric regulation of the proteolytic activity of α-thrombin activity using MUC1 as an upregulating effector molecule.

5.1 Introduction

In biochemistry, allostery is the regulation of an enzyme or protein by the binding of an effector molecule at the protein's allosteric site.[1] There are two main types of allosteric regulators: allosteric activators (where the binding event of the effector molecule increases the activity of the protein) and allosteric inhibitors (where the binding event of the effector molecule decreases the activity of the protein). Probably the most famous example of allosteric activation is the total conformational change of one subunit of haemoglobin upon the binding of oxygen on the Fe-containing active site.[1] Doing so induces the polymerization of adjacent subunits and enhances their affinities to oxygen, promoting the assembly of the tetra-subunit haemoglobin.

Considering the converse, allosteric regulation by inhibition is also prominent. Strychnine is an allosteric inhibitor of glycine,[2,3] which is a known post-synaptic inhibitory neurotransmitter in the mammalian spinal cord and brain stem.[4] Strychnine has the ability to bind post-synaptic glycine receptors on a secondary site to inhibit the binding of glycine on the glycine receptor.[2] Doing so reduces the frequency of inhibitory post-synaptic transmissions, thus leading to brain convulsions.

Since the revolutionary introduction of DNA and RNA aptamers as recognition devices in the last decade,[5,6] the attempt for aptamer-based allosteric regulation was considered. Soukup and Breaker considered the fusion of the anti-theophylline RNA aptamer sequence with that of the hammerhead ribozyme in an attempt to develop allosterically activating hammerhead ribozyme constructs using theophylline as an effector molecule.[7–10] Furthermore, the authors evolved a variant of the ribozyme that can exhibit specificity to derivatives of theophylline such as 3-methylxanthine.[11]

Recent efforts for nucleic acid-based allosteric regulation were exemplified by the use of both nucleic acids and proteins as allosteric effector molecules. In the former, an aptamer-based biosensor (a targeted reversibly attenuated probe, TRAP) was developed in which the ability of the aptamer to bind its analyte was dependent on the availability of an effector nucleic acid.[12] The central regime of the TRAP can bind a complementary nucleic acid (regNA, or regulatory nucleic acid) which can regulate the binding activity of the aptamer. The method was demonstrated successfully for the allosteric aptamer-based detection of ATP.[12] In the latter, the hairpin ribozyme was modified to include a specialized effector region.[13] The secondary structure of the original hairpin ribozyme contains two internal loop domains, A and B, each of them flanked by two helices that must interact to permit the site-specific cleavage to generate the 5′-hydroxyl and 2′,3′-cyclic phosphate.[14–17] In the design of Najafi-Shousahtari *et al.*, a third regulatory domain was added that is complimentary to a functional DNA, namely the anti-thrombin aptamer.[13] The presence of this sequence defines/guarantees the activity of the ribozyme to rely on the hybridization of the thrombin aptamer to the RNA complementary C domain. The presence of thrombin, which acts as an allosteric activator, neutralizes this effect and triggers the ribozyme to be catalytically active.

In the present scheme, DNA aptamers corresponding to anti-MUC1 sequences and anti-thrombin sequences were fused together – more specifically anti-MUC1 sequences were "inserted" into various positions along the primary sequence of the anti-thrombin sequence. This was done in the hope for allosteric regulation for thrombin with MUC1 as the effector molecule. The anti-MUC1 aptamer will be inserted in such as way such that the entire length of the aptamer will be mostly preserved to guarantee

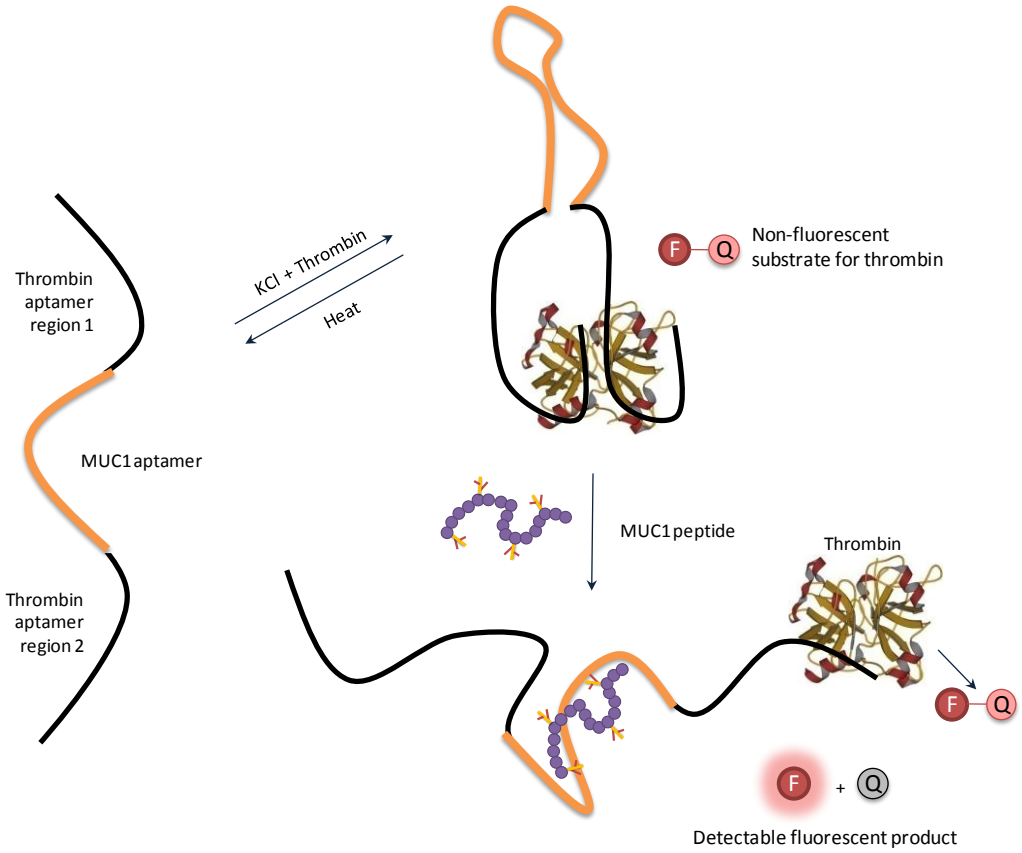

Figure 5-1. Schematic representation for allosteric regulation-controlled aptamer-based detection of MUC1. In this scheme, allosteric regulation for thrombin activity is controlled by MUC1 as the effector molecule. See text for details.

maximum binding capability to MUC1 peptides. On the other hand, the anti-thrombin aptamer will be interrupted at particular positions by the anti-MUC1 aptamer, but hopefully will still retain the ability to bind thrombin in sufficient quantities. Intense optimization of the constructs will use these two criteria as the starting point.

The overall scheme of detection is shown in Figure 5-1. In the presence of physiological salt and in the absence of MUC1 peptides, there will be preferential folding of the fusion aptamer construct to its G-quartet conformation,[18] in preparation for binding with thrombin. Upon doing so, the proteolytic activity of thrombin will be inhibited and

will thus be unable to cleave a non-fluorescent substrate bis-(p-tosyl-L-glycyl-L-prolyl-L-arginine amide) Rhodamine 110 (denoted F-Q) to a fluorescent product.[19] Upon the addition of MUC1, the peptide will act as an allosteric effector molecule since it has preferential binding to the fusion aptamer (this will come from optimization of the fusion aptamer construct, which involves retaining the entire anti-MUC1 sequence but interrupting the anti-thrombin sequence). This will result in the unfolding of the G-quartet conformation, thus releasing thrombin. The proteolytic activity of thrombin will then be restored and detectable fluorescence will be observed.

5.2 Results and Discussion

5.2.1 Insertion into the Anti-Thrombin Aptamer at Position G_8

To generate functional fusion aptamers, appreciable optimization was first performed to design for constructs of particular sequences (with anti-MUC1 aptamer sequences inserted into various positions in the anti-thrombin aptamer sequence). Insertion must happen to fulfill three conditions: (1) the two aptamers do *not* behave independently of each other (i.e. the binding of either analytes to its respective aptamer *does* affect the ability for the other analyte to bind its respective aptamer); (2) the fusion aptamer has the ability to bind and inhibit the proteolytic activity of thrombin; and (3) the binding efficiency of the fusion aptamer for MUC1 is higher than that of thrombin. As a starting point, we analyze the primary and secondary structure of the anti-thrombin aptamer. The aptamer, at its simplest form, is a 15-nucleotide single-stranded DNA oligonucleotide.[18] In the presence of KCl, it has the ability to fold into an antiparallel G-quadruplex, as shown in Panel A of Figure 5-2.

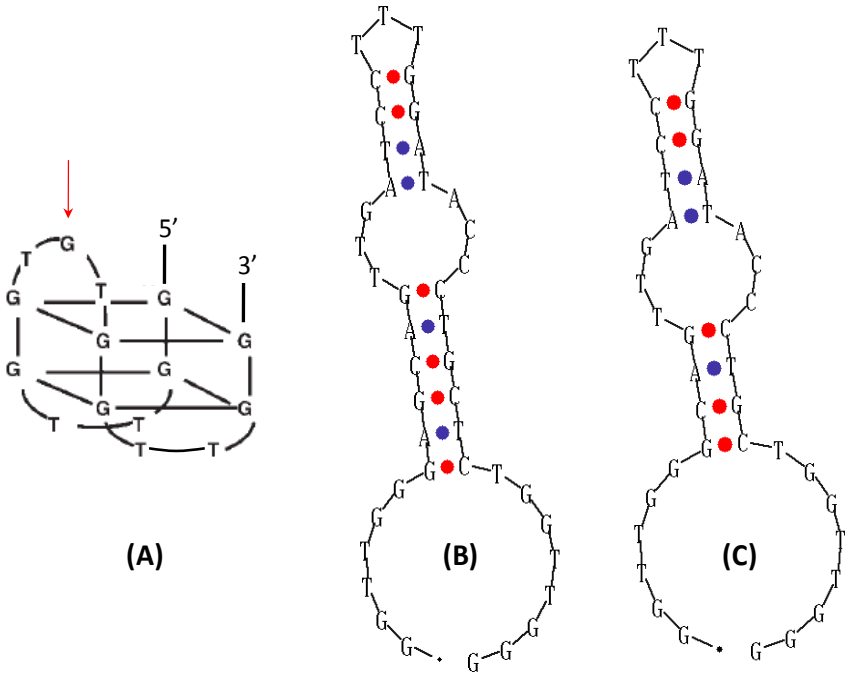

Figure 5-2. Primary sequence of (A) the anti-thrombin aptamer at its simplest form, and (B) Th-MUC1-Ap38-01 and (C) Th-MUC1-Ap42-02, both of which with anti-MUC1 sequences inserted in position G_8 of the anti-thrombin aptamer, shown by the red arrow. Some alterations in sequence were made as part of the optimization process.

Positions with the most potential for insertion of anti-MUC1 aptamer sequences are naturally those that are not involved in Hoogsteen hydrogen bonding to form G-quartets: T_3, T_4, T_7, G_8, T_9, T_{12} and T_{13}. We chose G_8 as a starting point (as shown by the arrow in Figure 5-2) by inserting the anti-MUC1 aptamer sequence at the G_8 position to generate two constructs, Th-MUC1-Ap38-01 and Th-MUC1-Ap42-02, both of which containing variable numbers of Watson-Crick base pairs in a stem region between the two aptamers. Their primary sequences are shown in Panel B and C of Figure 5-2. These constructs were designed this way as an attempt to understand the interaction of two fused aptamers in their linker regions – that is, to evaluate the number of base pairs

required to allow for sufficient communication between the two regimes as well as dependency in the binding of both analytes. To evaluate the ability for the fusion aptamers to bind the analytes of choice, we first performed dimethyl sulfate (DMS) chemical protection assays, to verify the ability of the fusion aptamers to fold accurately into anti-parallel G-quadruplexes, thus retaining the ability to bind thrombin. Since we have inserted the anti-MUC1 aptamer into the anti-thrombin aptamer (and not vice versa), it is reasonable to believe that functional fusion aptamers will have a more difficult time folding accurately to bind thrombin than to bind MUC1. Accurate folding of the fusion aptamers to form G-quartets will result in protection of guanines involved in G-quartet formation (G_1, G_2, G_5, G_6, G_{10}, G_{11}, G_{14}, G_{15}) upon incubation with DMS, which methylates guanine residues *not* involved in Hoogsteen hydrogen bonding.[20] Treatment with piperidine will result in cleavage of damaged (e.g. methylated) guanine residues, and the cleavage pattern can be resolved with a sequencing gel.[20] DMS protection assays on Th-MUC1-Ap38-01 and Th-MUC1-Ap42-02 were performed under four conditions: in TE (10 mM Tris-HCl, 100 μM EDTA, pH = 7.4) buffer, in 1 M NaCl, in 1 M KCl, and in 1 M LiCl. While KCl and NaCl are known to promote the formation of G-quadruplexes by chelating at the centre of G-quartets (K^+ is better than Na^+ in general), Li^+ and the presence of no salt is known to inhibit the formation of G-quadruplexes.[22] Shown in Figure 5-3 is a 12% sequencing polyacrylamide gel of the piperidine cleavage pattern of the two DMS-modified fusion aptamers under the four salt conditions.

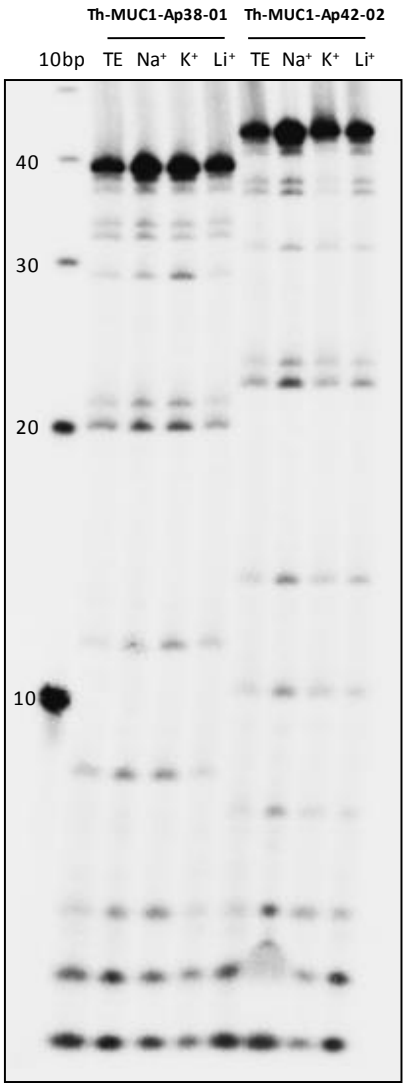

Figure 5-3. 12% sequencing polyacrylamide gel of DMS-modification pattern of Th-MUC1-Ap38-01 and Th-MUC1-Ap42-02 in TE buffer, 1 M NaCl, 1 M KCl and 1 M LiCl.

From Figure 5-3, it is clear that there are no salt species-dependency on the cleavage pattern of guanines in Th-MUC1-Ap38-01 and Th-MUC1-Ap42-02. If G-quartet formation did occur, one would expect to see protection from DMS methylation on guanine residues expected to form quartets especially under the 1 M KCl condition. Unfortunately this was not observed for Th-MUC1-Ap38-01 and Th-MUC1-Ap42-02.

One possible reason to explain the failure observed in these two fusion aptamers was in the geometry of the anti-thrombin aptamer region, which was altered upon modification at the G_8 position. What was originally a clean 3-nucleotide (GTG) loop would now become much more messy with the insertion of a 25 nucleotide anti-MUC1 aptamer sequence, along with linker regions. Other options were sought, in particular in the design of other constructs with insertion of the anti-MUC1 aptamer at a different position.

5.2.2 Insertion into the Anti-Thrombin Aptamer Between Positions T_{12} and T_{13}

In both 2004 and 2005, Ikebukuro *et al.* also performed experiments on fusion aptamers with thrombin.[22,23] Specifically, they fused the anti-thrombin aptamer sequence with that of the anti-adenosine aptamer sequence. As mentioned in Chapter 1, binding of two molecules of adenosine to its aptamer typically results in rectification of an otherwise floppy or unstable secondary structure, via purine-purine interactions.[24] In the case of Ikebukuro *et al.* the anti-adenosine aptamer was inserted between T_{12} and T_{13}. The advantage of doing this was that the overall geometry of the anti-thrombin aptamer could be maintained with "extensions" emanating from the T_{12} and T_{13} positions corresponding to the sequence of the secondary aptamer. In their results, Ikebukuro *et al.* showed that the addition of adenosine stabilizes the fusion aptamer system, allowing thrombin to bind, and thus inhibiting thrombin activity.[22,23] Note that this trend is exactly opposite from what we expect for MUC1 due to the nature of the analyte-aptamer interaction in the secondary aptamer. They also added additional stabilization base pairs before G_1 and after G_{15} as forms of stabilization of the anti-thrombin aptamer after insertion with the secondary aptamer. Since known success was observed with these optimized sequences, we proceeded to design fusion aptamers of thrombin and MUC1 with these conditions.

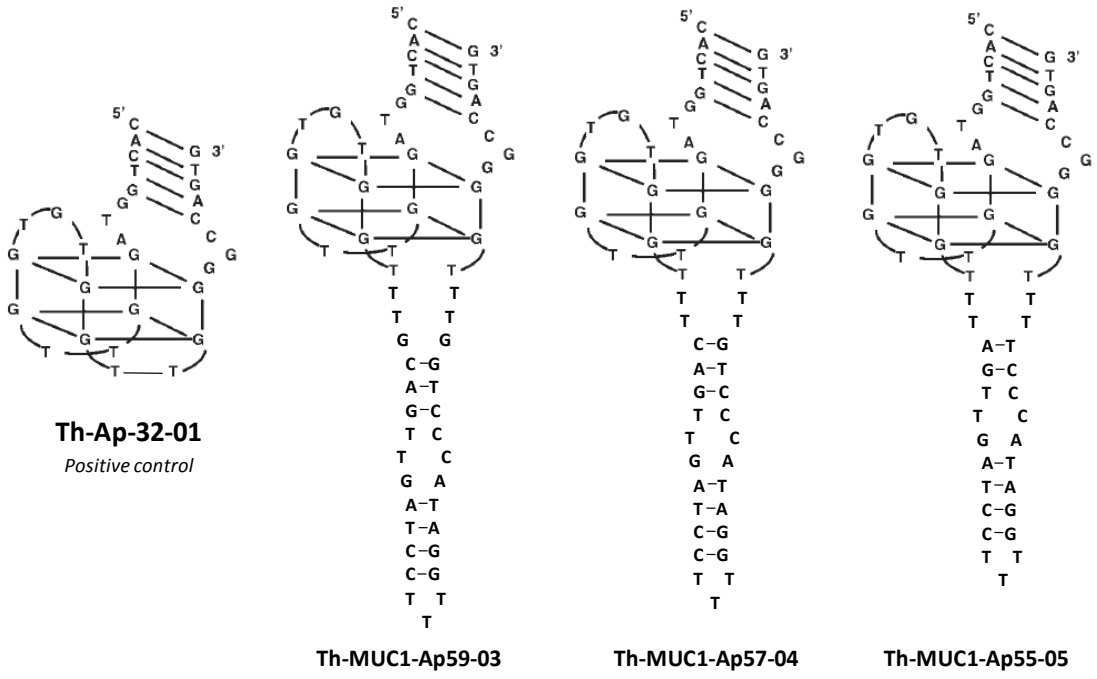

Figure 5-4. Primary sequence and predicted secondary structures for fusion aptamers Th-MUC1-Ap59-03, Th-MUC1-Ap57-04, and Th-MUC1-Ap55-05. Th-Ap32-01 was used a positive control containing only anti-thrombin aptamer sequences.

Shown in Figure 5-4 are the primary sequences and predicted secondary structures for four constructs. For subsequent construct optimization and testing, we decided to include Th-Ap32-01, which is just the anti-thrombin aptamer sequence with the additional stabilization base pairs before and after G_1 and G_{15} respectively. This construct will primarily serve as a positive control for both binding of thrombin and formation of G-quartets. Three fusion aptamer constructs were designed, each with varying numbers of base pairs and lengths in the linker region between the two aptamers. Optimization was for the selection of the best construct in terms of efficient "cross-talk" between the two domains, as well as the inability of the two aptamers to act independently of each other. As with Th-MUC1-Ap38-01 and Th-MUC1-Ap42-02,

sequencing gels were run to determine the ability of the three constructs to form G-quartets. We present on Panel A of Figure 5-5 a 12% sequencing polyacrylamide gel for the DMS chemical protection patterns of Th-Ap32-01, Th-MUC1-Ap59-03, Th-MUC1-Ap57-04, and Th-MUC1-Ap55-05. As shown for the lanes corresponding to Th-Ap32-01, very good protection of guanines was observed when the construct was incubated with 1 M KCl. Other salt species had the same effect as that of adding no salt (TE buffer): very little protection was observed. This result validates the ability of Th-Ap32-01 to act as a positive control for G-quartet formation. As for the remaining three fusion aptamer constructs, the addition of 1 M KCl had negligible effect on Th-MUC1-Ap57-04 as similar protection patterns were observed when the same construct was incubated with 1 M NaCl or 1 M LiCl. This result was unlike that for Th-MUC1-Ap59-03 and Th-MUC1-Ap55-05 which saw significant DMS protection in the presence of 1 M KCl. As part of the optimization process, care was taken such that equal ^{32}P counts per second (cps) were loaded onto each lane. The densitometric intensity value of guanine damage at G-quartet forming guanines in the presence of KCl was compared to that of the same guanine in TE buffer. In general, significantly higher DMS chemical protection was observed for Th-MUC1-Ap55-05 over Th-MUC1-Ap59-03, which allowed us to choose Th-MUC1-Ap55-05 as the fusion aptamer for further consideration. However, optimization of salt concentration is necessary if this fusion aptamer were to act as a biosensor for MUC1, since higher salt concentrations (such as 1 M KCl) may have unpredictable effects on the stability of both thrombin as well as MUC1. Considering the selection conditions for MUC1 (100 mM NaCl, 5 mM $MgCl_2$, pH = 7.4),[25] as well as thrombin's necessity for KCl, it was decided to evaluate the extent of G-quartet formation

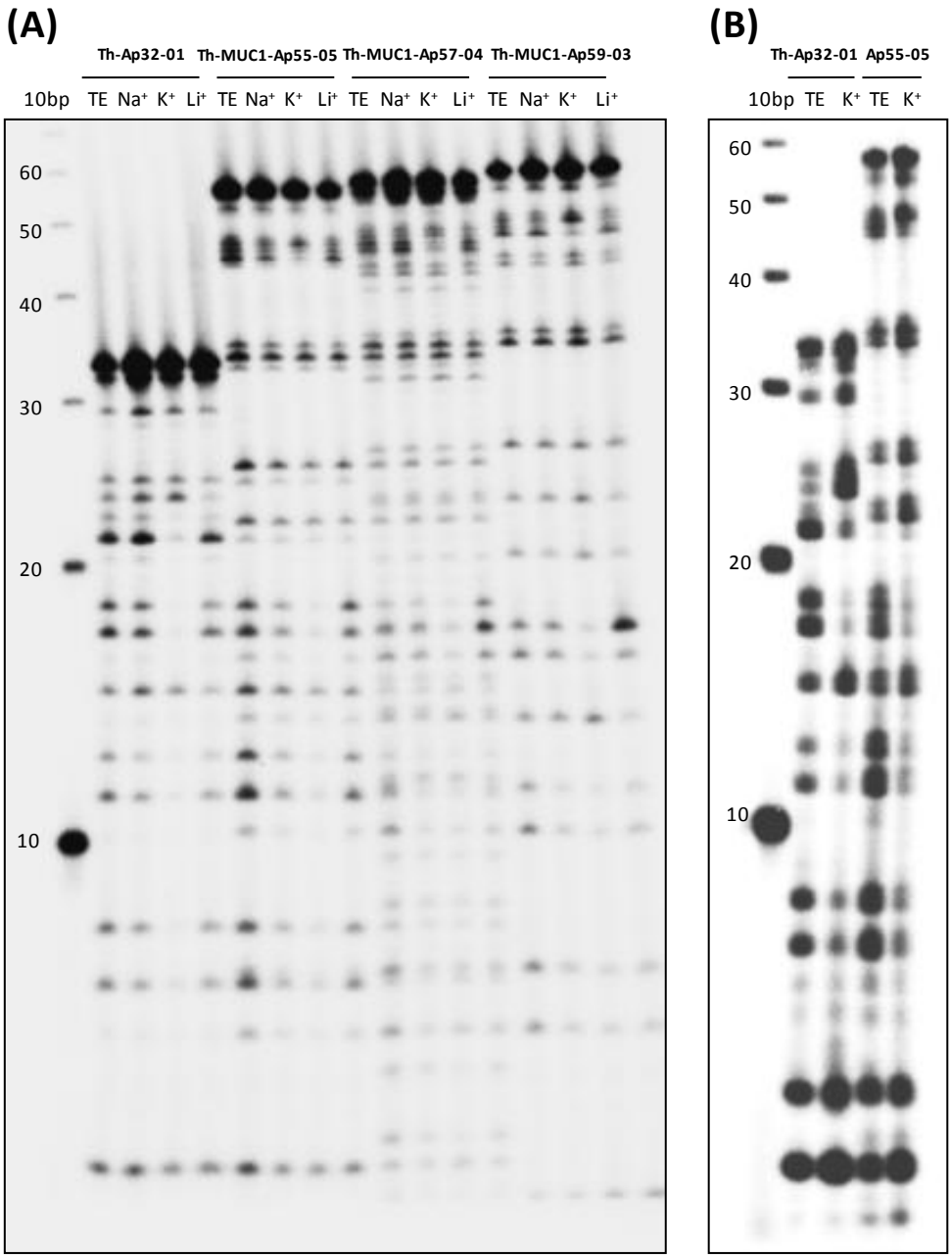

Figure 5-5. (A) 12% sequencing polyacrylamide gel depicting the piperidine cleavage patterns of DMS-modified Th-Ap32-01, Th-MUC1-Ap59-03, Th-MUC1-Ap57-04, and Th-MUC1-Ap55-05 in TE buffer, 1 M NaCl, 1 M KCl and 1 M LiCl. (B) 12% sequencing polyacrylamide gel depicting the piperidine cleavage patterns of DMS-modified Th-Ap32-01 and Th-MUC1-Ap55-05 in TE buffer and in 100 mM KCl (diluted from higher DNA and KCl [1 M] concentrations).

in the presence of 100 mM KCl. To make use of the new sought latent ability of Th-MUC1-Ap55-05 to fold into G-quartets at high efficiency in the presence of 1 M KCl, higher concentrations of Th-MUC1-Ap55-05 DNA (10 times higher) was allowed to fold in the presence of 1 M KCl overnight at 37 ℃. The samples were then diluted 10 times to result in Th-MUC1-Ap55-05 at the same original concentration in 100 mM KCl. DMS chemical protection, followed by piperidine cleavage was performed on both Th-MUC1-Ap55-05 and Th-Ap32-01 under these conditions. The resulting sequencing gel is shown on Panel B of Figure 5-5. From the figure, chemical protection was observed for guanine residues involved in G-quartet formation in the presence of 100 mM KCl, although the efficiency was not as great compared to that of 1 M KCl (Panel A). However, due to the fact that chemical protection efficiency was even worse for Th-MUC1-Ap55-05 with merely added 100 mM KCl without the dilution step (data not shown), this condition was chosen for subsequent experiments.

5.2.3 Gel Shift Assay for Thrombin

It is not sufficient to just evaluate the ability of the Th-MUC1-Ap55-05 fusion aptamer to fold into a G-quartet formation; it is equally necessary to validate its ability to bind thrombin, despite the interruption of the aptamer by the anti-MUC1 aptamer. We consider the binding of both Th-MUC1-Ap55-05 and Th-Ap32-01 to thrombin at various conditions: in TE buffer, in 100 mM KCl, and in 100 mM KCl with the addition of 1/10 of the total volume of a "non-specific" buffer (100 μM tRNA, 7.5 μM BSA, 100 mM NaCl, 10 mM Tris-HCl) to alleviate non-specific adsorption of thrombin to nucleic acids. We present Figure 5-6, which is an 8% non-denaturing (native) polyacrylamide gel depicting the gel shift. Several observations can be made. Firstly, thrombin has an

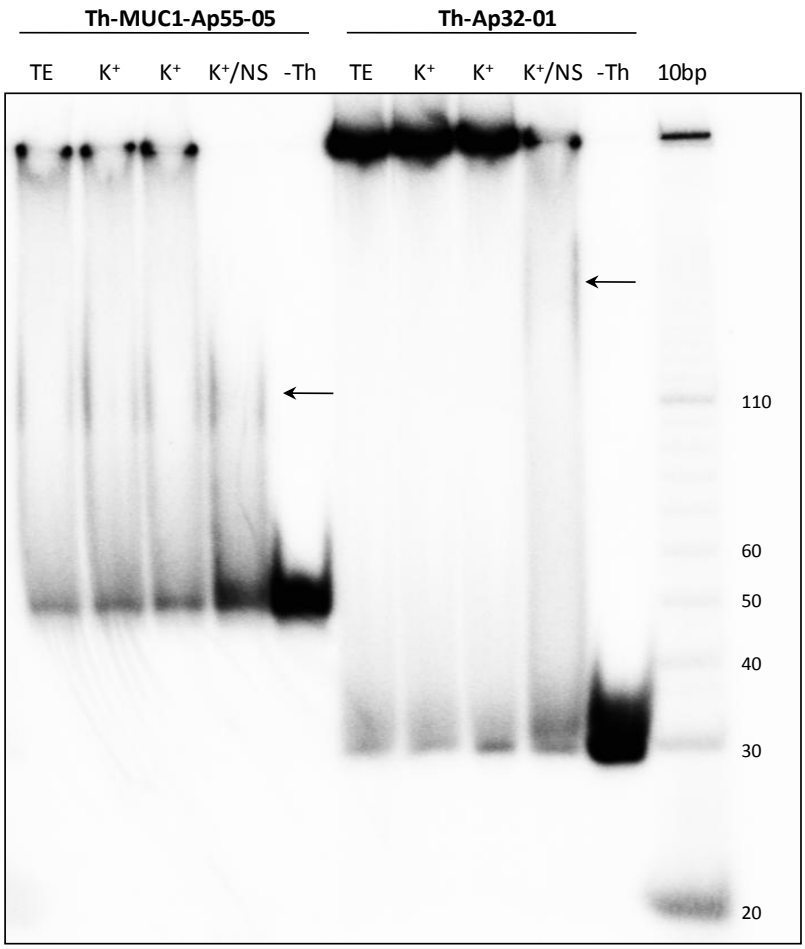

Figure 5-6. 8% non-denaturing (native) polyacrylamide gel depicting the gel shift of Th-MUC1-Ap55-05 and Th-Ap32-01 in the presence of thrombin. Lanes denoted "TE" and "K^+" refer to the salt condition (TE buffer and 100 mM KCl) in the presence of 2.13 μM thrombin. Lanes denoted "K^+/NS" refer to the addition of 100 mM KCl and a small amount (1/10 of the volume) of "non-specific" buffer (100 μM tRNA, 7.5 μM BSA, 100 mM NaCl, 10 mM Tris-HCl) in the presence of 2.13 μM thrombin. Lanes denoted "-Th" refer to the DNA alone. The arrows refer to the mobility of specific aptamer-analyte adducts.

inherent ability to absorb non-specifically to nucleic acid sequences. This is concluded by the observation that the lanes containing thrombin without the addition of the "non-specific" buffer saw significant aggregation at the position of the loading well. Secondly, the effect of the "non-specific" buffer was considerable since the addition of this buffer

resulted in a significantly smaller proportion of nucleic acid/protein aggregates, and a higher proportion of specific thrombin-aptamer conjugates (as denoted by the arrows). Thirdly, there was little preference for salt conditions for thrombin to bind to the aptamer since the formation of aggregates was observed when both Th-MUC1-Ap55-05 and Th-Ap32-01 were allowed to bind with thrombin in TE buffer and in 100 mM KCl. Since the shape and geometry of the anti-thrombin aptamer is well defined, this would provide evidence to say that thrombin (in the absence of KCl) promotes the folding of the aptamer into G-quartets. While both conditions (TE buffer and 100 mM KCl) resulted in adequate binding of thrombin, the latter condition was preferentially chosen since it guaranteed the formation of the G-quartet (Figure 5-5), which is an important step in the detection scheme for MUC1.

The specificity of the Th-MUC1-Ap55-05 for thrombin was also addressed. To dismiss the possibility that any nucleic acid could bind thrombin non-specifically, another DNA oligonucleotide with a similar length to that of Th-MUC1-Ap55-05 was evaluated for its ability to bind thrombin in the presence of 100 mM KCl. We present Figure 5-7 which is a native polyacrylamide gel showing the interaction of Th-MUC1-Ap55-05 and CT-59 (a non-related 59 nucleotide DNA oligonucleotide) with the addition of 2.13 μM thrombin in the presence of 100 mM KCl. Although CT-59 has two electrophoretic mobilities (probably due to two possible folding conformations), it is not at all affected by the presence of thrombin. This shows that the interaction between thrombin and Th-MUC1-Ap55-05 is a specific aptamer-analyte interaction.

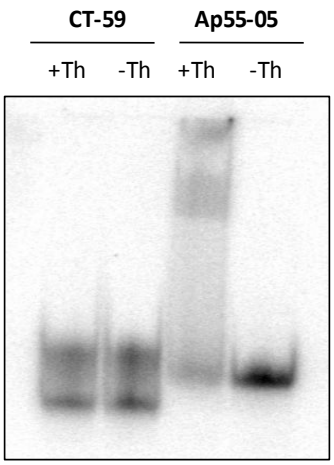

Figure 5-7. 8% non-denaturing (native) polyacrylamide gel showing the interaction of Th-MUC1-Ap55-05 and CT-59 with 2.13 μM thrombin. Lanes denoted "-Th" do not have thrombin, while lanes denoted with "+Th" have 2.13 μM thrombin along with "non-specific" buffer.

As shown in Figure 5-7, there was still significant aggregation of thrombin with Th-MUC1-Ap55-05, despite the addition of "non-specific" buffer. Further optimization was required to maximize the proportion of specifically-bound thrombin-aptamer adducts. At the end of the optimization process, it was concluded that it was the two tracking dyes used for non-denaturing polyacrylamide gels (xylene cyanol and bromophenol blue) that affected and influenced the ability for aggregate formation. Shown in Figure 5-8 is the non-denaturing polyacrylamide gel which featured the specific binding of Th-MUC1-Ap55-05 with 2.13 μM thrombin in the most optimized condition, specifically without the addition of xylene cyanol and bromophenol blue to the tracking dyes. Formation of specific thrombin-aptamer adducts was successful in both TE buffer as well as in 100 mM KCl, which was in accord with previous experimental results.

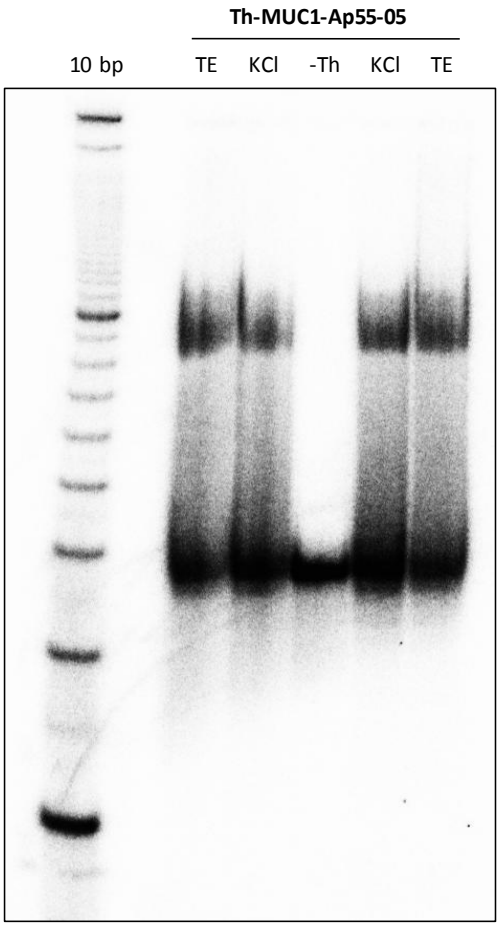

Figure 5-8. 8% non-denaturing (native) polyacrylamide gel showing the specific interaction of Th-MUC1-Ap55-05 and 2.13 μM thrombin. Lanes denoted "TE" refer to no salt conditions; lanes denoted "KCl" refer to 100 mM KCl; lanes denoted "-Th" refer to no addition of thrombin to the Th-MUC1-Ap55-05 oligonucleotide. Bromophenol blue and xylene cyanol were not added to the tracking dye.

To quantitate the interaction between thrombin and Th-MUC1-Ap55-05, another non-denaturing polyacrylamide gel was run with varying concentrations of thrombin. Quantification was from the percent specific complex formation and was densitometrically quantified with ImageQuant 5.2. The gel depicting concentration dependence of thrombin on Th-MUC1-Ap55-05 is shown on Figure 5-9.

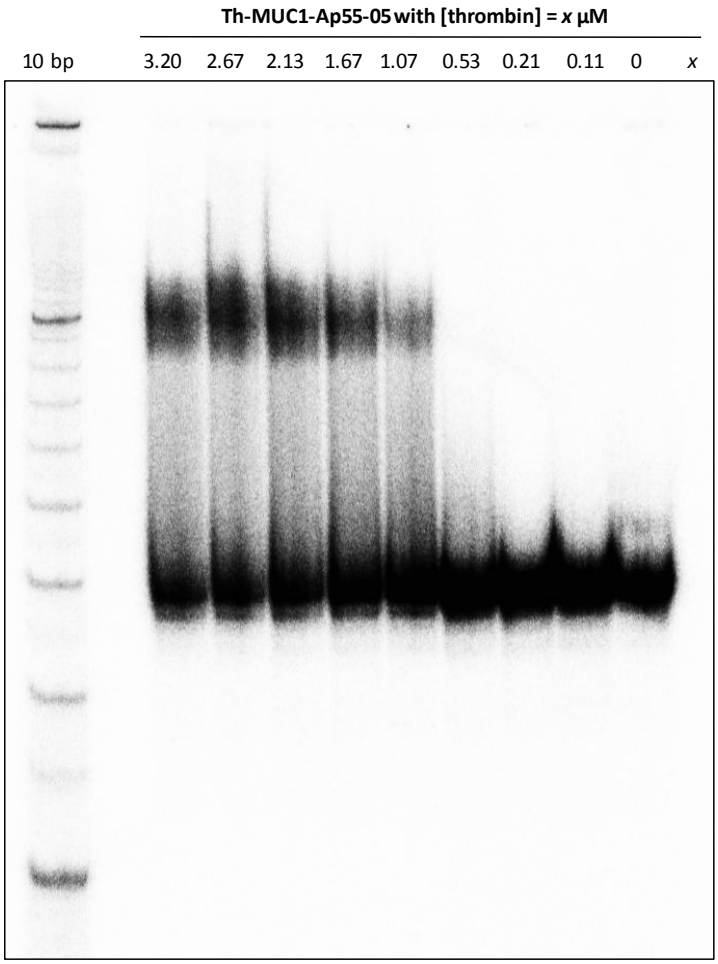

Figure 5-9. 8% non-denaturing (native) polyacrylamide gel showing the concentration dependence of thrombin on Th-MUC1-Ap55-05 in the presence of 100 mM KCl and with the addition of "non specific" buffer. Bromophenol blue and xylene cyanol were not added to the tracking dye.

Quantification of the signal was done with ImageQuant 5.2, in which the densitometric signals corresponding to the specific aptamer-analyte adduct was compared with that of the entire lane to extract a numerical value corresponding to percentage of complex formation. The number (percent complex formation) was plotted as a function of the concentration of thrombin, as shown in Figure 5-10. The concentration dependence

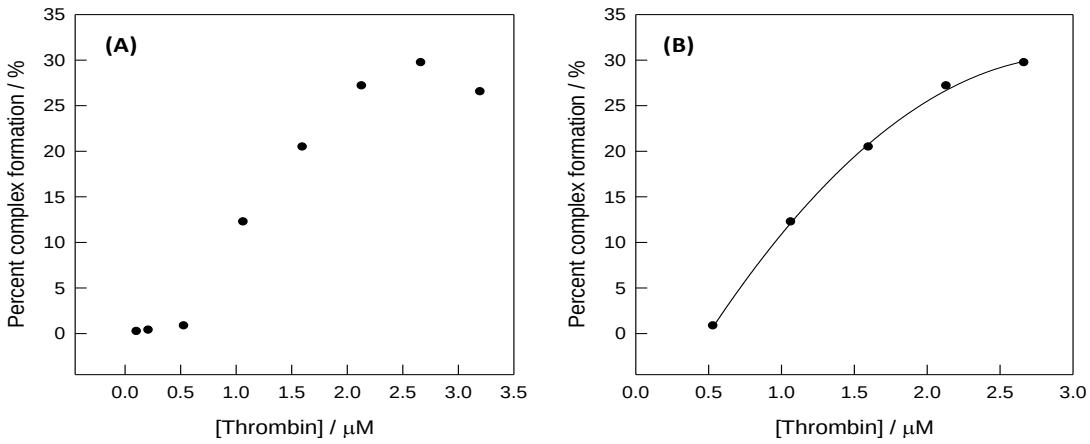

Figure 5-10. (A) Thrombin concentration dependence on the percent complex formation (as quantified from the nondenaturing polyacylamide gel on Figure 5-9) for fusion aptamer Th-MUC1-Ap55-05. (B) Thrombin concentration dependence on the percent complex formation for fusion aptamer Th-MUC1-Ap55-05 from a concentration range of 0.53 μM to 2.67 μM, with a quadratic regression overlay. Assuming that concentrations past 2.67 μM saturate the signal, the dissociation constant K_D was extracted as the concentration of thrombin in which 50% of the maximum signal (percent complex formation) was observed.

of thrombin (Panel A of Figure 5-10) on the percent complex formation is unlike that of typical Langmuir isotherms seen in Chapters 3, 4 and 5, in that a threshold concentration (approximately 0.5 μM) of thrombin was required to observe formation of the aptamer-analyte complex. At concentrations past 0.5 μM, monotonic increase in the percent complex formation was observed, until a decrease was observed from 2.67 μM to 3.2 μM. With the assumption that saturation will occur at concentrations higher than 2.67 μM, a regression was used to determine the dissociation constant of Th-MUC1-Ap55-05 for thrombin in the concentration range from 0.53 μM to 2.67 μM, as shown in Panel B of Figure 5-10. Here, K_D was defined as the concentration of thrombin in which the percent complex formation was 50% of that of the maximum percent complex formation. The

formalities of this can be derived from the Langmuir equation, where y is the signal (e.g. percent complex formation), y_{max} is the maximum signal, C is the concentration and K_D is the dissociation constant:

$$y = \frac{y_{max} C}{K_D + C} \quad (1)$$

When $C = K_D$, isolation for y becomes:

$$y = \frac{y_{max} K_D}{K_D + K_D} \quad (2)$$

$$y = \frac{y_{max} K_D}{2K_D} \quad (3)$$

$$y = \frac{y_{max}}{2} \quad (4)$$

which is to say that K_D is the concentration of thrombin which results the formation of 50% of the maximum number of analyte-aptamer adducts. Solving the quadratic regression for $\frac{y_{max}}{2}$, assuming y_{max} is the percent complex formation when [thrombin] = 2.67 μM, a dissociation constant of 1.22 μM was extracted. This is considerably (and reasonably) larger than the direct K_D for thrombin and its aptamer.[18] Considering that the concentration of thrombin in blood is in the low nanomolar to low micromolar range,[26] this system may be applicable for direct detection in blood using physiological thrombin.

Time constraints in the duration of my M.Sc. degree have limited further progress in this project. The next step would be to optimize the conditions to observe clear gel shifts by adding MUC1 peptides with Th-MUC1-Ap55-05. After proving the ability for

Th-MUC1-Ap55-05 to bind MUC1, optimization will take place in the proteolytic reaction carried out by thrombin and F-Q. Once parameters are optimized, more optimization will involve varying the ratio of the three species in solution (thrombin, MUC1 and Th-MUC1-Ap55-05) before beginning detection of MUC1 and generating concentration dependence plots.

5.3 Conclusion

The present study demonstrates that it was indeed possible to fuse two aptamers together and retain the binding ability for at least one of the analytes to bind. In an attempt to develop fusion aptamers corresponding to anti-MUC1 and anti-thrombin sequences to result in allosteric regulation of thrombin activity by MUC1 effector molecules, 5 fusion aptamer designs were tested for their ability to fold into G-quartets. This was confirmed with DMS chemical protection assays and piperidine cleavage. Th-MUC1-Ap55-05 was selected for gel shift assays with thrombin. Clear gel shifts were observed, and quantification of signal predicted a dissociation constant of Th-MUC1-Ap55-05 for thrombin to be 1.22 μM. More experiments are necessary to validate the ability of MUC1-Ap55-05 to bind MUC1, and to fully characterize the biosensing applicability of this fusion aptamer for MUC1.

5.4 Experimental Section

5.4.1 DNA Purification and Preparation

The synthetic fusion aptamer sequences Th-Apt-32, Th-MUC1-Ap38-01, Th-MUC1-Ap42-02, Th-MUC1-Ap59-03, Th-MUC1-Ap57-04, and Th-MUC1-Ap55-05, and control oligonucleotide CT59-4 (TCA CTA TGG TCA GCG TCT CGC ACT CGA

GAG AAG CAA GAG AAC GAG TCA GGT CGA CTA AA) were purchased from Core DNA Services, Inc. (Calgary, AB) and size-purified using denaturing (50% urea, w/v) polyacrylamide gel electrophoresis (PAGE). Quantification was done on a Cary 300Bio UV-Visible spectrophotometer (Varian Instruments) using an absorbance of 260 nm estimated for single stranded DNA. Oligonucleotides were end-labeled with ^{32}P (using standard kinasing procedures), and then PAGE purified following a pre-treatment with 10% piperidine (v/v) at 90 ℃ for 3 min followed by lyophilization.

5.4.2 Chemical Protection Assay with DMS (Dimethyl Sulfate)

Folding of fusion aptamers to G-quartet conformation was performed by adding 5 μL of salt (concentration and cationic species was optimized) to 2 μL of 50 μM DNA, 1 μL of 300 cps (counts per second) ^{32}P-labeled DNA, 6 μL of TE (10 mM Tris-HCl, 100 μM EDTA, pH = 7.4) buffer, and 1 μL of 1 M Tris-HCl. Before addition of salt, the aptamers were denatured for 2 min at 100 ℃ and placed on ice immediately. After addition of salt, the aptamers were incubated at 37 ℃ for at least 2 hours to promote the formation of the G-quartets. 16 μL samples of G-quartet forming aptamers were added 2.5 μL DMS (dimethyl sulfate) solution (3% v/v DMS in ddH_2O) and 2.5 μL DMS buffer solution (200 mM sodium cacodylate in ddH_2O). The chemical modification of guanines by DMS was allowed to take place for 0.5 hour. In the meantime, a stock "stop" solution mastermix was made by the addition of 100 μL glycogen (15 mg/15 mL ddH_2O) and 5 μL of β-mercaptoethanol to 1000 μL of ddH_2O. 130 μL of "stop" was added to each DMS reaction. This was followed by the addition of 375 μL of 100% ethanol stored at -20 ℃. The samples were placed on dry ice for 5 min or until the solution became viscous. The samples were centrifuged for 40 min at 4 ℃ to complete the ethanol

precipitation procedure. The supernatant was removed and the pellet was washed with 150 μL washes of 70% ethanol 3 times. 100 μL of 10% piperidine (v/v) in ddH_2O was added to the samples and the cleavage reaction was allowed to occur for 0.5 hour at 90 ℃. The samples were then immediately vacuum-concentrated to dryness. 80 μL of ddH_2O were added to the samples and were vacuum concentrated again to dryness. The samples were loaded on 12% denaturing polyacrylamide sequencing gels. Images and densitometry of sequencing gels were obtained using a Typhoon 9410 phosphorimager and quantitated with ImageQuant 5.2 (Amersham Bioscience).

5.4.3 Gel Shift Assay with Thrombin

The experimental protocol here refers to the optimized conditions for the gel shift assay with thrombin; see text for details. Aptamers were first allowed to fold to the G-quartet conformation in the presence of KCl prior to native gel shift assay with thrombin. This was performed in 7.3 μL samples containing 2 μL of 50 μM DNA, x μL of ^{32}P-labeled DNA with at least 1000 cps, (7.3 – x) μL TE buffer, and 4.7 μL of 4 M KCl. Folding was allowed to take place for at least 2 hours at 37°C. 1.5 μL of salt-incubated DNA (at a concentration of 6.6 μM) was then added to 2 μL of 4X binding buffer (1X = 50 mM Tris-HCl, 100 mM NaCl, 1 mM $MgCl_2$, 5% glycerol, pH = 7.4), 2 μL of thrombin (diluted with 50 mM sodium citrate, 200 mM NaCl, 0.1% PEG, pH = 6.5), 1 μL of "non-specific buffer" (100 μM tRNA and 7.5 μM BSA (bovine serum albumin) in 10 mM Tris-HCl, 100 mM NaCl, pH = 7.4) and 3.5 μL TE buffer. The binding of thrombin to the fusion aptamer was allowed to occur for 5 min at 37 ℃. The gel shift was performed with an 8% native polyacrylamide gel in 0.5X TBE buffer by running at a power of approximately 6 W for approximately 5-6 hours at 4 ℃.

5.5 References

1. Lodish, H.; Berk, A.; Matsudaira, P.; Kaiser, C. A.; Krieger, M.; Scott, M. P.; Zipursky, S. L.; Darnell, J. *Molecular Cell Biology*, Fifth edition; W. H. Freeman and Company: New York, **2004**.
2. Purves, D.; Augustine, G. J.; Fitzpatrick, D.; Hall, W. C.; LaMantia, A.-S.; McNamara, J. O.; White, L. E. *Neuroscience*, Fourth edition; Sinauer Associates: Sunderland, MA, **2008**.
3. Rajendra, S.; Lynch, J. W.; Schofield, P. R. *Pharmacol. Therapeut.* **1997**, *73*, 121 – 146.
4. Lynch, J. W. *Physiol. Rev.* **2004**, *84*, 1051 – 1095.
5. Ellington, A. D.; Szostak, J. W. *Nature* **1990**, *346*, 818 – 822.
6. Tuerk, C.; Gold, L. *Science* **1990**, *249*, 505 – 510.
7. Soukup, G. A.; Breaker, R. R. *Structure* **1990**, *7*, 783 – 791.
8. Soukup, G. A.; Breaker, R. R. *Proc. Natl. Acad. Sci. U. S. A.* **1990**, *96*, 3584 – 3589.
9. Soukup, G. A.; Breaker, R. R. *Trends Biotechnol.* **1990**, *17*, 469 – 476.
10. Soukup, G. A.; Breaker, R. R. *Curr. Opin. Struc. Biol.* **2000**, *10*, 318 – 325.
11. Soukup, G. A.; Emilsson, G. A. M.; Breaker, R. R. *J. Mol. Biol.* **2000**, *298*, 623 – 632.
12. Cong, X.; Nilsen-Hamilton, M. *Biochemistry* **2005**, *44*, 7945 – 7954.
13. Najafi-Shoushtari, S. H.; Famulok, M. *Blood Cell Mol. Dis.* **2007**, *38*, 19 – 24.
14. Ferre-D'amare, A. R.; Rupert, P. B. *Biochem. Soc. Trans.* **2002**, *30*, 1105 – 1109.
15. Hampel, K. J.; Pinard, R.; Burke, J. M. *Methods Enzymol.* **2001**, *341*, 566 – 580.

16. Esteban, J. A.; Banarjee, A. R.; Burke, J. M. *J. Biol. Chem.* **1997**, *272*, 13629 – 13639.

17. Fedor, M. J. *Biochem. Soc. Trans.* **2002**, *30*, 1109 – 1115.

18. Bock, L. C.; Griffin, L. C.; Latham, J. A.; Vermaas, E. H.; Toole, J. J. *Nature* **1992**, *335*, 564 – 566.

19. Pavlov, V.; Shlyahovsky, B.; Willner, I. *J. Am. Chem. Soc.* **2005**, *127*, 6522 – 6523.

20. Maxam, A.; Gilbert, W. *Methods Enzymol.* **1980**, *65*, 499 – 560.

21. Sen, D.; Gilbert, W. *Nature* **1990**, *344*, 410 – 414.

22. Ikebukuro K.; Yoshida W.; Sode K., *Nucleic Acids Symp. Ser.* **2004**; 48:231 – 232.

23. Ikebukuro K.; Yoshida W.; Sode K., *Nucleic Acids Symp. Ser.* **2005**; 49:83 – 84.

24. Lin, C. H.; Patel, D. J. *Chem. Biol.* **1997**, *4*, 817 – 832.

25. Ferreira, C. S. M.; Matthews, C. S.; Missailidis, S. *Tumor Biol.* **2006**, *27*, 289 – 301.

26. Lee, M.; Walt, D. *Anal. Biochem.* **2000**, *282*, 142 – 146.

CHAPTER 6

CONCLUSION AND FINAL REMARKS

6.1 Summary

In this thesis, the premise of aptamer-based biosensing has been explored. Specifically, a combination of electrochemical and optical methods has been employed for novel sensor development – this demonstrates the wide versatility of readout methods which can be used for aptamer-based biosensors. Our study began with a voltammetric detection method for a model protein lysozyme (Chapter 2), in which the cyclic voltammatric signal of DNA-binding electrostatic redox marker $[Ru(NH_3)_6]^{3+}$ decreased upon the incubation of lysozyme on anti-lysozyme aptamer-modified Au electrodes. This study, in combination with others, has expanded the realm of electrochemical aptamer-based biosensors to include the use of electrostatic redox markers to probe for analyte-induced conformational changes in the secondary structure of the aptamer.

Our subsequent studies (Chapters 3 through 5) focussed on the development of novel sensors for mucin 1 (MUC1), a cell-associated glycoprotein over-expressed and ubiquitous in detectable levels in the serum of patients with early epithelial adenocarcinomas. In Chapter 3, we explored the detection of MUC1 in a DNA hybridization scheme with quantum dot-based fluorescence readout, at detection limits comparable to presently-used ELISA assays for the same antigen. It was from this study

that important knowledge regarding the conformational change of the anti-MUC1 aptamer before and after binding of analyte was extracted. This knowledge was pertinent for the transforming of MUC1 detection methodologies to improved electrical ones, in which the incubation of MUC1 to either methylene blue (MB)-tagged anti-MUC1 aptamer-modified Au electrodes or anti-MUC1 aptamer-modified electrodes resulted in the decrease in oxidation current (as measured with square wave voltammetry) of tagged-MB or solution-diffused MB, respectively (Chapter 4). It was also from this study that the use of methylene blue electrochemistry for aptamer-based biosensing, in general, was evaluated: important parameters for MB-based sensor optimization were considered such as pH dependencies and electron transfer kinetics. In Chapter 5, we considered a unique fusion aptamer-based optical scheme for the detection of MUC1 based on allosteric regulation. By the fusion of an anti-thrombin aptamer sequence with that of an anti-MUC1 aptamer sequence, we were able to generate fusion aptamer constructs, in the hope of finding an optimized sequence that would use MUC1 peptides as an effector molecule to allosterically regulate the binding (and hence, loss of proteolytic activity) of thrombin to its aptamer sequence. Intense optimization has resulted in the discovery of one sequence Th-MUC1-Ap55-05 with the ability to both fold into the correct secondary structure for thrombin binding, and to bind thrombin.

6.2 Future Work

The very reason why researchers around the globe choose to focus their research in the realm of aptamer-based biosensors is not hard to comprehend. The complexities involved and inherent difficulties that are characteristic of their protein counterparts – antibodies – render nucleic acid aptamers much more suitable and applicable for the

ongoing fabrication of miniature, portable, electrical surface reaction-based sensors for protein biomarkers. In particular, the trend is now for the development of alternative diagnostic methodologies for tumour markers, of which adenocarcinomas are typically diagnosed through imaging techniques (particular for lung cancer) such as chest radiography, computed tomography scans. Verification of the diagnostic often involves the use of the invasive technique of needle biopsy.[1] In Chapters 3 through 5, we reported serum-based detection methodologies towards MUC1, a glycoprotein known to be expressed at elevated concentrations in almost all epithelial adenocarcinomatous tissues. We foresee the expansion of these aforementioned projects in the hope for increased sensitivity and specificity of these methodologies for the detection of MUC1.

In particular, with regards to the quantum dot-based fluorescence readout method described in Chapter 3, we envision the utilization of our newly-found capability in quantum dot (QD) surface-modification procedures to propose simple signal-on and signal-off aptamer-based biosensors (based on the conformational change of the aptamer upon analyte binding) using quencher-modified aptamer strands conjugated to quantum dots. The proposed schematic is shown in Figure 6-1. As shown in Panel A of the figure, the incubation of MUC1 peptides to quencher-tethered anti-MUC1 aptamer-modified quantum dots will result in the unfolding of the aptamer to an elongated conformation. This may be measured by an increase in fluorescence intensity due to the elimination of fluorescence resonance energy transfer (FRET). For thrombin detection (Panel B), incubation of thrombin will result in thrombin-induced folding of the quencher-tethered anti-thrombin aptamer-modified quantum dots to a G-quartet conformation. This brings the quencher closer to the nanoparticle surface, thus promoting the occurrence of FRET.

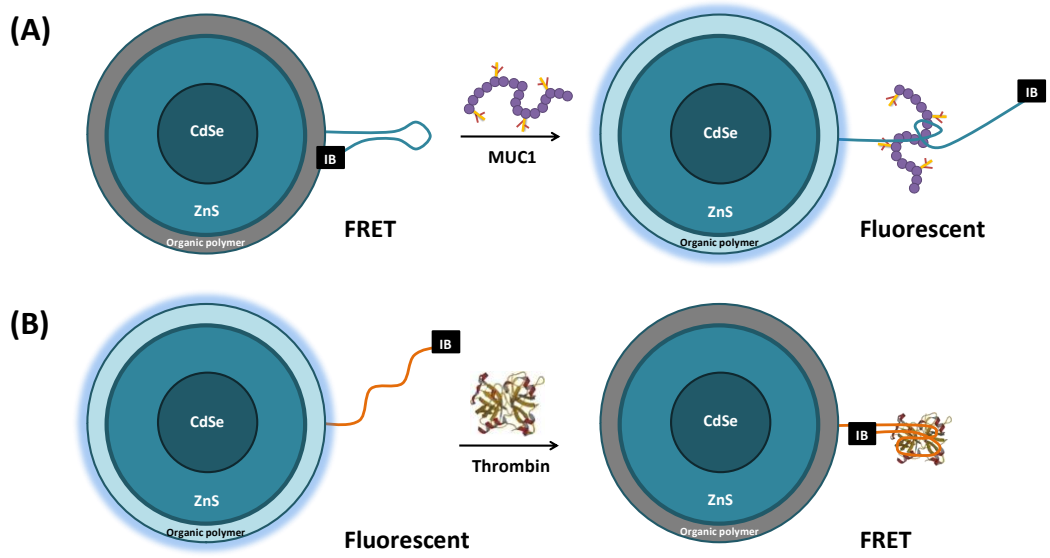

Figure 6-1. 'Signal-on' and 'signal-off' designs for the aptamer-based detection of MUC1 peptides (A) and thrombin (B) using fluorescence resonance energy transfer (FRET) as an energy transfer mechanism for control of quantum dot-based fluorescence readout.

With regards to the fusion aptamer-based detection protocol of MUC1 using the allosteric regulation of thrombin activity (Chapter 5), we envision the next step in the experimental plan to focus on the optimization of buffer conditions to guarantee the binding of both MUC1 and thrombin. Stoichiometry between the three species (fusion aptamer, thrombin, MUC1) will then be considered to optimize for the most favourable situation which can be used for detection of MUC1. This will be followed by optimization of conditions required for the proteolytic reaction of α-thrombin on the bis-(p-tosyl-L-glycyl-L-prolyl-L-arginine amide) Rhodamine 110 (F-Q) non-fluorescent substrate. Upon doing so, we can consider variations of the detection scheme in the hope for higher sensitivity. The first variation will utilize quantum dots as fluorophores, which have much more advantages compared to typical organic fluorophores (Figure 6-2).

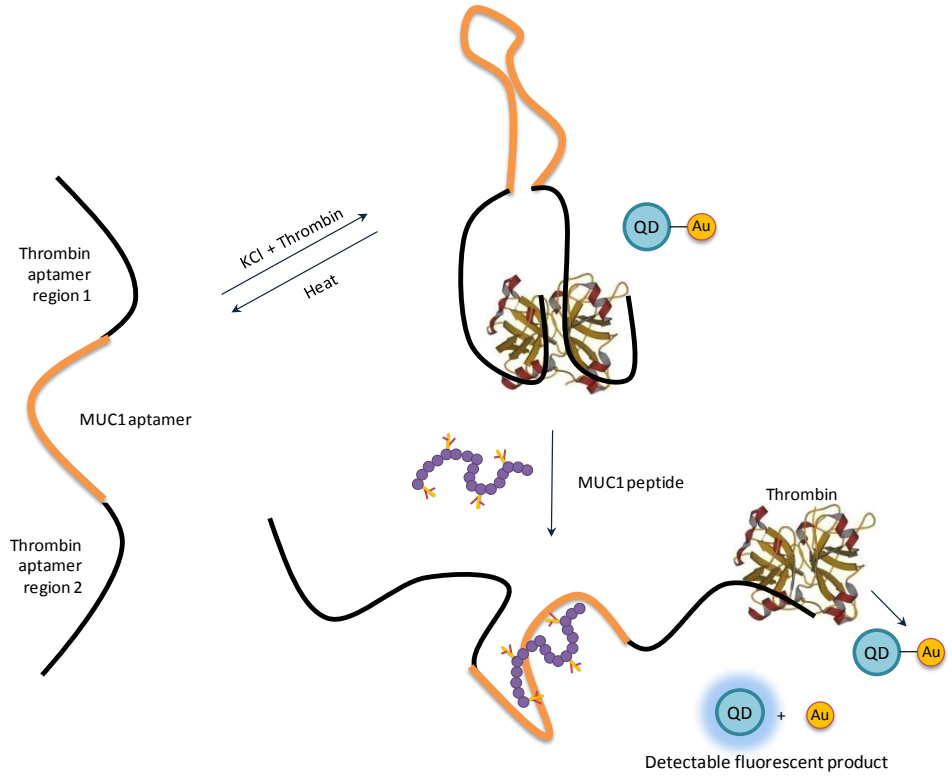

Figure 6-2. In the presence of physiological salt, the anti-thrombin aptamer folds into its inherent G-quartet secondary structure to allow the binding of thrombin. The inhibition of the proteolytic activity of thrombin prevents it from cleaving the peptide linker between QD and a Au nanoparticle. In the presence of MUC1, MUC1 binds to the anti-MUC1 aptamer thus releasing thrombin making it available to cleave the peptide linker between QD and Au. This results in significant increase in fluorescence emitted by the QD.

A specialized QD-Au nanoparticle conjugate system (hereon, QD-Au) will be designed (Figure 6-2) which can be used to assess the activity of thrombin. Human α-thrombin recognizes an amino acid sequence consisting of X-X-P-R-B-B[2] from N-terminus to C-terminus where X corresponds to hydrophobic amino acid residues, P for proline, R for arginine, and B for non-acidic amino acids at physiological pH. The cleavage location is the peptide bond on the C-terminus of R. To assess the activity of

thrombin, the QD-Au construct will be designed with a peptide linker: L-cysteinyl-L-alanyl-L-isoleucyl-L-prolyl-L-argininyl-L-glycyl-L-serinyl amide. The cysteine residue will be used to immobilize the peptide on the Au nanoparticle using the Au-S interaction with the β-carbon of cysteine; the amide moiety will be used to couple the linker to carboxy-terminated QDs. In the absence of MUC1, as shown in Figure 6-2, the proteolytic activity of thrombin will be inhibited and thus thrombin will not be able to cleave QD-Au. Quenching of the QD occurs by Au and minimal fluorescence will be observed. In the presence of MUC1, there will be preferential binding of MUC1 to anti-MUC1 aptamer compared to that of thrombin – this is due to the fact that MUC1 binds a fully undisrupted aptamer while thrombin binds a disrupted, less robust, aptamer. The binding of MUC1 should disrupt the secondary structure of the anti-thrombin aptamer leading to the release of α-thrombin. Released thrombin will restore the proteolytic activity of thrombin to cleave the bond between QD and Au. This will release QD from the quenching ability of Au, and significant fluorescence signal increase will be expected.

We can also consider an alternative to the scheme, which can use the conformational change exhibited by the fusion aptamer which is expected to occur in the presence of MUC1. We consider the double modification of the fusion aptamer at both the extreme 5′ end and the extreme 3′ end with fluorophore and quencher respectively. The fluorophore may be an organic fluorophore or a QD. As shown in Figure 6-3, in the presence of MUC1, the binding of MUC1 to the fusion aptamer will result in the unfolding of the G-quartet structure. Doing so will increase the distance between the fluorophore and the quencher leading to elimination of FRET. Increase in fluorescence intensity will be expected for increasing concentrations of MUC1 peptides.

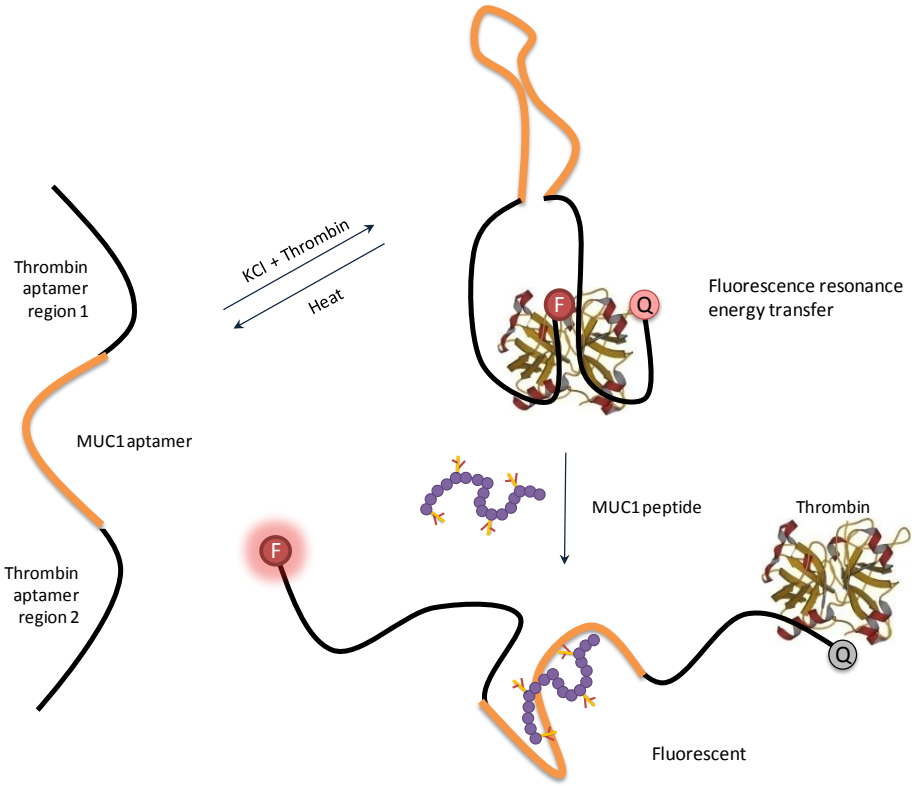

Figure 6-3. In the presentation of physiological salt, the anti-thrombin aptamer folds into its inherent G-quartet secondary structure to allow the binding of thrombin. In the presence of MUC1, MUC1 binds to the anti-MUC1 aptamer thus unfolding the G-quartet secondary structure. This increases the physical distance between a fluorophore and quencher, leading to the elimination of FRET. Increase in fluorescence intensity is expected.

6.3 Health Implications

From the research efforts around the globe on aptamer-based biosensors, we envision the future for health diagnostics to slowly transform from primarily protein-based assays to nucleic acid- (specifically, aptamer-) based devices, in particular for cancers. The specificity of these devices for cancers will arise from biomarkers, molecules that are found in bodily fluids that are specific to cancer patients. It is within our collective goal that it would be possible to permit the general individual in the

Canadian population to perform an early screening, thereby improving the prognosis in the event of a positive result indicating an early stage of cancer. We hope that it may be possible for these tests to be done even prior to the elicitation of regular symptoms. Ultimately, we aspire for the translation of research efforts in aptamer-based biosensors to an improved health for Canadians today.

6.4 References

1. Minna, J. D.; Schiller, J. H. *Harrison's Principles of Internal Medicine*, Seventeenth Edition; McGraw-Hill: **2008**.
2. Chang, J. Y. *Eur. J. Biochem.* **1985**, *151*, 21 7 – 224.